

Aus dem Max-Planck Institut für Kolloid und Grenzflächenforschung
Abteilung Grenzflächen

Introduction of a Thermo-sensitive Non-polar Species into Polyelectrolyte Multilayer Capsules for Drug Delivery

Dissertation
zur Erlangung des akademischen Grades
"doctor rerum naturalium"
(Dr. rer. nat.)
in der Wissenschaftsdisziplin Physikalische Chemie

eingereicht an der
Mathematisch-Naturwissenschaftlichen Fakultät
der Universität Potsdam

von
Michelle Elizabeth Prevot
Geboren am 05. Januar 1978 in Columbus, Georgia (Vereinigte Staaten)

Potsdam, den 30. Januar, 2006

This work is dedicated in loving memory to my grandmother Agatha Prevot. A person whose thirst for knowledge was never quenched, enabling education for my father, his siblings, and, eventually, me to be possible. With the completion of this work, her dreams come true.

Vorsitzender: Prof. Dr. Bechman

Gutachter: Prof. Dr. Möhwald, Prof. Dr. Decher, Dr. Prof. Sukhorukov

Beisitzer: Prof. Dr. Decher, Prof. Dr. Lashewsky, Prof. Dr. Mohwald, Prof. Dr. Strehmel,
Prof. Dr. Sukhorukov, Priv. Doz. Tauer,

Tag der mündlichen Prüfung: 19.06.2006

Table of Contents

Table of Contents	vi
List of Figure	ix
List of Equations	xii
Nomenclature	xiii
Chapter 1-General Introduction	1
Chapter 2-Literature Survey and Theory	3
2.1 Polyelectrolytes.....	3
2.2 Complexes.....	4
2.3 Flat Films	5
2.4 Capsules	6
2.5 PNIPAM	7
2.6 Permeability of LbL Films.....	9
2.7 Intermolecular Forces	9
References.....	13
Chapter 3-Methods of Characterization	19
3.1 Confocal Laser Scanning Microscopy (CLSM)	19
3.2 Raman Spectroscopy.....	22
3.3 UV/VIS Spectroscopy.....	24
3.4 Scanning Electron Microscopy	24
3.5 Scanning Force Microscopy	26
3.6 Zeta Potential Measurement	27
3.7 Ellipsometry	28
3.8 Differential Scanning Calorimetry.....	30
3.9 Neutron Reflectivity.....	31
3.10 Instrumental Detail.....	33
References.....	35
Chapter 4-Polyelectrolyte multilayers as an encapsulation vehicle	37
4.1 Introduction.....	37
4.2 Fluorescent Probes.....	38
Preparation	38
Results.....	40
4.3 PNIPAM inside CaCO ₃ cores	45
Preparation	45
Results.....	46
4.4 PNIPAM inside PS templated capsules	52
Preparation	52
Results.....	54
4.5 PNIPAM as an absorption and release agent.....	57

4.6 Salt effect on PNIPAM LCST	64
4.7 Comparison of encapsulation techniques.....	68
4.8 Conclusions.....	70
Reference	71
Chapter 5- Polyelectrolyte multilayer permeability alteration	
with wax particles layers	75
5.1 Introduction.....	75
5.2 Wax Particle Characterization	76
5.3 Flat films	77
Preparation.....	77
Results.....	78
5.4 Capsules	82
5.4.1 CaCO ₃	82
Preparation	82
Results	83
5.4.2 Melamine Formaldehyde	86
Preparation	86
Results	86
5.4.3 Polystyrene.....	89
Preparation	89
Results	89
5.5 Conclusions.....	97
References.....	97
Chapter 6 General Conclusions.....	99
Zusammenfassung.....	101
Abstract	102
Acknowledgments	103
Appendix I Materials.....	AI-1
Appendix II Supporting SEM images	AII-1
Appendix III Supporting AFM images	AIII-1
Appendix IV Publications	AIV-1

List of Figures

Figure 2.5.1 PNIPAM solubility above and below the Lower Critical Solution Temperature	8
Figure 2.7.1 Hydrogen bonding in bulk water	13
Figure 3.1.1 Principle of Confocal Microscopy.....	20
Figure 3.1.2 Principles of Fluorescent Recovery After Photobleaching	21
Figure 3.4.1 Layout of a typical SEM.....	25
Figure 3.5.1 Principle of AFM.....	26
Figure 3.6.1 Potential of a charged surface.....	28
Figure 3.7.1 Ellipsometry layout	29
Figure 3.8.1 Layout of DSC.....	30
Figure 3.8.2 Typical DSC curve for a polymer	31
Figure 3.9.1 Simulation of the specular neutron reflectivity as a function of q from a silicon/air interface.....	32
Figure 3.9.2 Simulation of the specular neutron reflectivity as a function of q from a silicon wafer with a film on top	32
Figure 3.9.3 Neutron sample interaction.....	33
Figure 4.2.1 Preparation schema of CaCO ₃ cores.....	39
Figure 4.2.2 CaCO ₃ core top and cross section of cores bottom	40
Figure 4.2.3 Coated CaCO ₃ cores top pictures are with 6 layers and below with 16 layers	41
Figure 4.2.4 CaCO ₃ core after 16 layers	42
Figure 4.2.5 SEM images of capsules after 6 and 16 layers of PSS/PAH.....	42
Figure 4.2.6 Confocal image of (PAH-FITC/PSS) 8.....	43
Figure 4.2.7 CLSM images of microcapsules.....	44
Figure 4.3.1 Scheme presenting CaCO ₃ core co-synthesis with PNIPAM and then the LbL deposition of PSS and PAH to form capsules.....	46
Figure 4.3.2 SEM of CaCO ₃ cores.....	46
Figure 4.3.3 SEM of CaCO ₃ cores with co-synthesized PNIPAM	47
Figure 4.3.4 SEM of (PAH/PSS) ₄ capsules from CaCO ₃ cores.....	47
Figure 4.3.5 SEM of (PAH/PSS) ₄ capsules from CaCO ₃ cores with encapsulated PNIPAM	48
Figure 4.3.6 Confocal images of (PAH/PSS) ₄ capsules from CaCO ₃ cores	48
Figure 4.3.7 Confocal images of (PAH/PSS) ₄ capsules from CaCO ₃ cores with encapsulated PNIPAM.....	49
Figure 4.3.8 Raman Spectroscopy of CaCO ₃ cores with and without PNIPAM.....	49
Figure 4.3.9 Raman Spectroscopy of capsules templated on CaCO ₃ cores.....	50
Figure 4.3.10 Raman Spectroscopy vibration assignment for CaCO ₃ cores with and without PNIPAM	50
Figure 4.3.11 Raman Spectroscopy vibration assignment for capsules templated on CaCO ₃ cores with and without PNIPAM	50

Figure 4.4.1 Ship in a bottle encapsulation scheme.....	53
Figure 4.4.2 Representative SEM pictures of capsules before and after PNIPAM synthesis.....	54
Figure 4.4.3 AFM images of dried capsules before and after PNIPAM encapsulation.....	55
Figure 4.4.4 Raman confocal spectra of pure PNIPAM purchased from Aldrich and the PNIPAM found inside the capsules	55
Figure 4.4.5 Series of confocal pictures revealing encapsulated PNIPAM only inside capsules	56
Figure 4.5.1 Release of Methylene Blue from a membrane	58
Figure 4.5.2 Confocal images of (PAH/PSS) ₄ capsules from CaCO ₃ cores with FITC	60
Figure 4.5.3 Confocal images of (PAH/PSS) ₄ capsules from CaCO ₃ cores with encapsulated PNIPAM with FITC	61
Figure 4.5.4 CaCO ₃ encapsulated PNIPAM (PSS/PAH) ₄ treated with Orange II overnight and washed until supernatant was clear.....	62
Figure 4.5.5 CaCO ₃ encapsulated PNIPAM (PSS/PAH) ₄ added to microscope slide.....	65
Figure 4.6.1 DSC of bulk PNIPAM with different ions and concentrations	66
Figure 4.6.2 Dependence of LCST of PNIPAM with various concentrations of different salts	66
Figure 4.7.1 Raman Spectroscopy of PNIPAM encapsulated in capsules templated on CaCO ₃ cores and PS cores	69
Figure 5.2.1 Wax types and their properties	77
Figure 5.2.2 DSC of wax particles.....	77
Figure 5.3.1 Schematic representation of the formation of a uniform hydrophobic barrier layer of paraffin atop the polyelectrolyte multilayer	78
Figure 5.3.2 Variation of the ellipsometric thickness of the (PAH/PSS) ₆ and (PAH/PSS) _{7.5} /wax samples with annealing time	79
Figure 5.3.3 Neutron reflectivity of multilayers measured in air	81
Figure 5.3.4 Neutron reflectivity of multilayers measured in D ₂ O.....	81
Figure 5.4.1 Scheme of capsule fabrication with wax layer via method	82
Figure 5.4.1.1 CaCO ₃ templated (PAH/PSS) ₄ capsules.....	84
Figure 5.4.1.2 CaCO ₃ templated (PAH/PSS) ₄ capsules after heating.....	84
Figure 5.4.1.3 CaCO ₃ templated (PAH/PSS) ₂ (PAH/-wax) ₂	84
Figure 5.4.1.4 CaCO ₃ templated (PAH/PSS) ₂ (PAH/-wax) ₂ capsules after heating	85
Figure 5.4.1.5 CaCO ₃ (PAH/PSS) ₂ (+wax022/PSS) ₂	85
Figure 5.4.2.1 FRAP curves of MF templated capsules	86
Figure 5.4.2.2 (PAH/PSS) ₄ MF templated capsule.....	87
Figure 5.4.2.3 (PAH/PSS) ₃ (PAH/-wax) (wax not heated) templated capsule	87
Figure 5.4.2.4 CLSM picture of heated MF templated capsules with wax	89
Figure 5.4.3.1 Capsule layer continent layout	90
Figure 5.4.3.2 Scheme of capsule fabrication with wax layer via method 2	90
Figure 5.4.3.3 Sample 2 (PAH/PSS) _{8.5bil}	91
Figure 5.4.3.4 Sample 2h (PAH/PSS) _{8.5bil} heated (60°C 1hr).....	91
Figure 5.4.3.5 Sample 3a (PAH/PSS) _{8.5bil} + (-wax) (before core dissolution).....	92

Figure 5.4.3.6 Sample 3ah (PAH/PSS) _{8.5bil} + (-wax) (before core dissolution) heated (60°C 1hr)	92
Figure 5.4.3.7 Sample 3b (PAH/PSS) _{8.5bil} + (-wax) (after core dissolution)	92
Figure 5.4.3.8 Sample 3bh (PAH/PSS) _{8.5bil} + (-wax) (after core dissolution) heated (60°C 1hr)	93
Figure 5.4.3.9 FRAP curves of PS templated capsules.....	94
Figure 5.4.3.10 Separated FRAP curves of PS templated capsules.....	94
Figure 5.4.3.11 Confocal image of Sample 3a and 3ah	95
Figure 5.4.3.12 Confocal image of Sample 3bh	95
Figure 5.4.3.13 PS (10µm core) (PSS/PAH) ₁₄ . (after core removal) (added -wax dissolved in acetone). Not heated	96

List of Equations

Equation 2.1.1 Henderson-Hasselbalch equation	3
Equation 2.7.1 Keesom interaction energy	10
Equation 2.7.2 Debye interaction energy.....	10
Equation 2.7.3 London dispersion interaction energy	10
Equation 2.7.4 Total Van der Waals interaction energy.....	10
Equation 2.7.5 Vans der Waals interaction energy in terms of the Hamacker constant.	11
Equation 2.7.6 Interaction energy attributed to the double layer force	11
Equation 3.1.1FRAP equation	21
Equation 3.1.2 linalized FRAP equation	22
Equation 3.2.1-2 Derivation of Raman equation	22
Equation 3.2.3-6 Derivation of Raman equation	23
Equation 3.2.7 Raman equation.....	23
Equation 3.3.1 Beer-Lambert Law.....	24
Equation 3.6.1 Smoluchowski equation.....	27
Equation 3.7.1 Definition of Δ	29
Equation 3.7.2 Definition of ψ	29
Equation 3.7.3 Fresnel equation.....	29
Equation 3.9.1 Definition of Q	31
Equation 5.3.1.1 CaCO ₃ crystallization reaction	83
Equation 5.3.2.1 Fraction of sealment	88

Nomenclature

APS	Ammonium Peroxodisulfate
AFM	Atomic Force Microscopy
bil	bilayer
CaCO ₃	Calcium Carbonate
CLSM	Confocal Laser Scanning Microscopy
DSC	Differential Scanning Calorimetry
FITC	Fluorescein isothiocyanate
FRAP	Fluorescence Recovery After Photobleaching
LbL	Layer-by-Layer
LCST	Lower Critical Solution Temperature
MF	Melamine Formaldehyde
MRho	Methacryloxyethyl thiocarbonyl rhodamine B
PAH	Poly (allylamine hydrochloride)
PNIPAM	Poly (N- isopropyl acrylamide)
PS	Polystyrene
PSS	Poly (styrene sulfonate)
SEM	Scanning Electron Microscope
SLD	Scattering Length Density
SFM	Scanning Force Microscopy
TEMDA	Tetramethylethylenediamine
THF	Tetrahydrofuran
UV/Vis	Ultraviolet/ Visible Spectroscopy

Chapter 1- General Introductions

"When we decode a cookbook, every one of us is a practicing chemist. Cooking is really the oldest, most basic application of physical and chemical forces to natural materials."

Arthur E. Grosser

Indeed, in our everyday life we encounter many aspects of physical and chemical forces. Cooking is an example, but the simple acts of washing our hands or taking medicine for a cold are, as well. In the case of washing our hands the soap we use decreases the surface tension of water, allowing the dust particles to dissolve into the water. Soap also acts as an amphiphile that will form micelles around the excess oil on our skin. And it is more than likely that when we take a tablet for a cold, it is the result of years of research on encapsulating the drug into a shell to protect it from the low pH of the stomach, but then letting it release in the intestines. Today many medicines are coated such that the release profile is very slow, in order to offer hours of relief from our ails.

This work will present two ways that can be used as possible delivery systems that will have a way to encapsulate an active molecule and then tune the release properties of the active species. The first method will discuss the incorporation of active molecules into polyelectrolyte multilayer capsules. This will be done using two encapsulation methods. The second approach to tune the release properties is by

controlling the permeability of the container itself. This will be done by introducing a material that, after heating, forms a layer that greatly reduces permeability. In this work both systems are responsive to stimuli, in this case, to heat. One system exhibits a reversible effect, and the other possesses an irreversible effect. The layout of the thesis is as follows.

Chapter 2 - Literature Survey and Theory will introduce the basics, from what a polyelectrolyte is to the principles of intermolecular interaction theory necessary to understand this work.

Chapter 3 - Method of Characterization and Materials will discuss the fundamentals of the most relevant methods of characterization used in this work. This chapter will also detail the experimental parameters of the instruments used.

Chapter 4 - Polyelectrolyte multilayers as an encapsulation vehicle will discuss the use of polyelectrolyte multilayer capsules used as containers to trap active molecules.

Chapter 5 - Polyelectrolyte multilayer permeability alteration with wax particles will discuss the use of hydrophobic species that, upon heating, form a barrier layer to alter the permeability of capsules.

Chapter 6 - General Conclusions will summarize the main findings of this work.

Chapter 2 - Literature Survey and Theory

2.1 Polyelectrolytes

An electrolyte is a substance which dissociates into free ions when dissolved, to produce an electrically conductive medium. A polyelectrolyte is a polymer in which the repeating unit possesses an electrolyte [1]. This means that when a powder of a polyelectrolyte is dissolved in an aqueous solution the electrolyte will disassociate, resulting in a charge on the polymer that is compensated by a counterion in solution. Examples of natural polyelectrolytes are DNA, polysaccharides and proteins.

A polyelectrolyte can be classified according its charge and whether it is a “strong” or “weak” polyelectrolyte. If after dissolving in an aqueous solution the resulting polyelectrolyte is positive, it is referred to as a polycation. Conversely, if the resulting polyelectrolyte is negative, it is referred to as a polyanion. In many cases a polyelectrolyte can and will completely disassociate within a normal pH range. These are referred to as “strong” polyelectrolytes. There are other polymers that only partially dissociate upon dissolution in an aqueous solution. These are referred to as “weak” polyelectrolytes. The dependence of the pH value on the dissociation constant is described by the Henderson-Hasselbalch equation [2] seen below.

$$pH = pK_a - \log \frac{[acid]}{[base]}$$

Equation 2.1.1 Henderson-Hasselbalch equation

Here the pK_a is the dissociation constant, [acid] is the molar concentration of acid, and [base] is the molar concentration of base. It is clearly understood that if the electrolyte on the polymer did not completely dissolve, the polyelectrolyte is not fully charged. The Henderson-Hasselbalch equation then is also a simple expression which determines at a given pH the percentage of the polyelectrolyte in the protonated, neutral or deprotonated form.

2.2 Complexes

It is well known that opposite charges attract. This is also the case of polyanions and polycations. When these two are mixed they bind and precipitate, forming a complex. The attractive force involved is Coulombic and the main driving force for this is the entropy gain when the counterions are released into solution. Since the attractive force is dependent on the ability to be attracted to an opposite charge, it is intuitive that the addition of an electrolyte or salt - that will dissolve into its respective ions which carry a charge - can affect this attractive force. Investigations on this effect were performed by Dautzenberg. He found that in the case of strong polyelectrolytes the addition of a low concentration of salt leads to a lower amount of aggregates. However, at higher concentrations, a secondary aggregation took place, which lead to the large aggregates to precipitate out of solution [3]. This can be explained by the DLVO theory, which will be discussed later in this chapter. When a complex consists of a weak polyelectrolyte and a strong polyelectrolyte, the addition of salt leads to a complete dissolution of the complex [4]. In the case of a weak polyelectrolyte the charge density changes depending on the pH. To investigate the effect of the charge density on complexes, a copolymer of strong polyelectrolyte and a neutral species were synthesized. This synthesis leads to a polyelectrolyte with a defined charge density that can be discretely varied. When combining a polyelectrolyte with a high charge density and a polyelectrolyte with a low charge density, a complex could be formed at non-stoichiometric conditions, whereas a with mixing ratio close to 1:1 only flocculation was observed. When a complex could be formed, it also dissolved upon the addition of salt [5].

2.3 Flat Films

Coulombic interactions do not only occur between polyelectrolytes. If a surface is also charged, an attractive force can be possible. When a charged surface is placed in a polyelectrolyte solution, the polyelectrolyte will adsorb onto the surface. If the adsorbing polyelectrolytes completely cover the surface, the charge of the system will now carry the charge of the polyelectrolyte. This is referred to as charge reversal. When this occurs the surface can be washed in water and then placed in a solution of another polyelectrolyte with a charge opposite to that of the first polyelectrolyte. In the presence of the second polyelectrolyte, it will adsorb on top of the first one. A difference between complexes and a surface is that this process can be repeated as many times as desired. This process is called layer-by-layer (LbL) assembly and leads to a multilayer film, with the first major work being reported by Decher et al [6,7]. The internal structure of the films has been investigated by neutron reflectivity. These investigations reveal that the structure is continuous, striated, and interdigitated [8,9]. When the film is comprised of a species that induces some water structuring, like a hydrophobic species, a more individual film could be realized [10]. Films comprising of as many as 200 layers have been reported [11]. Since the paper by Decher in 1992, the work done on LbL has largely increased due to its ease and versatility. To date, many substrates have been used, including glass, quartz, silicon wafers, mica, and gold surfaces. In addition to the many available substrates, many layer constituents have been realized, including polyelectrolytes, biopolymers, inorganic particles, and many others too numerous to list here. A list of used layer constituents is available in the following references [12,13,14].

Most multilayer films are built using electrostatic interaction between oppositely-charged polyelectrolytes; however, these are not the only interactions available when a multilayer film is wanted. Kotov stated that hydrophobic interaction arising from the carbon backbone of the polymer also plays a major role [15]. Other interactions that can be exploited to build multilayer films are hydrogen bonding [16,17] and specific interactions [18].

Multilayer films, like complexes, are also susceptible to environmental effects. These environmental effects include the presence and concentration of salt [19,20], the pH of films built from weak polyelectrolytes [21,22]. For this specific case of films produced on a surface that are dried, the humidity in the air can affect the thickness of the film [23]. Studies have also been done to calculate the content of water in films that are dried. Films measured at ambient conditions were found to contain 10-20% water, which could be removed upon excessive heating [24].

2.4 Capsules

The extension of LbL onto a spherical substrate has lately been a topic of great interest. If LbL is performed on a spherical sacrificial substrate, after the desired number of layer is deposited, the substrate can be removed, leaving a hollow shell. This is referred to as a capsule. Colloid spheres have been used to this effect. The colloidal spheres can be introduced into a polyelectrolyte solution and left for the polyelectrolyte to absorb on the surface. The colloidal particles can be removed from the polyelectrolyte solution by filtration [25,26,27] or by the now widely-used centrifugation method. As with the flat films, the substrates and layer constituents are vast. To date many cores have been employed, ranging from organic particles to inorganic crystals, including melamine formaldehyde (MF) [27,28,29], CaCO_3 [30,31,32], Polystyrene (PS) [29,33,34], SiO_2 [35], and MnCO_3 [36]. As with flat films, hydrogen bonding can also be used to build capsules [37].

Initially much work was done investigating the basic properties of the capsule membrane, including the thickness of the membrane wall, the pH [38], salt [39], and temperature sensitivity [40,41]. Other properties that have been investigated include their permeability and mechanical properties [42,43,44].

Lately, multilayered polyelectrolyte microcapsules have been of particular interest due to their possible use as microcontainers [31,45,46]. Proteins [32,47], enzymes [48], DNA, inorganic salts [49] and polymers can be encapsulated using various techniques. Such encapsulated polymers could also act as adsorbents for substrates or as substrates

themselves and could be used for chemical reactions inside the capsules that will thus be employed as microreactors or as a drug delivery system. Recently, they have been used for the synthesis of inorganic particles in a restricted volume [50]. Synthesized polymers were chosen depending on their stimuli-responsive properties [51]: metal complexants [52] for reversible complex formation in the presence of metal ions, acid or basic polymers for their pH-responsive properties [38], and thermo-responsive properties [53].

2.5 PNIPAM

Poly (N-isopropylacrylamide) is a polymer of much interest due to its novel reversible, thermo-sensitive property; the first major work was reported in 1968 by Heskins and Guillet [54]. Some of its thermodynamic properties in comparison to some of its neighbors like poly (acrylic acid) and poly (methacrylate) were also discussed [55]. It is a special polymer in that its solubility actually decreases when the temperature is increased. The Lower Critical Solution Temperature (LCST) is often discussed when characterizing the polymer [56], which is simply the temperature at which the polymer is no longer soluble. PNIPAM is a neutral polymer that at room temperature is water soluble through strong hydrogen bonding (see section 2.7). However, above 32°C the hydrogen bonding is disrupted and water no longer acts as a suitable solvent. At this temperature, PNIPAM undergoes a coil to globule transition where it preferentially makes hydrogen bonds with neighboring polymer chains. This collapse is caused by the disruption of the hydrogen bonding network between the amide bonds of the PNIPAM and water. As hydrogen bonds are affected by salt, the LCST of PNIPAM is influenced and can be tuned by salts. Some investigations to this effect have been performed [57,58]. The transition is displayed on a molecular level in Figure 2.5.1.

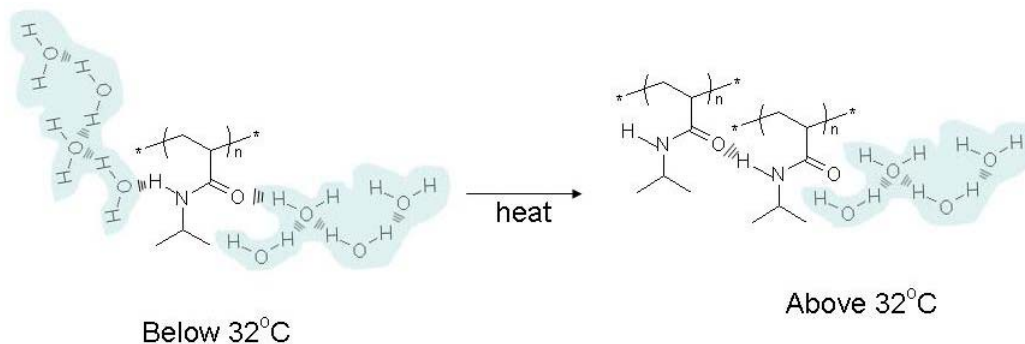


Figure 2.5.1 PNIPAM solubility above and below the Lower Critical Solution Temperature.

PNIPAM has been synthesized in many ways, resulting in many different architectures. Some polymerization methods employed include free radical polymerization [59], redox initiation in aqueous media, emulsion polymerization [60] and ionic polymerization. Some of the resulting architectures are linear, microgel particles [60,61] macrogel particles, micelles [59], and, when copolymerized with a charged species, flat films [62]. More details of PNIPAM synthesis and architectures are presented in an excellent review by Schild [63]. It has been shown that PNIPAM can act like a sponge, since in its swollen state it can absorb dyes [64] or metal ions, making it of interest in drug delivery or waste water treatment [60].

PNIPAM has been already investigated in conjunction with polyelectrolyte multilayers. Caruso et al found that multilayers consisting of PNIPAM could adsorb Rhodamine and upon heating release the absorbed dye [65] Sukhishvili et al formed capsules with PNIPAM as one of the layer constituents using hydrogen bonding. This system was thermo-responsive [66]. Glinel et al used block co-polymers, including PNIPAM, to construct capsules with the traditional electrostatic interaction. The capsule permeability was greatly reduced upon heating. In both of these systems, however, the PNIPAM did not exhibit full thermo-sensitive behavior, since the PNIPAM movement was seriously restricted [67].

2.6 Permeability control of LbL films

As seen in section 2.4 capsules are of great interest as a semi-permeable membrane [68] which is impermeable for large molecules, however, very permeable for small molecules. This is a result of the many pores created in the film during the core dissolution. In many drug delivery or controlled release applications this is not acceptable. Therefore recent investigations have focused on the permeability control of capsules. As many of the properties of capsules can be tuned by the layer constituents, there are many options for controlling the permeability. In the case of all capsules - regardless of the components employed - a thicker layer results in an overall lower permeability. In the case of capsules prepared with a weak polyelectrolyte one can alter the pH in order to change the permeability [69,34]. In the case of weak polyelectrolytes the charge density of the polyelectrolyte changes with the pH. In capsules formed in pH ranges in which the weak polyelectrolyte contained many charges, changing the pH to a range in which the chain is not as charged, will cause the chains that are still charged to repel, thus altering the permeability. Another option is to introduce enough flexibility or mobility to the multilayer constituents that they can rearrange, thereby sealing the pores [70]. Yet another way to control the permeability of the capsule is to simply add additional polyelectrolyte layers after the core has been removed to fill in the pores created during core removal [71]. The heating and even autoclaving of capsules has been of interest in recent investigations [40,41].

2.7 Intermolecular force Theory

In this work many interactions will be discussed. As shown from the literature survey it is clear that in order to understand the many interactions, some background information about these interactions is necessary. Three forces that lie between permanent and induced dipoles are singled out due to their r^6 dependence. They are Keesom forces, Debye forces, and London forces [72,73].

Van der Waals

Keesom forces, or orientation forces, occur between two freely rotating, permanent dipoles. This interaction between atoms or molecules is a function of r (the distance between the dipoles), the relative orientation of the dipole moments u_1 and u_2 , and the changes in the orientation due to thermal motion. The interaction is described with Equation 2.7.1

$$w_K(r) = -\frac{u_1^2 u_2^2}{3(4\pi\epsilon\epsilon_0)^2 kTr^6} = -\frac{C_K}{r^6}$$

Equation 2.7.1 Keesom interaction energy

where ϵ is the dielectric constant of the medium, ϵ_0 is the dielectric constant of vacuum, k is Boltzmann constant and T is the temperature.

Debye forces, or induction forces, are the force between a permanent dipole and an induced dipole. In the case of two different molecules possessing permanent dipole u_1 and u_2 and polarizabilities α_{o1} and α_{o2} , their net dipole-induced dipole interaction energy can be described with Equation 2.7.2.

$$w_D(r) = -\frac{u_1^2 \alpha_{o2} + u_2^2 \alpha_{o1}}{(4\pi\epsilon\epsilon_0)^2 r^6} = -\frac{C_D}{r^6}$$

Equation 2.7.2 Debye interaction energy

London forces, or dispersion forces, are the interaction between two non-polar species. They have an interaction energy described in Equation 2.7.3.

$$w_L(r) = -\frac{3\alpha_1\alpha_2(h\nu_1)(h\nu_2)}{2(4\pi\epsilon_0)^2 r^6 h\nu_1 + h\nu_2} = -\frac{C_L}{r^6}$$

Equation 2.7.3 London dispersion interaction energy

where $h\nu_1$ and $h\nu_2$ are the first ionization potentials of the molecules and h is the Planck constant.

These three equations are normally put together because they are always attractive and they all have an r^6 dependence. Combined, they are referred to as the Van der Waals force, which can be written as

$$w_{vdw}(r) = \frac{C_K + C_D + C_L}{r^6}$$

Equation 2.7.4 Total Van der Waals interaction energy

To calculate the interaction between two planes at distance D one has to integrate over all Van der Waals forces of points within these planes. This yields a D^{-2} dependence with interaction constants merging into a Hamaker constant A , according to.

$$w_{vdw}(D) = \frac{A}{12\pi D^2}$$

Equation 2.7.5 Vans der Waals interaction energy in terms of the Hamaker constant.

Double layer forces

Another class of forces that are repulsive in nature is the double layer force. This force arises when a surface with dissociable groups is placed in water. The charges that dissociate will be compensated by opposite charges in solution or adsorbed at the surface. The expression that describes the distribution near the interface is the Poisson-Boltzmann equation. The Poisson-Boltzmann equation requires that a non-linear second-order differential to be solved [74]. The distribution, σ , is affected by the concentration of salt in the solution. The Debye length, κ^{-1} , is the characteristic decay length of the double layer. Basically, it is the “thickness” of the double layer. The interaction energy of the electric double layer is seen in Equation 2.7.6.

$$w_{el}(D) = \frac{2\sigma^2}{\kappa\epsilon\epsilon_0} e^{-\kappa D}$$

Equation 2.7.6 Interaction energy attributed to the double layer force

The combination of the Van der Waals forces and the electric double layer force is known as the DLVO theory after Derjaguin, Landau, Verwey and Overbeek. The DLVO theory describes the total interaction energy between two surfaces as a function of distance. From Equations 2.7.5 and 2.7.6 it can be seen that at long ranges and extremely short distances the Van der Waals contribution to the total potential is dominant. However, in the intermediate D , the electric double layer forces are dominant. For many years the DLVO theory has been the solid foundation which one uses to describe the interaction between two surfaces. But at very, very close range, the DLVO no longer completely describes all the effects seen between two interacting bodies. These forces are referred to as non-DLVO forces.

Non-DLVO Forces

At distances that are within a few nanometers from a surface the DLVO theory fails to describe all the interactions that occur. These forces, not described by the DLVO theory, can be attractive, repulsive or oscillatory in nature and are known as steric forces, hydration forces, solvation forces, and hydrophobic forces. Steric forces normally refer to the case at small distances that the Stern layer (see section 3.6) overlaps. The solvation (or structuring) of solvent molecules at a surface is determined primarily by the geometry of molecules and their arrangement around a constraining boundary. It is also important to appreciate that solvation forces do not arise simply because liquid molecules tend to arrange in semi-ordered layers at surfaces. They result from the disruption or change of this ordering during the approach of a second surface. If there were no change, there would be no solvation force. Solvation forces depend not only on the properties of the intervening medium but also on the chemical and physical properties of the surfaces. The short-distance interactions are usually referred to as solvation forces, structural forces, or – when the medium is water – hydration forces. Hydrophobic forces arise from species that are inert to water or cannot bind to water. The case where a hydrophobic species is in an aqueous environment is an entropically unfavorable one. Therefore the hydrophobic species are drawn together to reduce the surface to water.

Hydrogen bonding

Finally, a force that cannot be explained by the DLVO theory or by the non-DLVO forces is hydrogen bonding. It is a special case of attractive directional dipole-dipole interactions that is of extreme importance for this work. Hydrogen bonding takes its name from the fact that it always involves a hydrogen atom. In particular, if hydrogen is bonded to an electronegative atom, the electron will spend more time around the electronegative atom, leaving a partial positive charge on the hydrogen and a partial negative charge on the electronegative atom. Species that take the role of the electronegative atom are known as hydrogen bonding donors, and examples of good hydrogen bonding donors are oxygen, nitrogen, and fluorine. Hydrogen bonding is useful in nature because of its directional dependence as well as its semi-strong nature. It has strength from 10-40kJ/mole. This is in comparison to Van der Waals forces which have a

bond strength $\sim 1\text{kJ/mol}$ and covalent bonds whose strength is 500kJ/mol . It is important because it is an interaction that is strong but not so strong that it is unbreakable. Water is a special case of an associated liquid, or liquids that displays hydrogen bonds, since it has two hydrogens and one oxygen. The oxygen of one water atom has two lone pairs of electrons, each of which can form a bond with hydrogens on two other water molecules. This can repeat, so that every water molecule is H-bonded with four other water molecules. It forms a structure in bulk that can be seen below.

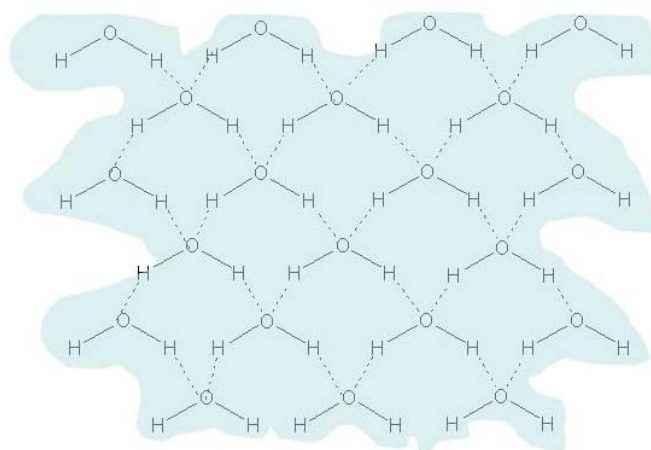


Figure 2.7.1 Hydrogen bonding in bulk water

References

- 1 Hara, M.; Editor, *Polyelectrolytes: Science and Technology*. ed.; 1993; 'Vol.' p 399 pp.
- 2 Atkins, P.; de Paula, J., *Atkins' Physical Chemistry, 7th Edition*. ed.; 2002; 'Vol.' p 1149 pp.
- 3 Dautzenberg, H., Polyelectrolyte Complex Formation in Highly Aggregating Systems. 1. Effect of Salt: Polyelectrolyte Complex Formation in the Presence of NaCl. *Macromolecules* **1997**, 30, (25), 7810-7815.
- 4 Dautzenberg, H.; Karibyants, N., Polyelectrolyte complex formation in highly aggregating systems. Effect of salt: response to subsequent addition of NaCl. *Macromolecular Chemistry and Physics* **1999**, 200, (1), 118-125.
- 5 Dautzenberg, H.; Jaeger, W., Effect of charge density on the formation and salt stability of polyelectrolyte complexes. *Macromolecular Chemistry and Physics* **2002**, 203, (14), 2095-2102.

- 6 Decher, G.; Hong, J. D.; Schmitt, J., Buildup of Ultrathin Multilayer Films by a Self-Assembly Process.3. Consecutively Alternating Adsorption of Anionic and Cationic Polyelectrolytes on Charged Surfaces. *Thin Solid Films* **1992**, 210, (1-2), 831-835.
- 7 Decher, G., Fuzzy nanoassemblies: Toward layered polymeric multicomposites. *Science* **1997**, 277, (5330), 1232-1237.
- 8 Schmitt, J.; Grunewald, T.; Decher, G.; Pershan, P. S.; Kjaer, K.; Losche, M., Internal Structure of Layer-by-Layer Adsorbed Polyelectrolyte Films - a Neutron and X-Ray Reflectivity Study. *Macromolecules* **1993**, 26, (25), 7058-7063.
- 9 Losche, M.; Schmitt, J.; Decher, G.; Bouwman, W. G.; Kjaer, K., Detailed structure of molecularly thin polyelectrolyte multilayer films on solid substrates as revealed by neutron reflectometry. *Ibid.***1998**, 31, 8893-8906.
- 10 Arys, X.; Fischer, P.; Jonas, A. M.; Koetse, M. M.; Laschewsky, A.; Legras, R.; Wischerhoff, E., Ordered polyelectrolyte multilayers. Rules governing layering in organic binary multilayers. *Journal of the American Chemical Society* **2003**, 125, (7), 1859-1865.
- 11 Zhai, L.; Cebeci, F. C.; Cohen, R. E.; Rubner, M. F., Stable Superhydrophobic Coatings from Polyelectrolyte Multilayers. *Nano Letters* **2004**, 4, (7), 1349-1353.
- 12 Arys, X.; Jonas, A. M.; Laschewsky, A.; Legras, R., Supramolecular polyelectrolyte assemblies. *Supramolecular Polymers* **2000**, 505-563.
- 13 Bertrand, P.; Jonas, A.; Laschewsky, A.; Legras, R., Ultrathin polymer coatings by complexation of polyelectrolytes at interfaces: suitable materials, structure and properties. *Macromolecular Rapid Communications* **2000**, 21, (7), 319-348.
- 14 Decher, G., Polyelectrolyte Multilayers, an overview. In *Multilayer Thin Films*, ed.; Decher, G.; Schlenoff, J. B., 'Ed.'^'Eds.' Wiley-VCH: **2003**; 'Vol.' p^pp 1-46.
- 15 Kotov, N. A., Layer-by-layer self-assembly: The contribution of hydrophobic interactions. *Nanostructured Materials* **1999**, 12, (5-8), 789-796.
- 16 Sukhishvili, S. A.; Granick, S., Layered, erasable, ultrathin polymer films. *Journal of the American Chemical Society* **2000**, 122, (39), 9550-9551.
- 17 Sukhishvili, S. A.; Granick, S., Layered, erasable polymer multilayers formed by hydrogen-bonded sequential self-assembly. *Macromolecules* **2002**, 35, (1), 301-310.
- 18 Hong, J. D.; Lowack, K.; Schmitt, J.; Decher, G., Layer-by-layer deposited multilayer assemblies of polyelectrolytes and proteins: From ultrathin films to protein arrays. *Progress in Colloid & Polymer Science* 1993, 93, (TRENDS IN COLLOID AN), 98-102.
- 19 Decher, G.; Schmitt, J., Fine-tuning of the film thickness of ultrathin multilayer films composed of consecutively alternating layers of anionic and cationic polyelectrolytes. *Progress in Colloid & Polymer Science* **1992**, 89, (Trends Colloid Interface Sci. VI), 160-4.
- 20 Ferreira, M.; Rubner, M. F., Molecular-Level Processing Of Conjugated Polymers.1. Layer-By-Layer Manipulation Of Conjugated Polyions. **1995**, 28, (21), 7107-7114.

- 21 Mendelsohn, J. D.; Barrett, C. J.; Chan, V. V.; Pal, A. J.; Mayes, A. M.; Rubner, M. F., Fabrication of microporous thin films from polyelectrolyte multilayers. *Langmuir* **2000**, 16, (11), 5017-5023.
- 22 Dubas, S. T.; Schlenoff, J. B., Polyelectrolyte multilayers containing a weak polyacid: Construction and deconstruction. *Macromolecules* **2001**, 34, (11), 3736-3740.
- 23 Kugler, R.; Schmitt, J.; Knoll, W., The swelling behavior of polyelectrolyte multilayers in air of different relative humidity and in water. *Macromolecular Chemistry and Physics* **2002**, 203, (2), 413-419.
- 24 Farhat, T.; Yassin, G.; Dubas, S. T.; Schlenoff, J. B., Water and ion pairing in polyelectrolyte multilayers. *Langmuir* **1999**, 15, (20), 6621-6623.
- 25 Turkenburg, D. H.; Antipov, A. A.; Thathagar, M. B.; Rothenberg, G.; Sukhorukov, G. B.; Eiser, E., Palladium nanoclusters in microcapsule membranes: From synthetic shells to synthetic cells. *Physical Chemistry Chemical Physics* **2005**, 7, (10), 2237-2240.
- 26 Petrov, A. I.; Antipov, A. A.; Sukhorukov, G. B., Base-acid equilibria in polyelectrolyte systems: From weak polyelectrolytes to interpolyelectrolyte complexes and multilayered polyelectrolyte shells. *Macromolecules* **2003**, 36, (26), 10079-10086.
- 27 Radtchenko, I. L.; Sukhorukov, G. B.; Möhwald, H., Incorporation of macromolecules into polyelectrolyte micro- and nanocapsules via surface controlled precipitation on colloidal particles. *Colloids and Surfaces a-Physicochemical and Engineering Aspects* **2002**, 202, (2-3), 127-133.
- 28 Gao, C.; Moya, S.; Lichtenfeld, H.; Casoli, A.; Fiedler, H.; Donath, E.; Möhwald, H., The decomposition process of melamine formaldehyde cores: the key step in the fabrication of ultrathin polyelectrolyte multilayer capsules. *Macromolecular Materials and Engineering* **2001**, 286, (6), 355-361.
- 29 Antipov, A. A.; Sukhorukov, G. B.; Fedutik, Y. A.; Hartmann, J.; Giersig, M.; Möhwald, H., Fabrication of a novel type of metallized colloids and hollow capsules. *Langmuir* **2002**, 18, (17), 6687-6693.
- 30 Antipov, A.; Shchukin, D.; Fedutik, Y.; Zhanaveskina, I.; Klechkovskaya, V.; Sukhorukov, G.; Möhwald, H., Urease-catalyzed carbonate precipitation inside the restricted volume of polyelectrolyte capsules. *Macromolecular Rapid Communications* **2003**, 24, (3), 274-277.
- 31 Volodkin, D. V.; Petrov, A. I.; Prevot, M.; Sukhorukov, G. B., Matrix polyelectrolyte microcapsules: New system for macromolecule encapsulation. *Langmuir* **2004**, 20, (8), 3398-3406.
- 32 Shenoy, D. B.; Sukhorukov, G. B., Microgel-based engineered nanostructures and their applicability with template-directed layer-by-layer polyelectrolyte assembly in protein encapsulation. *Macromolecular Bioscience* **2005**, 5, (5), 451-458.
- 33 Fang, M.; Grant, P. S.; McShane, M. J.; Sukhorukov, G. B.; Golub, V. O.; Lvov, Y. M., Magnetic bio/nanoreactor with multilayer shells of glucose oxidase and inorganic nanoparticles. *Langmuir* **2002**, 18, (16), 6338-6344.
- 34 Déjугnat, C.; Sukhorukov, G. B., pH-Responsive Properties of Hollow Polyelectrolyte Microcapsules Templated on Various Cores. *Ibid.* **2004**, 20, (17), 7265-7269.

- 35 Köhler, K.; Shchukin, D. G.; Möhwald H.; Sukhorukov, G. B., Thermal Behavior of Polyelectrolyte Multilayer Microcapsules. 1. The Effect of Odd and Even Layer Number. *Journal of Physical Chemistry B* **2005**, 109, (39), 18250-18259.
- 36 Antipov, A. A.; Shchukin, D.; Fedutik, Y.; Petrov, A. I.; Sukhorukov, G. B.; Möhwald, H., Carbonate microparticles for hollow polyelectrolyte capsules fabrication. *Colloids and Surfaces a-Physicochemical and Engineering Aspects* **2003**, 224, (1-3), 175-183.
- 37 Kozlovskaya, V.; Ok, S.; Sousa, A.; Libera, M.; Sukhishvili, S. A., Hydrogen-bonded polymer capsules formed by layer-by-layer self-assembly. *Macromolecules* **2003**, 36, (23), 8590-8592.
- 38 Mauser, T.; Déjugnat, C.; Sukhorukov, G. B., Reversible pH-dependent properties of multilayer microcapsules made of weak polyelectrolytes. *Macromolecular Rapid Communications* **2004**, 25, (20), 1781-1785.
- 39 Antipov, A. A.; Sukhorukov, G. B.; Möhwald, H., Influence of the ionic strength on the polyelectrolyte multilayers' permeability. *Langmuir* **2003**, 19, (6), 2444-2448.
- 40 Köhler, K.; Shchukin, D. G.; Sukhorukov, G. B.; Möhwald, H., Drastic Morphological Modification of Polyelectrolyte Microcapsules Induced by High Temperature. *Macromolecules* **2004**, 37, (25), 9546-9550.
- 41 Köhler, K.; Shchukin, D. G.; Möhwald, H.; Sukhorukov, G. B., Thermal Behavior of Polyelectrolyte Multilayer Microcapsules. 1. The Effect of Odd and Even Layer Number. *Journal of Physical Chemistry B* **2005**, 109, (39), 18250-18259.
- 42 Prevot, M.; Cordeiro, A. L.; Sukhorukov, G. B.; Lvov, Y.; Besser, R. S.; Möhwald, H., Design of a microfluidic system to investigate the mechanical properties of layer-by-layer fabricated capsules. *Macromolecular Materials and Engineering* **2003**, 288, (12), 915-919.
- 43 Gao, C. Y.; Leporatti, S.; Moya, S.; Donath, E.; Möhwald, H., Stability and mechanical properties of polyelectrolyte capsules obtained by stepwise assembly of poly(styrenesulfonate sodium salt) and poly(diallyldimethyl ammonium) chloride onto melamine resin particles. *Langmuir* **2001**, 17, (11), 3491-3495.
- 44 Müller, R.; Köhler, K.; Weinkamer, R.; Sukhorukov, G.; Fery, A., Melting of PDADMAC/PSS Capsules Investigated with AFM Force Spectroscopy. *Macromolecules* **2005**, 38, (23), 9766-9771.
- 45 Déjugnat, C.; Halozan, D.; Sukhorukov, G. B., Defined picogram dose inclusion and release of macromolecules using polyelectrolyte microcapsules. *Macromolecular Rapid Communications* **2005**, 26, (12), 961-967.
- 46 Ibarz, G.; Dähne, L.; Donath, E.; Möhwald, H., Smart micro- and nanocontainers for storage, transport, and release. *Advanced Materials* **2001**, 13, (17), 1324-1327.
- 47 Petrov, A. I.; Volodkin, D. V.; Sukhorukov, G. B., Protein-calcium carbonate coprecipitation: A tool for protein encapsulation. *Biotechnology Progress* **2005**, 21, (3), 918-925.
- 48 Tiourina, O. P.; Antipov, A. A.; Sukhorukov, G. B.; Larionova, N. I.; Lvov, Y.; Möhwald, H., Entrapment of α -chymotrypsin into hollow polyelectrolyte microcapsules. *Macromolecular Bioscience* **2001**, 1, (5), 209-214.

- 49 Sukhorukov, G. B.; Susha, A. S.; Davis, S.; Leporatti, S.; Donath, E.; Hartmann, J.; Möhwald, H., Precipitation of inorganic salts inside hollow micrometer-sized polyelectrolyte shells. *Journal of Colloid and Interface Science* **2002**, 247, (1), 251-254.
- 50 Dähne, L.; Leporatti, S.; Donath, E.; Möhwald, H., Fabrication of micro reaction cages with tailored properties. *Journal of the American Chemical Society* **2001**, 123, (23), 5431-5436.
- 51 Sukhishvili, S. A., Responsive polymer films and capsules via layer-by-layer assembly. *Current Opinion in Colloid & Interface Science* **2005**, 10, (1,2), 37-44.
- 52 Shchukin, D. G.; Radtchenko, I. L.; Sukhorukov, G. B., Micron-scale hollow polyelectrolyte capsules with nanosized magnetic Fe₃O₄ inside. *Materials Letters* **2003**, 57, (11), 1743-1747.
- 53 Kohler, K.; Shchukin, D. G.; Sukhorukov, G. B.; Möhwald, H., Drastic morphological modification of polyelectrolyte microcapsules induced by high temperature. *Macromolecules* **2004**, 37, (25), 9546-9550.
- 54 Heskins, M.; Guillet, J. E., Solution properties of poly(N-isopropylacrylamide). *Journal of Macromolecular Science, Chemistry* **1968**, 2, (8), 1441-55.
- 55 Eliassaf, J., Aqueous solutions of poly(N-isopropylacrylamide). *Journal of Applied Polymer Science* **1978**, 22, (3), 873-4.
- 56 Schild, H. G.; Tirrell, D. A., Microcalorimetric detection of lower critical solution temperatures in aqueous polymer solutions. *Journal of Physical Chemistry* **1990**, 94, (10), 4352-6.
- 57 Freitag, R.; Garret-Flaudy, F., Salt effects on the thermoprecipitation of poly-(N-isopropylacrylamide) oligomers from aqueous solution. *Langmuir* **2002**, 18, (9), 3434-3440.
- 58 Rasmusson, M.; Routh, A.; Vincent, B., Flocculation of Microgel Particles with Sodium Chloride and Sodium Polystyrene Sulfonate as a Function of Temperature. *Ibid.* **2004**, 20, 3536-3542.
- 59 Zhang, J. X.; Qiu, L. Y.; Zhu, K. J.; Jin, Y., Thermosensitive micelles self-assembled by novel N-isopropylacrylamide oligomer grafted polyphosphazene. *Macromolecular Rapid Communications* **2004**, 25, (17), 1563-1567.
- 60 Saunders, B. R.; Crowther, H. M.; Morris, G. E.; Mears, S. J.; Cosgrove, T.; Vincent, B., Factors affecting the swelling of poly(N-isopropylacrylamide) microgel particles: fundamental and commercial implications. *Colloids and Surfaces, A: Physicochemical and Engineering Aspects* **1999**, 149, (1-3), 57-64.
- 61 Pelton, R., Temperature-sensitive aqueous microgels. *Advances in Colloid and Interface Science* **2000**, 85, (1), 1-33.
- 62 Jaber, J. A.; Schlenoff, J. B., Polyelectrolyte Multilayers with Reversible Thermal Responsivity. *Macromolecules* **2005**, 38, (4), 1300-1306.
- 63 Schild, H. G., Poly (N-Isopropylacrylamide) - Experiment, Theory and Application. *Progress in Polymer Science* **1992**, 17, (2), 163-249.

- 64 Sershen, S. R.; Westcott, S. L.; Halas, N. J.; West, J. L., Temperature-sensitive polymer-nanoshell composites for photothermally modulated drug delivery. *Journal of Biomedical Materials Research* **2000**, 51, (3), 293-298.
- 65 Quinn, J. F.; Caruso, F., Thermoresponsive nanoassemblies: Layer-by-layer assembly of hydrophilic-hydrophobic alternating copolymers. *Macromolecules* **2005**, 38, (8), 3414-3419.
- 66 Kozlovskaya, V.; Ok, S.; Sousa, A.; Libera, M.; Sukhishvili, S. A., Hydrogen-bonded polymer capsules formed by layer-by-layer self-assembly. *Macromolecules* **2003**, 36, (23), 8590-8592.
- 67 Glinel, K.; Sukhorukov, G. B.; Möhwald, H.; Khrenov, V.; Tauer, K., Thermosensitive hollow capsules based on thermoresponsive polyelectrolytes. *Macromolecular Chemistry and Physics* **2003**, 204, (14), 1784-1790.
- 68 Hammond, P. T., Form and function in multilayer assembly: New applications at the nanoscale. *Advanced Materials* **2004**, 16, (15), 1271-1293.
- 69 Antipov, A. A.; Sukhorukov, G. B.; Leporatti, S.; Radtchenko, I. L.; Donath, E.; Möhwald, H., Polyelectrolyte multilayer capsule permeability control. *Colloids and Surfaces a-Physicochemical and Engineering Aspects* **2002**, 198, 535-541.
- 70 Ibarz, G.; Dähne, L.; Donath, E.; Möhwald, H., Controlled permeability of polyelectrolyte capsules via defined annealing. *Chemistry of Materials* **2002**, 14, (10), 4059-4062.
- 71 Ibarz, G.; Dähne, L.; Donath, E.; Möhwald, H., Resealing of polyelectrolyte capsules after core removal. *Macromolecular Rapid Communications* **2002**, 23, (8), 474-478.
- 72 Israelachvili, J. N., Intermolecular and surface forces. ed.; Academic Press: London, **1992**; 'Vol.' p.
- 73 Butt, H. J.; Graf, K.; Kappl, M., *Physics and Chemistry of Interfaces*. ed.; **2003**; 'Vol.' p 350 pp.
- 74 Bosio, V. Interactions of multilayer coated surfaces studied by colloidal probe Atomic Force Microscopy. Universität Potsdam, Potsdam, **2003**.

Chapter 3 - Method of Characterization and Materials

As can be seen from Chapter 2, the fabrication of multilayer systems is versatile and easy. The resulting structure, however, is small and quite complex. To gain insight or specific knowledge of the system various techniques are needed. The techniques used to analyze the systems discussed in the work are a mixture of microscopy, spectroscopy, and reflectivity methods. Some methods give surface and morphology information, while other methods allow a look inside the system. Combining the knowledge gained from all the measurements with one another gives a better understanding of the whole system. The principles and layout of the methods used in this work are described in this chapter.

3.1 Confocal Laser Scanning Microscopy (CLSM)

Confocal Microscopy is a method that is widely used in many fields for obtaining high-resolution images, 3-D reconstructions, or for obtaining images in-situ, meaning in solution. The main advantage of confocal microscopy over other microscopy methods is the ability to produce blur-free images of thick specimens and various but defined levels [1,2].

The Confocal Laser Scanning Microscope works by pointwise illumination and pointwise detection, which, coupled with a deflection mechanism (the static beam),

becomes a scanning beam. To achieve this light is emitted from a laser that after passing through the illuminating pinhole is deflected by a dichroic mirror, or beam splitter. After the light passes the beam splitter it expands to fill the pupil of the objective lens. The objective lens then focuses the light onto the sample. After the light hits and is reflected from the sample, it is focused again by the objective lens and then passes through the beam splitter. Once the light passes the beam splitter it is transmitted or rejected by the detector pinhole. After passing the detector pinhole the light is detected by a photomultiplier tube (PMT). The confocal principle comes from the fact that light that comes from the focal plane will come into focus just as it comes to the pinhole. Light that comes from below the focal plane will come into focus before the pinhole and continue diverging until it is rejected by the pinhole. Conversely, light originating from above the focal plane would come into focus only after the pinhole; therefore it is rejected by the pinhole. The PMT converts the light signal into a digital signal that is recorded by a computer as an intensity which becomes a pixel of a picture. After scanning in the x-y direction, a full picture is reconstructed by the computer. It is also possible to move the stage in the z direction with a computer-controlled fine-stepping method. It is also possible to make 3-D pictures of the specimen by taking successive 2-D x-y scans and assembling them.

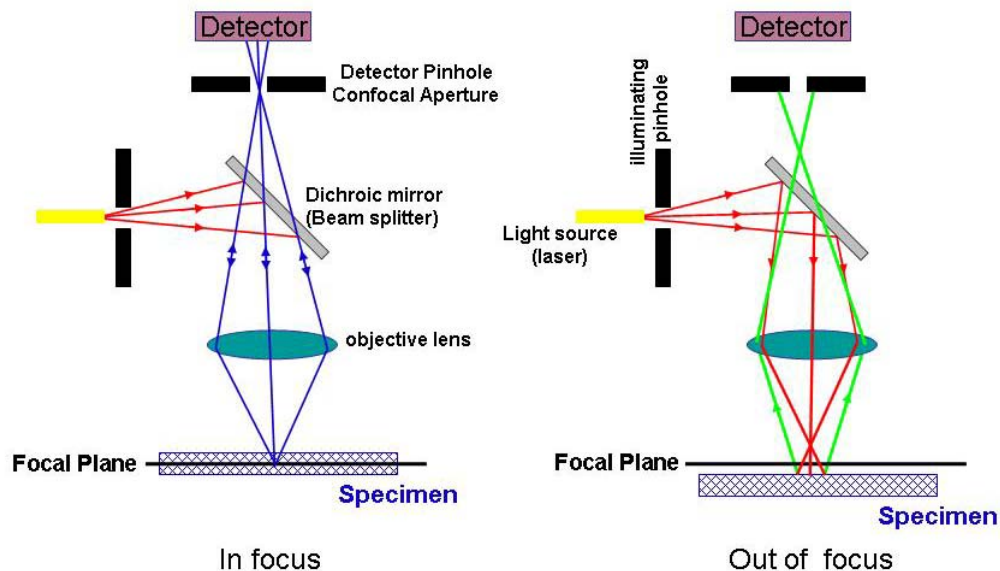


Figure 3.1.1: Principle of Confocal Microscopy

One exploitation of the confocal technique is the ability to investigate the cross section of samples while in situ. In the case of microcapsules one can carry out experiments and investigate phenomena exclusively inside the capsule wall. One investigation that can be done with Confocal Microscopy which is of particular interest is “Fluorescence Recovery After Photobleaching”, also referred to as FRAP. An image of the process is shown in Figure 3.1.2. FRAP is used to determine the permeability of a membrane. To achieve this, a fluorescent species is introduced into the suspension of the material to be investigated. The laser is then focused on the inside of the capsule wall. The wavelength of light that the dye absorbs is used to illuminate the region of interest at high intensity. The high intensity laser light destroys the dye molecules so that they no longer fluoresce. This is referred to as bleaching. At this point the interior of the capsule is dark. Then the intensity of the fluorescence will increase, since the bleached dye is diffusing out and fluorescing molecules diffuse into the capsule. This is referred to as recovery.

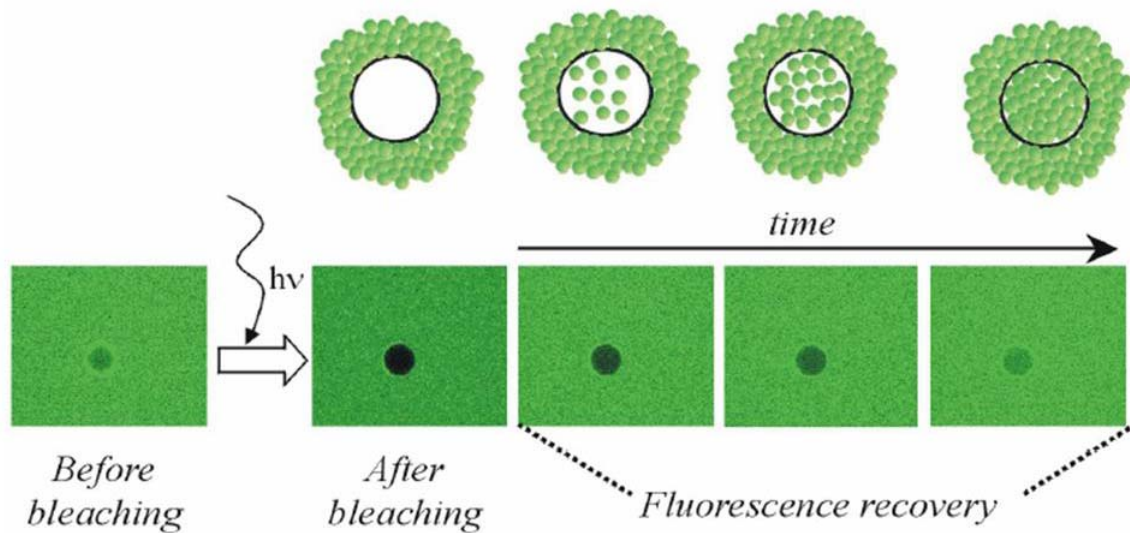


Figure 3.1.2 Principles of Fluorescent Recovery After Photobleaching [3].

From reference [3] we know.

$$\frac{I_{(t)} - I_s}{I_o - I_s} = e^{\frac{-3Pt}{r}}$$

Equation 3.1.1

If one knows the initial intensity I_o , the radius of the capsule r , the intensity when the intensity has recovered I_s , and the intensity at time t , $I_{(t)}$ one can calculate the permeability, P_o . The linearized form of equation 3.1.2 is

$$\ln(I_{(t)} - I_s) = -\frac{3P}{r}t + \ln(I_o - I_s)$$

Equation 3.1.2

3.2 Raman Spectroscopy

Raman confocal microscopy is a method based on the Raman effect that was first predicted by Adolf Gustav Smekal (1923) and then theoretically described by Heisenberg (1925), Schrödinger (1926) and Dirac (1927). In 1928 a physicist named Chandrasekhara Venkata Raman first experimentally proved that the wavelength of a small amount of radiation scattered from a molecule differs from the incident wavelength [4,5]. For this he received the Nobel Prize in 1931, and this technique now carries his name.

To understand the Raman effect one must take into consideration that when the beam with frequency ν_{ex} is incident upon a sample, the resulting electric field can be described as

$$E = E_o \cos(2\pi\nu_{ex}t) \tag{3.2.1}$$

where E_o is the amplitude of the wave. When this electric field interacts with the electron cloud of the sample, it induces a dipole moment, μ , of the bond defined as αE , where α is the polarizability of the bond. Substituted into equation 3.2.1 one obtains

$$\mu = \alpha E = \alpha E_o \cos(2\pi\nu_{ex}t) \tag{3.2.2}$$

Assuming that α depends linearly on the distance between the nuclei of the bond this can be described as

$$\alpha = \alpha_o + (r - r_{eq}) \left(\frac{\partial \alpha}{\partial r} \right)$$

3.2.3

where r and r_{eq} are the instantaneous and equilibrium distances, respectively. The change in the distances fluctuates with the frequency ν_v according to the equation

$$r - r_{eq} = r_m \cos(2\pi\nu_v t)$$

3.2.4

where r_m is the maximum distance between the nuclei relative to their equilibrium position. If equation 3.2.4 is substituted into equation 3.2.3 the following is obtained.

$$\alpha = \alpha_o + \left(\frac{\partial \alpha}{\partial r} \right) r_m \cos(2\pi\nu_v t)$$

3.2.5

Now if equation 3.2.5 is inserted into equation 3.2.2 the induced dipole moment of the bond can be described as

$$\mu = \alpha_o E_o \cos(2\pi\nu_{ex} t) + E_o r_m \left(\frac{\partial \alpha}{\partial r} \right) \cos(2\pi\nu_v t) \cos(2\pi\nu_{ex} t)$$

3.2.6

Now knowing that $\cos(x) \cos(y) = [\cos(x+y) + \cos(x-y)]$ equation 3.2.7 is obtained

$$\mu = \alpha_o E_o \cos(2\pi\nu_{ex} t) + \frac{E_o}{2} r_m \left(\frac{\partial \alpha}{\partial r} \right) \cos[2\pi(\nu_{ex} - \nu_v)t] + \frac{E_o}{2} r_m \left(\frac{\partial \alpha}{\partial r} \right) \cos[2\pi(\nu_{ex} + \nu_v)t]$$

3.2.7

where the first, second and third terms are referred to Rayleigh scattering, Stokes and Anti-Stokes respectively. From this derivation to describe the Raman effect one sees that it is dependant on and measures the change in the polarizability of a molecule as a function of distance [6,7].

In a typical Raman experiment a monochromatic light source is introduced into a diffraction-limited spot on the sample. Upon interacting with the sample, the monochromatic light is scattered into the three Rayleigh, Stokes and Anti-Stokes forms. Most of the light is elastically scattered, which means that there is virtually no loss in energy (Rayleigh scattering). Only 1 in 10^6 to 10^7 photons created from the scattering event are inelastically scattered or meaning an energy change in the beam. Energy loss $(\nu_{ex} - \nu_v)$ corresponds to the Stokes shift and $(\nu_{ex} + \nu_v)$ energy gain corresponds to the Anti-Stokes shift. As most of the photons are unchanged before the light continues on

towards the detector, there is first a holographic filter which removes the Rayleigh scattered light. The light continues through a “multi-mode” fiber until it reaches the detector. The “multi-mode” fiber also serves as a pinhole introducing the confocal capability of the instrument. Since Anti-Stokes scattering occurs from vibronically excited states and these are much less populated than the ground state, the Stokes lines are more intense and are therefore used in this work.

3.3 UV/VIS Spectroscopy

UV/Vis Spectroscopy is a class of spectroscopy that measures the absorbance of a substance in the UV/Vis range. The absorbance is defined as the log of the intensity of the incoming light I_0 , divided by the intensity of the light after passing through the sample, I . The concentration, c of the substance and the pathlength, l through the sample and the molar extinction coefficient ϵ are related by the Beer-Lambert law.

$$A = \log_{10} \frac{I_0}{I} = cl\epsilon$$

Equation 3.3.1 Beer-Lambert Law

If one knows the molar extinction coefficient of a substance one can measure the absorbance, A to calculate the concentration of the sample [8,7].

3.4 Scanning Electron Microscopy

Scanning Electron Microscopy is an important method for capsule analysis. It gives not only an overall view of the capsules but also provides a view of the structure and morphology of the capsule wall.

The principle of SEM is that electrons are formed with a gun by heating and exciting the filament; in this case a LaB_6 , the cathode, and then are accelerated toward an

anode. Once electrons are formed they are conducted down the column, where they are focused with condenser lenses (electromagnet coils) into a fine spot. At this point the electrons go through an objective lens where they are deflected with scanning coils to raster the electrons over the sample. During the beam interaction with the samples many scattering events occur, creating many types of electrons classified by their energy. After inelastic scattering by the sample, the secondary electrons are collected by the secondary electron detector. The secondary electrons come from within a nanometer from the surface, giving special information about the surface. These collected electrons are used to modulate the intensity of a CRT that is rastered in conjunction with the raster-scanned primary beam [7,9,10].

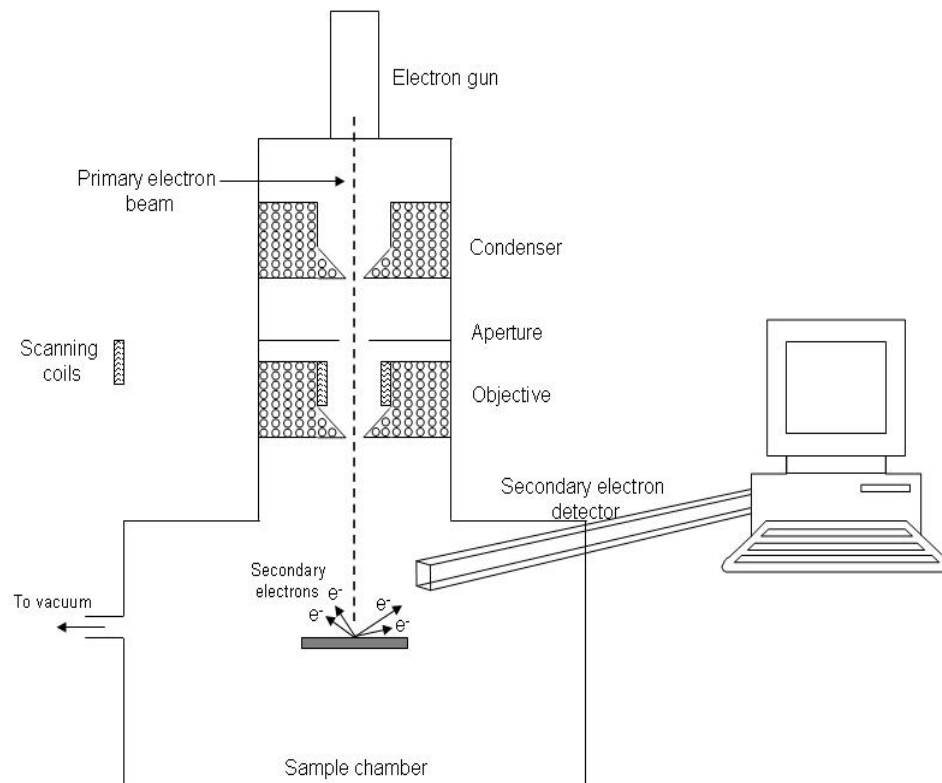


Figure 3.4.1 Layout of a typical SEM

3.5 Scanning Force Microscopy

Scanning Force Microscopy (SFM) also known as Atomic Force Microscopy (AFM) is a method invented in 1986 by Binnig, Quate, and Gerber [7,11,12]. AFM is of interest for this work because it is a non-destructive method that provides a 3-D surface profile of a sample, and can be utilized in many environments, i.e. vacuum, air, and liquid. As can be seen in Figure 3.5.1, an AFM consists of a sharp tip attached to a cantilever. The deflection of a flexible cantilever is measured by the “beam-bounce” method. In this method light from a laser source is illuminated on the backside of the cantilever which then after reflection from a mirror passes to a position-sensitive detector. The detector consists of four closely set photodiodes. When the cantilever is in a normal position it reflects the light to the middle of the detector. The AFM has many advantages over SEM, including the fact that it can supply an exact thickness value, and the fact that it does not destroy the sample. There are also disadvantages, however, including the fact that AFM is slower and can measure only a limited area. In contrast, SEM can measure large areas quickly, but the sputtering process inhibits the measurement of the sample with other techniques.

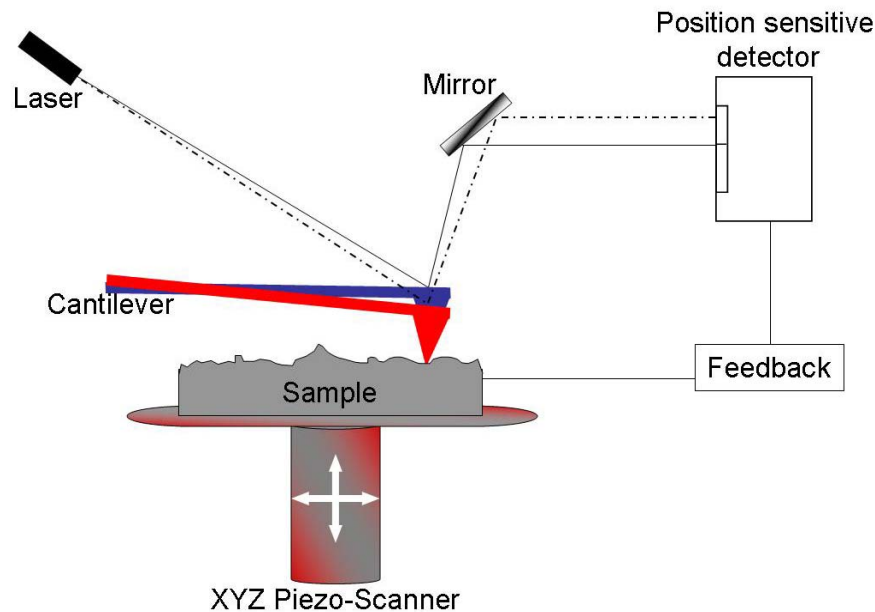


Figure 3.5.1 Principle of AFM

3.6 Zeta Potential Measurement

Zeta Potential Measurement is a method widely used to determine the charge of a surface, and size of a particle [10,13].

This technique measures the electrophoretic mobility of a particle, which is defined as $u_E = v/E$. This is achieved by applying an electric field across a solution containing the particles and an electrolyte. When the electric field, E is present the particles will start to move in the direction of the oppositely-charged electrode. The velocity, v of the particle in solution is a function of the strength of the electric field, E the dielectric constant, ϵ the viscosity of the medium, η and the zeta potential of the particle, ζ . All of the variables are related by Equation 3.6.1 the Smoluchowski equation.

$$u_E = \frac{\epsilon\zeta}{\eta}$$

Equation 3.6. 1

To interpret the zeta potential ζ of a particle one must look at the surface of a particle. If one takes a particle with a negative surface charge, there will be many positive counterions that are temporarily bonded to the surface of the particle. These particles comprise the Stern layer. The outside of this layer is where the Stern potential is located. Moving away from the surface are the ions that are in rapid thermal movement, known as the diffuse double electrical layer. The zeta-potential is defined as the potential at the distance from the surface where counterions inside still move with the particle, whereas those outside are not sufficiently attracted and thus their motion is determined by thermal energy. This is pictorially represented in Figure 3.6.1.

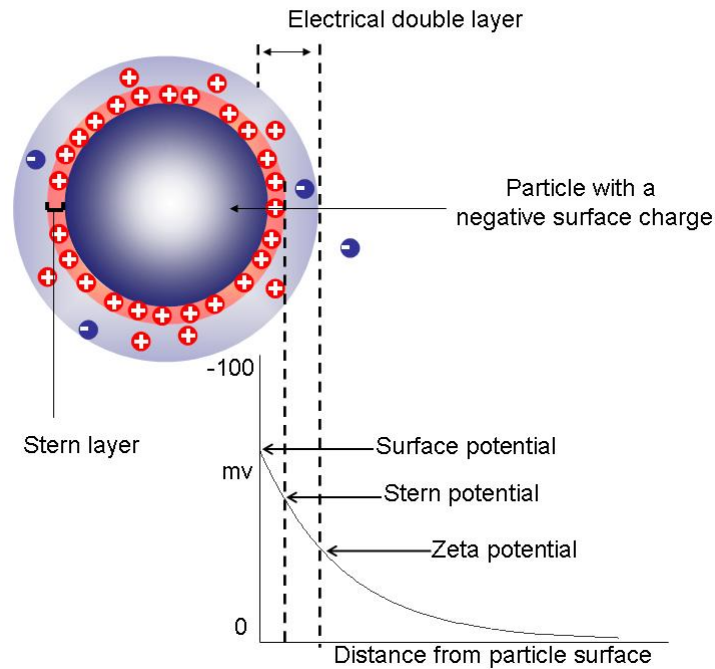


Figure 3.6. 1: Potential of a charged surface

3.7 Ellipsometry

Ellipsometry is a specular optical technique used to measure the thickness of thin films. It is of particular interest, because it is a non-destructive method which has a resolution ranging from angstroms to micrometers, and the only sample requirement is that it reflects laser light. The electric field vector of light, \vec{E} , has two components, p and s. p refers to light that is parallel to the plane of incidence and s is light perpendicular to the plane of incidence. In ellipsometry one measures the change in polarization state of light after interacting with a surface [10, 12,14]. The layout of a typical experiment is seen below.

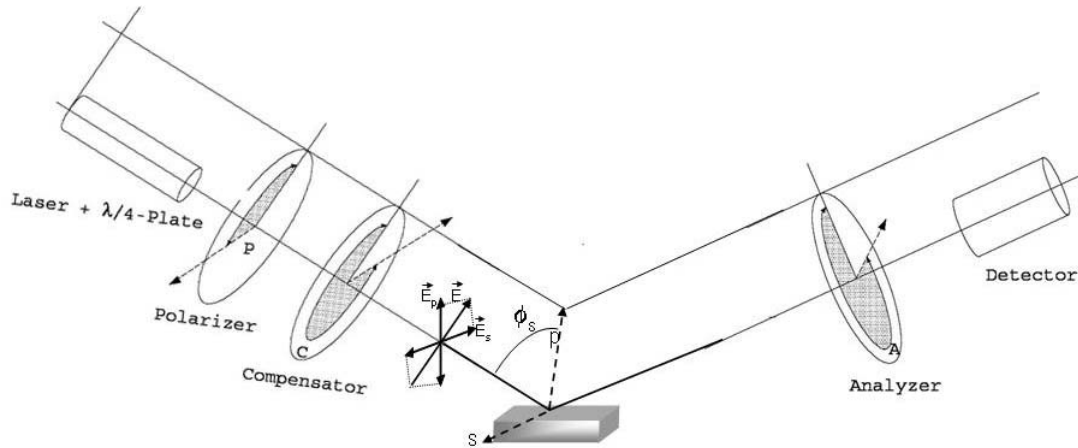


Figure 3.7.1 Ellipsometry layout

The polarizer and compensator are used to produce any desired state of polarization of the incident light. After reflection the state of polarization is changed and analyzed by the analyzer. In a typical experiment, two quantities, Δ and Ψ , are measured which are defined in equations below

$$\Delta = (\delta_p^r - \delta_s^r) - (\delta_p^i - \delta_s^i)$$

Equation 3.7.1

$$\tan \psi = \frac{\left| \frac{E_p^r}{E_s^r} \right|}{\left| \frac{E_p^i}{E_s^i} \right|}$$

Equation 3.7.2

where Δ and Ψ refer to the change in phase and the change in the amplitude of the light respectively. The superscript r is the reflected light and i is the incident light. The values Δ and Ψ are then placed into Equation 3.7.3 to obtain the thickness of the sample.

$$\tan \psi e^{i\Delta} = \frac{R_p}{R_s}$$

Equation 3.7.3 Fresnel equation

3.8 Differential Scanning Calorimetry

Differential scanning calorimeter (DSC) is a thermo-analytical technique in which the amounts of heat required to increase the temperature of a sample and reference are measured as a function of temperature. Using this method one can measure the helix-coil transition in DNA, protein denaturation to crystallization, and the melting or decomposition of a polymer [7,15].

DSC works on the principle of slowly and simultaneously heating a sample and a reference, both in aluminum pans, with the same amount of energy being put into both. The DSC monitors the amount of energy that must be introduced into the system to increase the temperature in comparison to the reference. The temperature, at which the energy input into the sample changes, denotes that a transition has occurred. There are many types of transitions that can be observed: phase transition, glass transition, and the change in the conformation of a protein.

If one knows the amount of the sample in addition to the temperature difference between the pans, one can calculate the energy associated with the phase change.

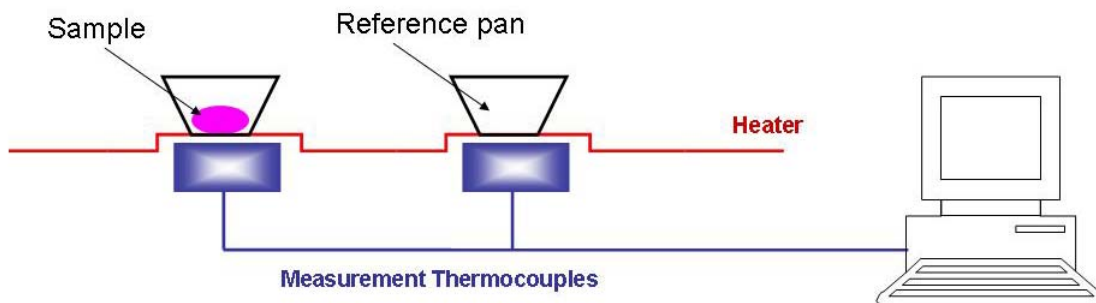


Figure 3.8.1 Layout of DSC

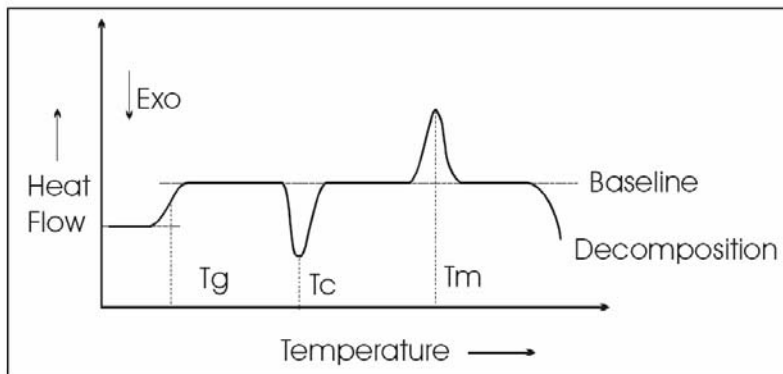


Figure 3.8.2 Typical DSC curve for a polymer: T_g- glass transition, T_c- crystallization temperature, T_m- Melting temperature and the decomposition of the polymer. From ref [16]

3.9 Neutron Reflectivity

Neutron Reflectivity is an interesting technique due to its surface sensitivity and contrast-matching ability. In the case of polyelectrolytes one can learn about the hydration of the polyelectrolytes in the film, especially when measured against D₂O in comparison to H₂O or air [17].

Neutrons are formed in a reactor or via a process called spallation. With guides the neutrons are lead through a chopper which through an offset in the phase of the chopper selects discrete energies of neutrons that are allowed to pass through slits and then to interact with the surface. After the interaction with the surface the neutrons pass through another slit and then to the detector. When interacting with the sample, some neutrons are scattered, which can be described by the following equation.

$$Q = \left(\frac{4\pi}{\lambda} \right) \sin\left(\frac{\theta}{2} \right)$$

Equation 3.9.1

where Q is the scattering vector, λ is the wavelength of the neutrons, θ is the scattering angle. In the case of a bare substrate at small angles all the neutrons are reflected by the samples (total reflection). If the angle is increased, some of the neutrons will refract or

enter the sample (critical edge). After the angle is increased past the critical edge the intensity of the refracted neutrons will increase as described by a Fresnel curve shown in Figure 3.9.1. In the case of samples with a film on top, some neutrons will be reflected from the top of the layer, and other neutrons will be reflected at the film/solid interface. These two beams of light will interfere constructively or destructively as a function of the angle. This type of interference results in fringes referred to as Kiessig fringes. The addition of the Fresnel curve and the Kiessig fringes is observed in typical reflectivity curves shown in Figure 3.9.2. The interaction of neutrons with a solid surface is shown in Figure 3.9.3.

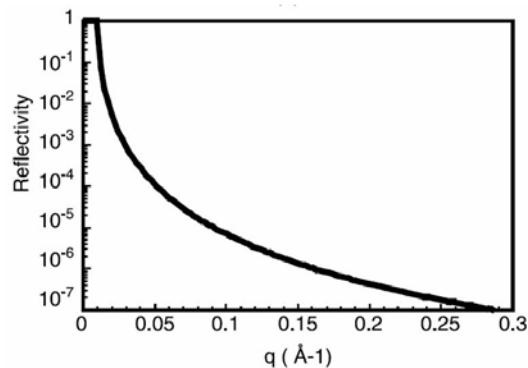


Figure 3.9.1 Simulation of the specular neutron reflectivity as a function of q from a silicon/air interface.

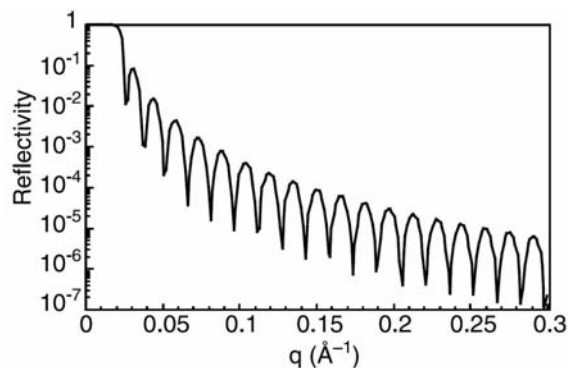


Figure 3.9.2 Simulation of the specular neutron reflectivity as a function of q from a silicon wafer with a film on top.

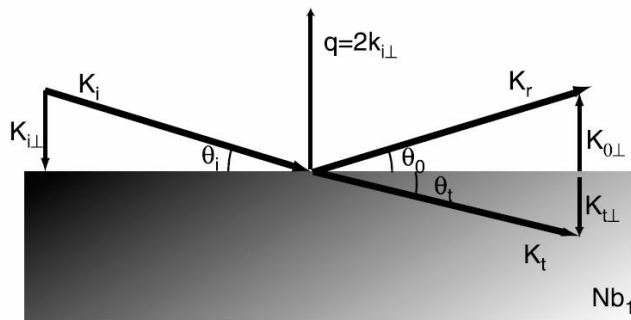


Figure 3.9.3 Neutron sample interaction

3.10 Instrumental Details

The CLSM data presented were conducted with a Leica TCS SP inverted confocal microscope system (Leica, Germany) with a 100x oil-immersion objective, and a numerical aperture of 1.4.

Raman Confocal microscopy spectra were measured at room temperature using a Confocal Raman Microscope (CRM200, Witec) equipped with a piezo scanner (P-500, Physik Instrumente) and a high NA microscope objective (x 60, NA = 0.80 or x 100 oil NA = 1.25, Nikon). In a typical experiment, a circularly polarized laser (diode-pumped Green laser, $\lambda=532\text{nm}$, CrystaLaser) was focused on the located material with a diffraction limited spot and the Raman light was detected and guided to an Avalanche Photodiode Detector (APD). The spectra were taken with an air-cooled CCD (PI-MAX, Princeton Instruments) behind a grating (600 mm^{-1}) spectrograph (Acton) with a resolution of 6 cm^{-1} .

All UV/Vis Spectra were taken with a Cary 50 Conc (Varian GmbH, Australia Pty Ltd). Cary software was used for measurement control and data acquisition.

Scanning electron microscopy images were taken using a Gemini 550 (Zeiss, Germany) using an excitation voltage of 3.0 KeV. A drop of solution was placed on a glass slide that was attached to a carbon film. After air drying at room temperature, the

samples were sputter coated with a few angstroms of Pt in order to have a conductive surface.

SFM images were recorded in dry state at 25°C using a Nanoscope III Multimode SFM (Digital Instruments Inc, USA). Samples were prepared by placing a drop of the suspension of interest onto a cleaved mica surface, which were then allowed to dry. The SFM images were processed by the Nanoscope III software or WSxM software (Nanotec, Spain).

Measurements were performed with a Zetasizer 3000HS system from Malvern Instruments Ltd. (Southborough, MA, USA).

The thickness of the film was determined in air with a null ellipsometer (Multiskop from Optrel, Berlin, Germany) at a fixed incidence angle of 70° and fixed wavelength of 5320 Å. A film refractive index of 1.54 was assumed to determine the thickness of the films. Because the refractive index of wax is about 1.48, the total film thickness determined by ellipsometry is slightly underestimated when a layer of wax is present atop the polyelectrolyte multilayer

The reflectivity, R , which is the ratio between the intensity of the incoming and the reflected beam, was measured as a function of Q . The experiments were performed with D_2O on the bottom of the experimental cell against a Si block above. In this case the lower medium has a higher SLD than the upper one. Under these conditions, $R= 1$ for Q below a critical value Q_c . Above Q_c , R decays with Q , and the shape of the dependence is a function of the area-averaged scattering length density profile normal to the interface. A beam of rectangular cross section was set by a slit system on the sample side. The studies were performed in a $\theta/2\theta$ geometry using the V6 monochromatic (wavelength $\lambda= 0.47$ nm) reflectometer [18,19] at the Hahn-Meitner Institute, Berlin, Germany.

References

- 1 Sheppard, C. J. R.; Shotton, D. M., Confocal Laser Scanning Microscopy. ed.; BIOS Scientific Publishers: Oxford, **1997**; 'Vol.' p 345.
- 2 Corle, T. R.; Kino, G. S., Confocal Scanning Optical Microscopy and Related Imaging Systems. ed.; Academic Press: San Diego, **1996**; 'Vol.' p 120.
- 3 Ibarz-Ric, G. Controlling internal structure and permeability of polyelectrolyte multilayer microcapsules. Universität Potsdam, Potsdam, **2003**.
- 4 Raman, C. V., A new radiation. Indian Journal of Physics **1928**, 2, 387-98.
- 5 Raman, C. V.; Krishnan, K. S., A new type of secondary radiation. Nature (London, United Kingdom) **1928**, 121, 501-2.
- 6 Colthup, N.; Daly, L. H.; Wiberley, S. E., Introduction to Infrared and Raman Spectroscopy. 3rd Ed. ed.; **1990**; 'Vol.' p 547 pp.
- 7 Skoog, D. A.; Holler, J. E.; Nieman, T. A., Principles of Instrumental Analysis. 5th ed.; Saunders College Publishing: Philadelphia, **1998**; 'Vol.' p 849.
- 8 Perkampus, H. H., UV Atlas of Organic Compounds. Second ed.; VCH-Verlangsgesellschaft: **1992**; 'Vol.' p 336.
- 9 Reimer, L., Scanning Electron Microscopy. ed.; Springer-Verlag: Berlin, **1985**; 'Vol.' 45, p 457.
- 10 Butt, H. J.; Graf, K.; Kappl, M., Physics and Chemistry of Interfaces. ed.; **2003**; 'Vol.' p 350 pp.
- 11 Binnig, G.; Quate, C. F.; Gerber, C., Atomic force microscope. Physical Review Letters **1986**, 56, (9), 930-3.
- 12 Bubert, H.; Jennet, H., Surface and Thin Film Analysis: A Compendium of Principles, Instrumentation, and Applications. ed.; Wiley-VCH: Weinheim, 2002; 'Vol.' p 336.
- 13 Malver Instruments., Zetasizer Nano Series User Manual. ed.; 2003; 'Vol.' p.
- 14 Motschmann, H.; Teppner, R., Ellipsometry in Interface Science, Novel methods to Study Interfacial Layers. ed.; Elsevier: **2001**; 'Vol.' p 41.
- 15 Hatakeyama, T.; Quinn, F., Thermal Analysis: Fundamentals and Applications to Polymer Science, 2nd Edition. ed.; **1998**; 'Vol.' p 336 pp.
- 16 Montenegro, R. V. D. Crystallization, Biomimetics and Semiconducting Polymers in Confined Systems. Universität Potsdam, Postdam, **2003**.
- 17 Cubitt, R.; Fragneto, G., Neutron reflection: principles and examples of applications. Scattering **2002**, 2, 1198-1208.
- 18 Mezei, F.; Golub, R.; Klose, F.; Toews, H., Focused Beam Reflectometer for Solid and Liquid Surfaces. Physica B **1995**, 213, 898-900.
- 19 <http://www.hmi.de/bensc/instrumentation/instrumente/v6/v6.html>.

Chapter 4- Polyelectrolyte multilayers as an encapsulation vehicle

4.1 Introduction

Encapsulation of various substances into different micro- and nanoparticles such as capsules, polymer spheres, liposomes, etc. has received considerable attention due to increased interest in biotechnology, medicine, catalysis, ecology, nutrition, and so forth [1]. As seen in chapter 2 the sequential layer-by-layer (LbL) deposition of polyelectrolyte was used to fabricate multilayer films flat macroscopic substrates utilizing electrostatic interaction between oppositely-charged macromolecules at each adsorption step. The extension of this technology toward colloidal species has enabled an alternating polyelectrolyte assembly on different kinds of supports. Encapsulation of macromolecules, proteins, and other bioactive materials into such type of microcapsules is of great interest for pharmaceuticals and biotechnology due to the possibilities for applying such systems as micro- and nanocontainers for drug delivery and controlled release and in catalysis. To date there are many approaches for encapsulating macromolecules into polyelectrolyte capsules using the LbL technique. The first method consists of the formation of particles out of molecules subjected to encapsulation. Dye and drug nanocrystals [2,3], protein aggregates, and compact forms of DNA [4,5] were used to template LbL assembly, thus leading to encapsulation. The second approach for encapsulation of macromolecules exploits preformed hollow capsules and incorporates

the macromolecules from the surrounding medium by switching the permeability of the hollow capsule shell [6,7]. The third method can be used for the incorporation of charged and noncharged macromolecules via fabrication of double-walled capsules with subsequent decomposition of the inner wall [8]. The fourth route of polymer encapsulation is via controlled polymeric synthesis inside the capsule, now also referred to as the “ship in a bottle” method [9]. These approaches have some disadvantages, such as formation of stable cores with certain surface properties for the first method, low incorporation efficiency for the second one, and confined usage of employed polymers for the other approaches. This work aims to elaborate a new approach for fabrication of polyelectrolyte capsules employing porous inorganic CaCO_3 microparticles as a template for polyelectrolyte capsule fabrication. Microcapsule formation is based on consecutive core coatings in solutions of two oppositely-charged polyelectrolytes (poly (styrene sulfonate) and poly (allylamine hydrochloride)) followed by core dissolution. The structures formed were studied by scanning electron and force microscopy and confocal Raman and laser-scanning fluorescence microscopy. The structure and properties of particles used in this study and the capacity of microcapsules for macromolecule entrapment will be discussed as well.

4.2 Fluorescent Probes

Preparation

Uniform, nearly spherical microparticles of CaCO_3 with a narrow size distribution were prepared by colloidal crystallization from supersaturated (relative to CaCO_3) solution. The process was initiated by rapid mixing of equal volumes of CaCl_2 and Na_2CO_3 solutions. The mixture was intensively agitated on a magnetic stirrer. The time course of the reaction was observed under a light microscope. The amorphous precipitate instantly formed upon mixing was found to transform more slowly into microparticles with spherical morphology. The diameter of microparticles increases with time up to 15-20 μm without an essential change in particle morphology. In parallel with colloidal

aggregation of primary nanoparticles of CaCO_3 into microspheres, the true crystallization of CaCO_3 into rhombohedral calcite microcrystals is also observed. We have found experimental conditions for CaCO_3 crystallization practically excluding the formation of all CaCO_3 microparticles except for microspherical ones. In a typical experiment, 0.33 M Na_2CO_3 solution (sodium carbonate was found to give more reproducible results in comparison with ammonium bicarbonate, as used in ref [10]) was rapidly poured into an equal volume of 0.33M solution of CaCl_2 at room temperature, and after intense agitation on a magnetic stirrer the precipitate was filtered off, thoroughly washed with pure water, and dried in air. The procedure results in highly homogeneous, spherical CaCO_3 microparticles with an average diameter ranging from 4 to 6 μm .

Polyelectrolyte microcapsules were prepared by alternating incubation of CaCO_3 microparticles (1% w/w in suspension) in PSS and PAH solutions (2 mg/mL), within 0.5M NaCl. Each adsorption cycle (10 min incubation, shaking) was completed with three centrifugation steps (200g, 5 min) followed by suspension in water containing 0.05M NaCl for 4 min. Washing procedures were used before the next polyelectrolyte was added and were applied to remove nonbound polymer. The last washing step was carried out in pure water. Then the treated microparticles were re-suspended in an Eppendorf tube by adding 0.1 M EDTA solution (pH 7.0 was adjusted by HCl) to dissolve the calcium carbonate core. After 30 min of agitation, the capsules were centrifuged (1500g, 5 min), the supernatant was removed, and the capsules were re-suspended in fresh EDTA. This washing procedure with EDTA was repeated three times; the resultant suspension of the formed microcapsules was washed four times with pure water and stored at 4 °C in water. To fabricate microcapsules with fluorescent-labeled polyelectrolyte, the same procedure was used with PAH-FITC.

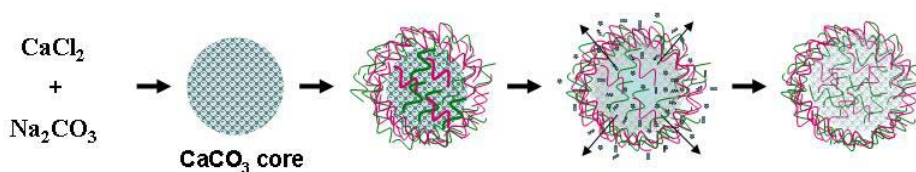


Figure 4.2.1 Preparation schema of CaCO_3 cores

Results

After following the core preparation procedure above, SEM pictures were taken of the resulting cores. Figure 4.2.2 shows cores that were synthesized, washed, dried and imaged.

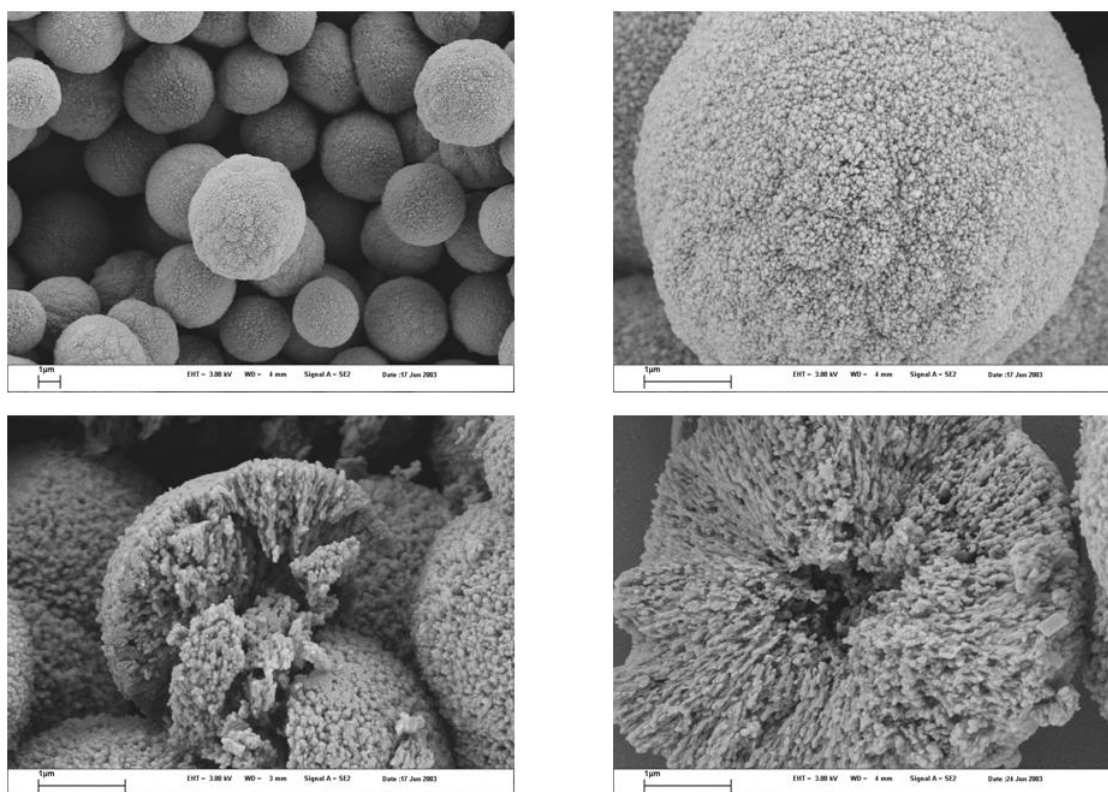


Figure 4. 2. 2: CaCO₃ core top and cross section of cores bottom. Scale bar in all images is 1 µm.

The picture in Figure 4.2.2 shows the resulting CaCO₃ particles. The top row shows whole cores, revealing the spherical and porous nature of the CaCO₃ cores. Mechanical pressure was applied to take pictures of the cross section of the cores that were on the SEM grid. The cross sectional pictures show lines, radial or striated from the center of the cores. This results from the crystal nucleation taking place in the inside followed by crystal growth outward.

Figure 4.2.3 shows SEM images of the coated cores, if the whole cores are used as a template for LbL as described above.

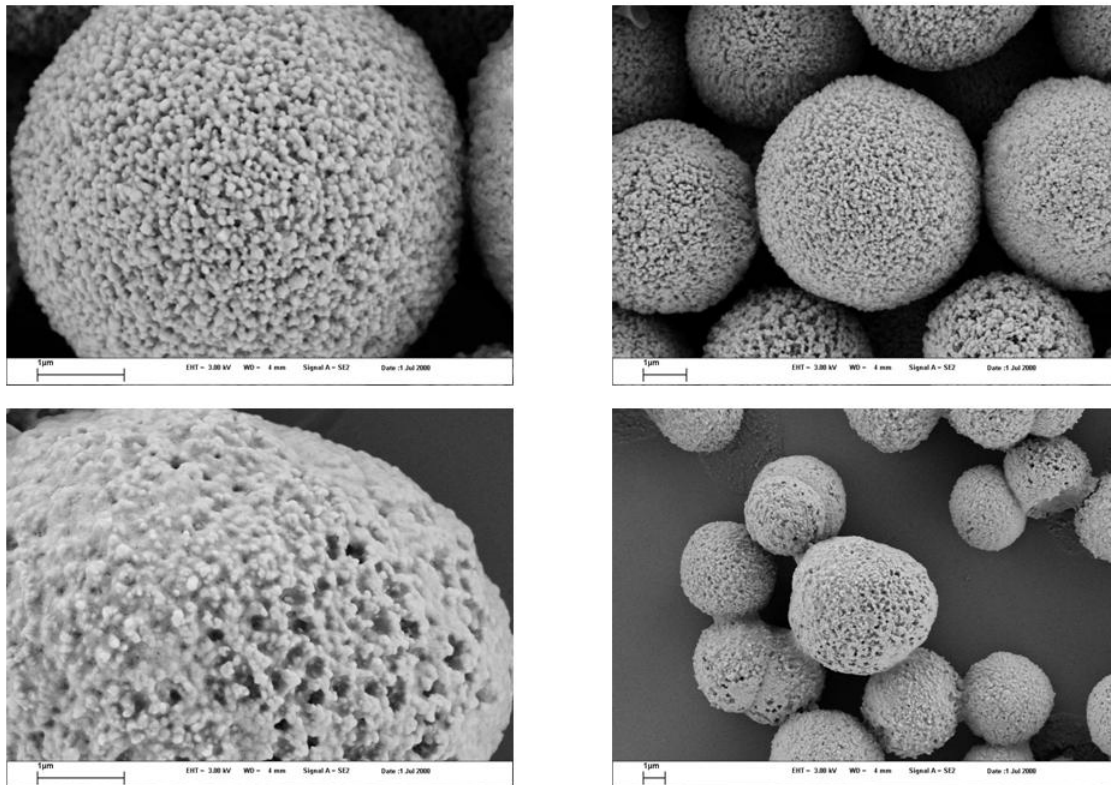


Figure 4. 2. 3: Coated CaCO₃ cores top pictures are with 6 layers and below with 16 layers. Scale bar in all images is 1 µm.

The CaCO₃ cores were templated with two different amounts of PSS and PAH absorbed on the surface. The top pictures show cores after 6 layers and the bottom pictures show 16 layers of PSS and PAH coating. Cores coated with 6 layers show that the surface roughness is decreased. This occurs even more so in the pictures with 16 layers of PSS and PAH on CaCO₃ cores. One can also observe that the definition of the shape is blurred by a “plastic” coating.

If mechanical stress is applied to cores with 16 layers of PSS and PAH the cross section of the coated core as seen in Figure 4.2.4 is obtained. In this image the typical striations that show the crystal growth are still present. But in addition to the radial lines of the interior, one can also see the polymeric coating resulting from the PSS and PAH.

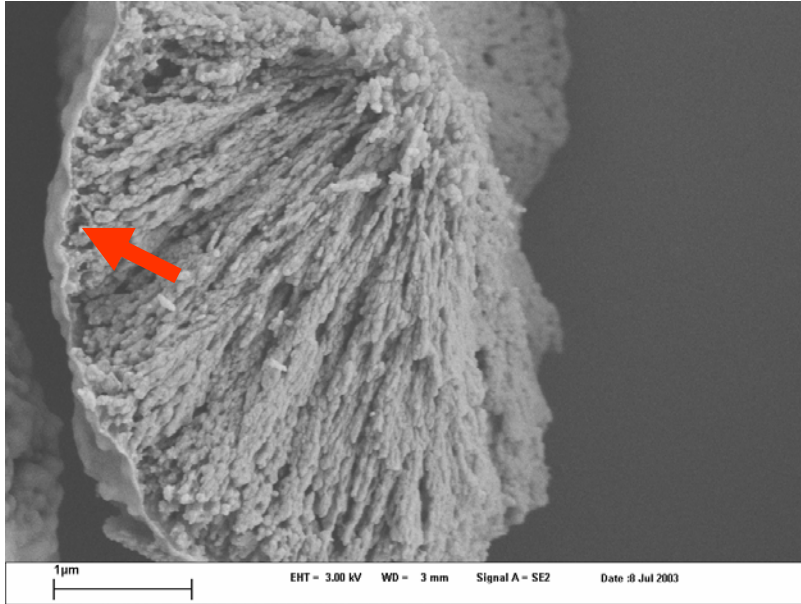


Figure 4. 2.4 Cross section of a CaCO₃ core after 16 layers. Scale bar is 1 μm. Arrow shows the polymeric coating on the surface of the particle.

If the CaCO₃ core is removed as also described above one obtains the following images. Note the porous and fiber-like structure of the surface.

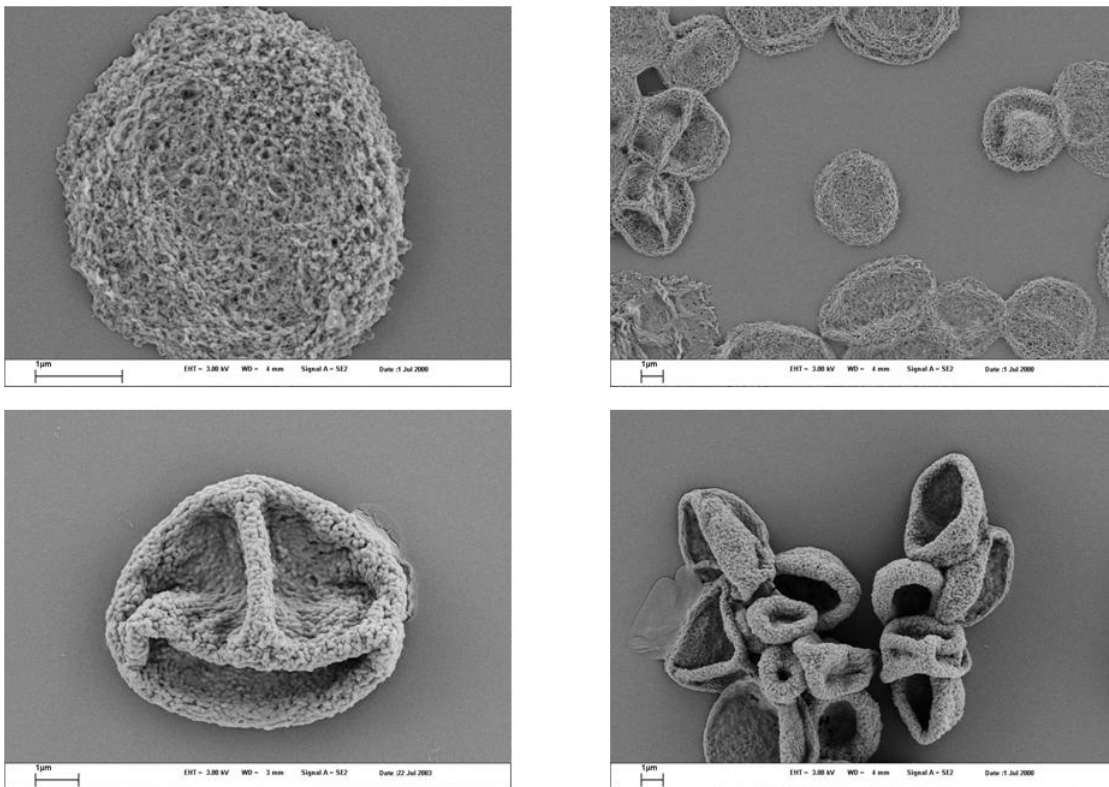


Figure 4.2. 5 SEM images of capsules after 6 and 16 layers of PSS/PAH. Scale bar in all images is 1 μm.

If a fluorescently-labeled polyelectrolyte is used one can gain much information about where the polyelectrolyte goes during the absorption step. When one uses a CaCO_3 core and FITC labeled PAH (FITC-PAH) and PSS to make the capsule the result is the following capsule, shown in Figure 4.2.6.

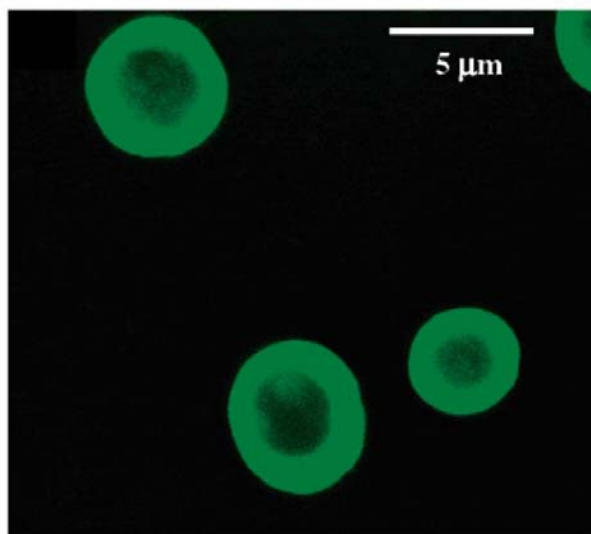


Figure 4. 2. 6 Confocal image of (PAH-FITC/PSS) 8 capsules

In figure 4.2.6 one can see a capsule consisting of 16 layers of (PAH-FITC/PSS). With fluorescence inside the capsules, it is evident that PAH is also present in the capsule interior. Therefore one can also assume that the PSS goes inside the core during the absorption steps. Thus, both polyelectrolytes are inside the microcapsule, forming a polyelectrolyte complex. This means that microcapsules formed on CaCO_3 cores have a matrix-type structure and the polyelectrolyte complex is not only precipitated at the wall. The polyelectrolyte complex between PSS and PAH inside the capsule may have an excess charge due to nonstoichiometry and it may therefore swell, trapped within the capsule, forming a gel-like structure. The diameter of the pores in the CaCO_3 microparticles is from 20 to 60 nm. This allows small molecules of PSS and PAH with a size of several nanometers to penetrate inside.

When unlabeled polyelectrolytes are used, the matrix left inside the CaCO_3 capsules will have no fluorescence. If a fluorescent dye like Bovine Serum Albumin labeled with FITC (BSA-FITC) or dextran-FITC is added to the capsules with a matrix

the pictures seen in Figure 4.2.7 are obtained. The fabrication of BSA-FITC, dextran-FITC, as well as the structures used for the entire work are illustrated in Appendix I The cross section of the capsule in Figure 4.2.7 B shows the non- uniformity of the matrix structure inside the capsule. This arises from the fact that PSS and PAH are unable to diffuse completely to the middle of the core.

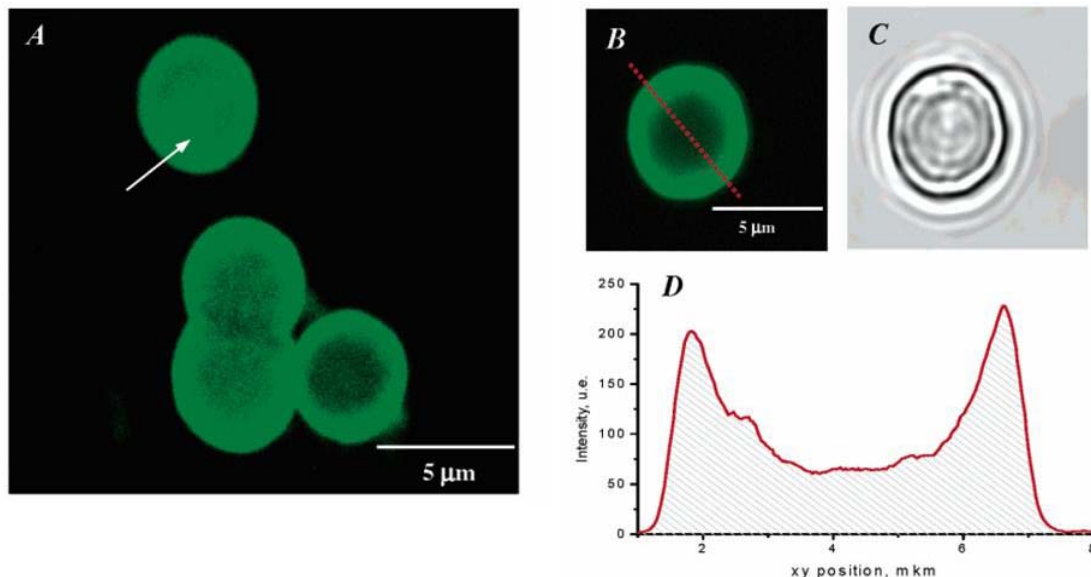


Figure 4.2.7 CLSM images of microcapsules (16 PEAP) after incubation with BSA-FITC(A) and dextran-FITC(B) followed by water washing. (C) Transmission confocal microscopy image of the capsule presented in image B. (D) The fluorescence profile for image B

Discussion

After the desirable number of PEAP was achieved, the calcium carbonate support was decomposed. This was accomplished by multiple washings in an EDTA solution that leads to the formation of a water-soluble complex between EDTA and Ca^{2+} . Thus, the polymeric microcapsules are formed. SEM images of capsules obtained using 6 and 16 layers were shown. The number of layers used affects the morphology of the structures formed. In the case of 6 layers, the capsule structure looks like a very porous network with many holes (Figure 4.2.5 top left). The surface morphology of the initial CaCO_3 microcores governs the morphology of the polyelectrolyte film formed on its surface and as a consequence the morphology of the capsules. After 16 layers, the morphology of the

capsules differs from that which was described for 6 PEAP. SEM images of such capsules are given in the bottom half Figure 4.2.5. These capsules have more defined folds indicating a visibly thicker wall, which is smoother than the previous capsules (6 layers) but still rough. Formation of polyelectrolyte complex on the surface of CaCO_3 cores hinders the diffusion of other polyelectrolytes during further treatment with PSS and PAH; this leads to formation of a thick wall in the case of 16 layers. Scanning Confocal Raman spectroscopy (will be shown later) and CLSM were used to determine the presence of a polyelectrolyte complex inside the capsule.

4.3 PNIPAM in CaCO_3 cores

Preparation

The CaCO_3 cores were prepared by vigorously stirring adding an equal amount of 1 M Na_2CO_3 all at once to 1M CaCl_2 in a small glass beaker that contained 5 ml of water. Upon addition of the second salt the solution immediately became cloudy, denoting the nucleation and growth of the CaCO_3 cores. After allowing the CaCO_3 to grow for 30 seconds, stirring was halted and the solution was transferred into Eppendorf tubes. It was then centrifuged (4000 rpm, 5 minutes) and washed 3 times to remove the excess NaCl, CaCl_2 , and Na_2CO_3 , to stop the CaCO_3 growth, and to remove the cores that were much smaller than the $5\mu\text{m}$ average. After washing the cores, the layer-by-layer assembly of polyelectrolytes and wax particles was performed until the desired number of layers was deposited. To encapsulate PNIPAM inside the CaCO_3 core, PNIPAM was dissolved in the 5 ml of water to which the CaCl_2 and Na_2CO_3 were added to. Once the desired number of layers was deposited, the core was removed with two washings in 0.1M HCl for 5 min and then washed in pure water until a neutral pH was reached.

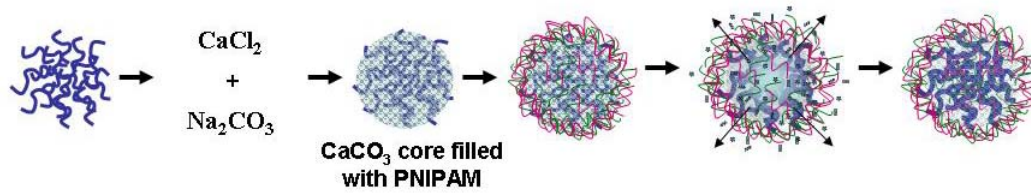


Figure 4. 3. 1 Scheme presenting CaCO₃ core co-synthesis with PNIPAM and then the LbL deposition of PSS and PAH to form capsules.

Results

Capsules templated on CaCO₃ that were co-synthesized with PNIPAM were measured with SEM, Raman, and Confocal microscopy. In Figures 4.3.2 and 4.3.3, SEM pictures of CaCO₃ cores with and without encapsulated PNIPAM are shown. In the case of CaCO₃ cores the typical porous, spherical structure is seen Figure 4.3.2. When during the synthesis of the core PNIPAM is added to the water a co-synthesis particle is obtained. In this sample, with PNIPAM encapsulated in the core (Figure 4.3.3) one can see that there is not only the amorphous structure of the CaCO₃ core but also spots where there appear to be smooth areas on the surface of the particle and projecting out of the particle.

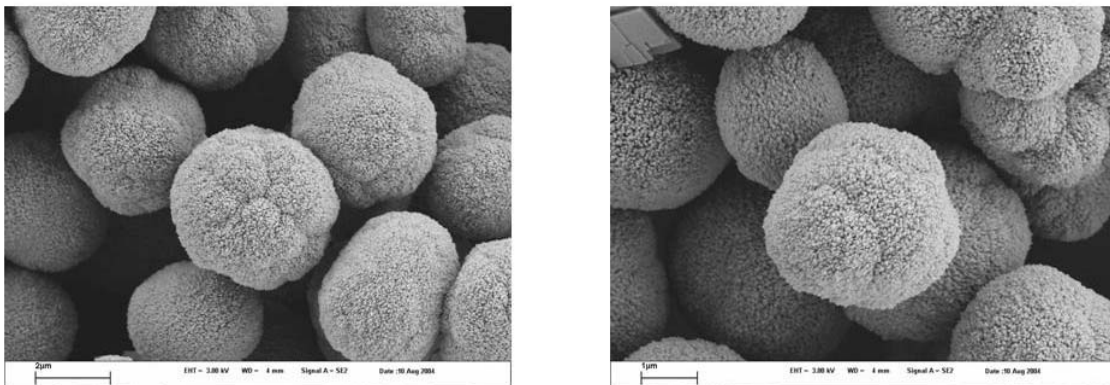


Figure 4. 3. 2 SEM images of CaCO₃ cores . The left scale bar is 2 μm and the right scale bar is 1 μm.

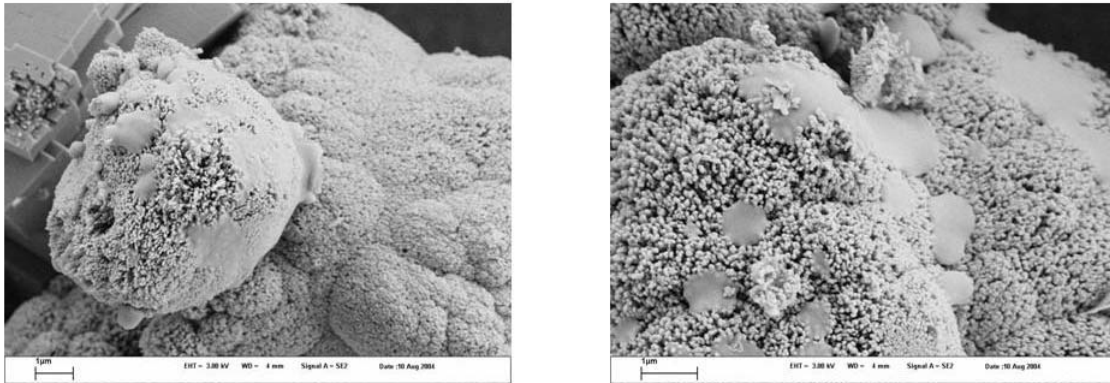


Figure 4. 3. 3 SEM of CaCO₃ cores with co-synthesized PNIPAM. Scale bar in both images is 1 µm.

When treating the particle with 0.1M HCl the CaCO₃ dissolves, leaving a capsule of the constituents employed, in this case PAH/PSS. Capsules consisting of four bilayers of (PAH/PSS) are shown in Figure 4.3.4. Results with capsules with the same number of layers and the same layer components, but on CaCO₃ co-synthesized with PNIPAM, are presented in Figure 4.3.5.

Capsules templated on plain CaCO₃ cores are spherical but not flat. The morphology of capsules prepared using the filled CaCO₃ cores is drastically different. In the left image of Figure 4.3.5, they in fact look like the native cores. The right image was taken only a few millimeters away on the same sample.

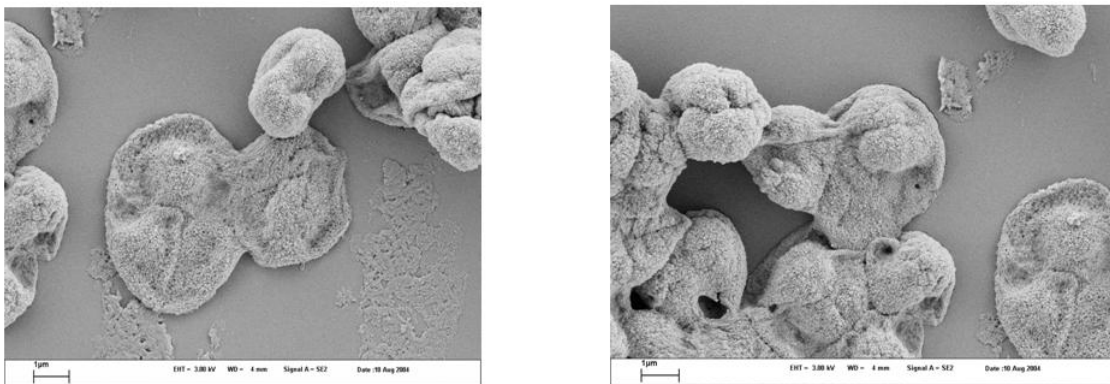


Figure 4. 3. 4 SEM of (PAH/PSS)₄ capsules from CaCO₃ cores. Both scale bars are 1µ.m

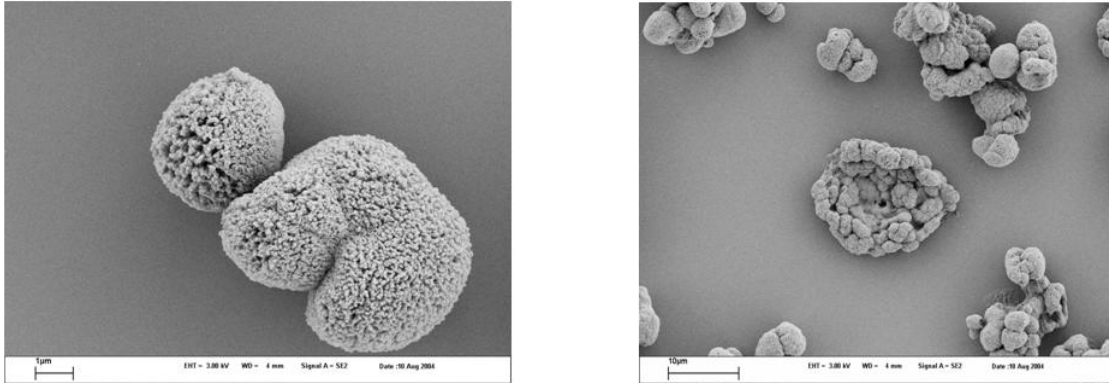


Figure 4. 3. 5 SEM of (PAH/PSS)₄ capsules from CaCO₃ cores with encapsulated PNIPAM. The left scale bar is 1 μm and the right scale bar is 10 μm.

In Figures 4.3.6 and 4.3.7 the optical transmission confocal pictures corresponding to the above SEM pictures are presented. In confocal microscopy, when looking at a cross-section or confocal plane it can be seen that in the case of unfilled cores, the capsules are spherical. This, however, is not the case for capsules made up of co-synthesized CaCO₃ particles. Another observation is that in the case of unfilled capsules, their size distribution is $5\mu\text{m} \pm 0.5\mu\text{m}$. When PNIPAM is inside the cores the resulting capsules have a size distribution between 7 and 17 μm.

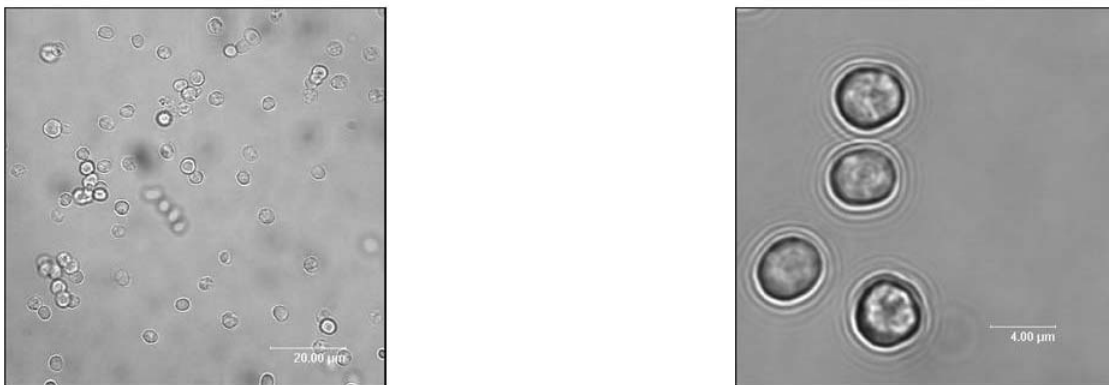


Figure 4. 3. 6 Confocal images of (PAH/PSS)₄ capsules from CaCO₃ cores.



Figure 4.3.7 Confocal images of (PAH/PSS)₄ capsules from CaCO₃ cores with encapsulated PNIPAM

To achieve a definite proof of the presence of PNIPAM inside the CaCO₃ cores and the resulting capsules, Raman Spectra are presented in Figure 4.3.8 and 4.3.9. Although it cannot be shown, fluorescence was observed during the measurement of the PNIPAM-MRho inside the CaCO₃.

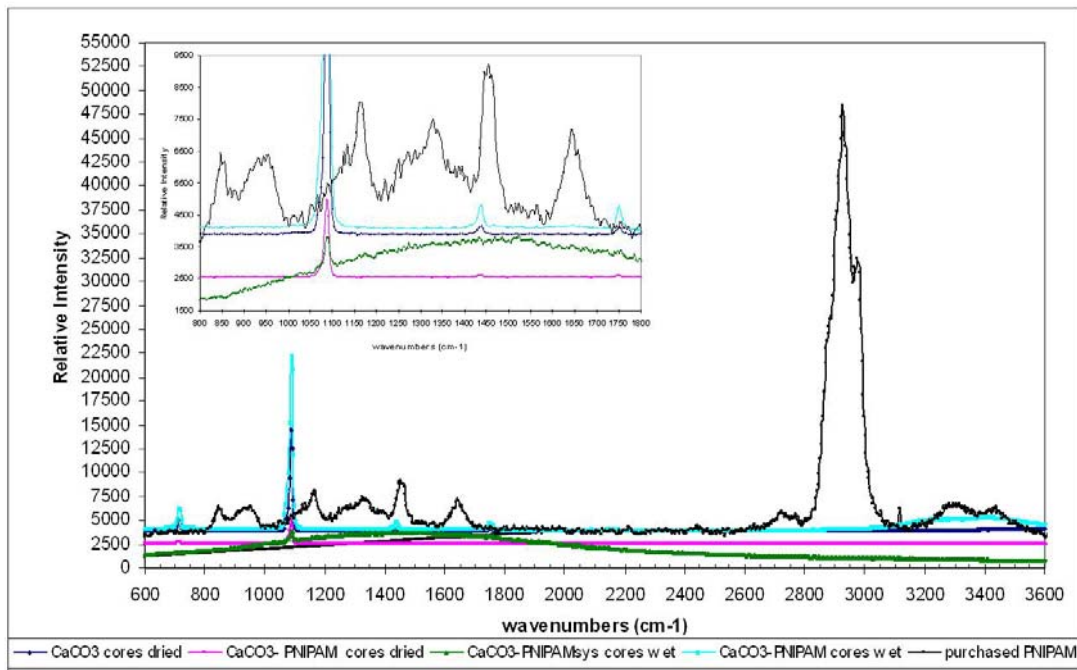


Figure 4.3.8 Raman Spectroscopy of CaCO₃ cores with and without PNIPAM.

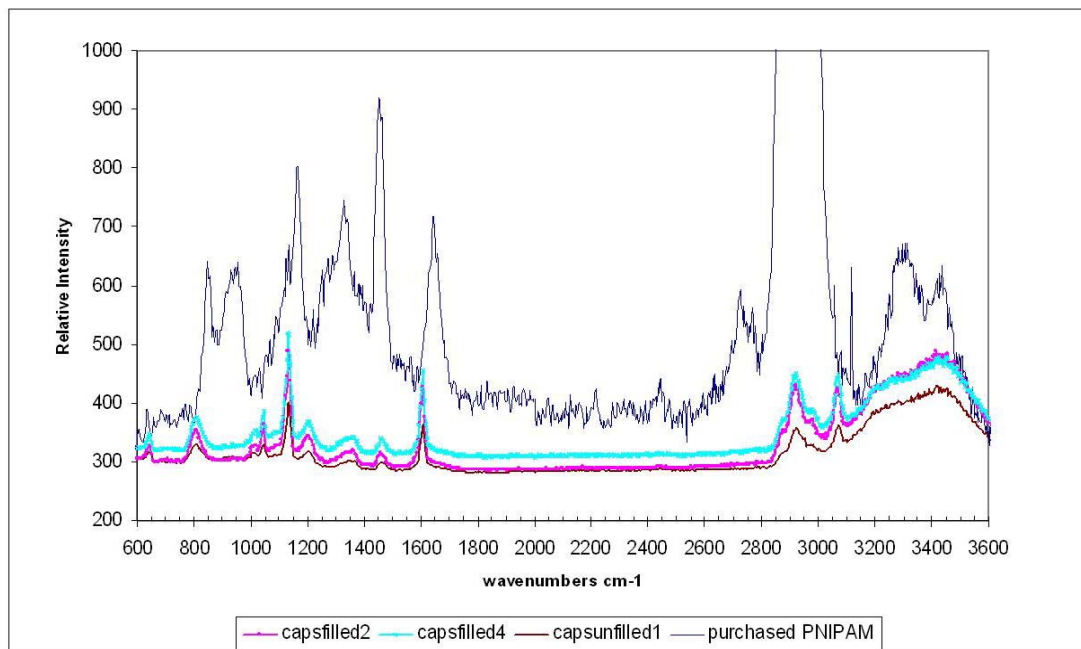


Figure 4.3.9 Raman Spectroscopy of capsules templated on CaCO₃ cores.

Assignments of the peaks seen in Figures 4.3.8 and 4.3.9 are presented in Figure 4.3.10 and 4.3.11 respectively.

Peak Position cm ⁻¹	Intensity	Assignment
1087	sh, s	CaCO ₃ , Internal stretching
1433	sh, w	CaCO ₃ , Internal stretching
1453	sh, m	CH ₂ stretching
1658	sh, m	R-N-C=O
1751	sh, w	CaCO ₃ , Internal stretching
2926	br, s	CH ₂ , CH ₃ stretching
3380-3430	br, w	-OH elongation

Absorption: s- strong, m- medium, w- weak, sh- sharp, br- broad.

Figure 4.3.10 Raman Spectroscopy vibration assignment for CaCO₃ cores with and without PNIPAM.

Peak Position cm ⁻¹	Intensity	Assignment
1131	sh, m	R-SO ₃ ⁻
1604	sh, m	aromatic stretching
2850-2950	br, m	CH ₂ , CH ₃ stretching
3380-3430	br, w	-OH elongation

Absorption: s- strong, m- medium, w- weak, sh- sharp, br- broad.

Figure 4.3.11 Raman Spectroscopy vibration assignment for capsules templated on CaCO₃ cores with and without PNIPAM.

The spectra presented in Figure 4.3.8 show a large peak between 2850-2950cm⁻¹ which can be attributed to the CH₂, CH₃ stretching of the PNIPAM backbone. The peaks at 1087 (cm⁻¹), and in the insert at 1433 cm⁻¹ and 1751 cm⁻¹ are attributed to internal stretching in the CaCO₃ [11]. The green curve (CaCO₃ co-precipitated with PNIPAM-MRho) shows a broad band between 1100 and 1800 cm⁻¹ that is probably caused by the fluorescence of the MRho.

The Raman spectra presented in Figure 4.3.9 shows, primarily from the absence the peaks at 1087, 1433, and 1751 cm⁻¹, that the CaCO₃ core has been completely dissolved and removed. Secondly the CH₂-CH₃ stretching peak normally at 2926 cm⁻¹ for the pure dried PNIPAM has a slight red shift to 2923 cm⁻¹ for unfilled capsules and to 2920 (cm⁻¹) for the capsule with PNIPAM. This shift in the CH₂-CH₃ can be attributed to two effects. The initial shift could be induced by the larger order found inside the capsule [17]. Another reason for the shift could be a result of the PNIPAM inside the capsules. Zhanpeisov et al report that there is a red shift in the CH₂-CH₃ stretching peak for polymers that can form hydrogen bonds with water [12]. Both of the reasons could cause a shift in the peak position, but due to the lack of separation of the bands associated to CH₂ and CH₃ and the unspecific nature of the CH₂-CH₃ peak it is hard to definitively say that PNIPAM is inside the CaCO₃ core.

Discussion

Raman alone cannot demonstrate whether there is PNIPAM inside the capsules templated on CaCO₃ cores. However, from the florescent interference in the Raman, SEM and confocal one could say that the PNIPAM was successfully encapsulated inside the core. In the SEM the presence of material on the surface of the core could only be PNIPAM.

It was shown that calcium carbonate forms porous particles and that the large pores in the CaCO₃ core are large enough for the polyelectrolytes PSS and PAH to penetrate inside the core. As CaCO₃ has a negative surface charge, PAH is applied first to

the core. After washing, the PSS is added to the core solution. During the adsorption of the polyelectrolytes, the polyelectrolytes adsorb not only on the surface but also in the interior of the pores of the particle, which is also electrostatically driven. The result is not a hollow capsule, but a capsule with a matrix structure as seen in Figures 4.2.6, 4.2.7, and 4.3.4. It is this matrix structure inside the capsules that in both cases causes the adsorption and accumulation of the dye species inside the capsule. In the case of the capsules templated on cores with PNIPAM, dye will also accumulate inside the matrix from the PSS and PAH. In the next section PNIPAM encapsulated inside a capsule with the “ship in a bottle method” will be discussed. In this case the encapsulated PNIPAM collapses above the LCST or high salt concentration. The capsules with PNIPAM inside the capsules obtained with the CaCO₃ method were also tested to see if a collapse of the PNIPAM could be seen. In this case a collapse was not observed. This is probably a result of the presence of the matrix inside the capsule. The matrix acts as a stabilizer and even inhibits PNIPAM from collapsing even though it was heated above the LCST.

4.4 PNIPAM in PS templated capsules

Preparation

Microcapsules were fabricated with the LbL method by alternate adsorption of PAH and PSS (both were in 0.5 M NaCl). A 10 μm polystyrene template was first coated with PAH for twenty minutes. After the adsorption step the sample was centrifuged at 6000 rpm for 30 seconds. The supernatant was removed and washed three times with water. This procedure was repeated until 18 layers of PAH/PSS were adsorbed. After the desired number of layers was deposited, the core was removed, leaving a hollow shell. To achieve this THF was added to the coated PS cores and they were then washed three times with THF to ensure all PS remnants were removed. Figure 1 A-E.

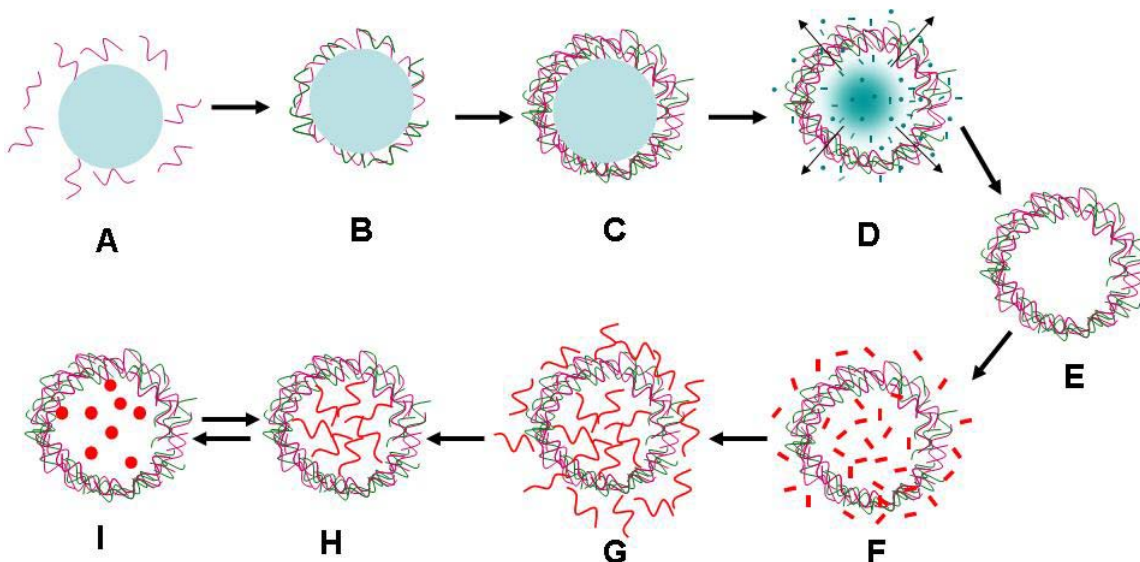


Figure 4. 4. 1 Ship in a bottle encapsulation scheme

PNIPAM was encapsulated inside the capsules with a method proposed by Dähne et al [9]. The NIPAM was weighed to have an overall 0.5M solution with an overall 8 ml volume. MRho and APS were weighed out to be 0.5% and 1% by moles of the NIPAM, respectively. The NIPAM and MRho were dissolved together and APS was dissolved alone, but all were dissolved in Milli-Q water that had N_2 bubbled through it to remove the dissolved O_2 . The hollow (PAH/PSS) shells were then added to a mixture of the NIPAM monomers and the MRho. This mixture was allowed to come to equilibrium by stirring and bubbling with N_2 for four hours.

After establishing equilibrium, the NIPAM/capsule/MRho mixture was cooled in an ice bath. Then the APS and 50 μ L of TMEDA were added, starting the reaction. After the reaction was finished, (one hour) the capsules were centrifuged and washed with water leaving the labeled PNIPAM only inside the capsules. This is shown in Figure 4.4.1 F-I. The supernatant from the reaction was saved and dialyzed exhaustively against water and freeze dried. Figure F-H

Results

In Figure 4.4.2 a representative SEM picture before and after PNIPAM synthesis is shown. Before encapsulation the capsules are flat and collapsed. After the encapsulation one can see the presence of small particles. These particles are PNIPAM that precipitated and formed particles upon drying. In Figure 4.4.3 AFM images are presented. In the case before encapsulation the double wall thickness of the capsule is around 55 nm [13]. After the encapsulation of PNIPAM the double wall thickness increases to between 170 and 230 nm. This large increase in thickness denotes the presence of the dried PNIPAM microgel that is restrained inside the capsule. Figure 4.4.4 compares the Raman spectra of capsules with those of a dried PNIPAM. The major C-H stretching bands ($2800-3000\text{cm}^{-1}$) [14] and the broad band between $1580-1720\text{cm}^{-1}$ which are assigned to amide [15] that are present in the PNIPAM as purchased are also present inside the capsule, giving chemical proof of the presence of the PNIPAM inside the capsule.

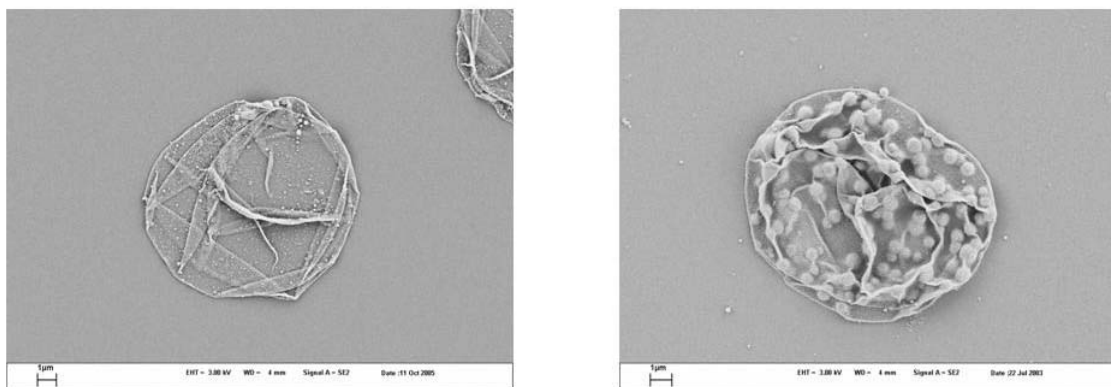


Figure 4.4. 2 Representative SEM pictures of capsules before (left) and after PNIPAM synthesis (right). Particle formation inside the capsule after the polymerization is due to the presence of PNIPAM which upon drying forms particles. Scale bar in both images is 1 µm

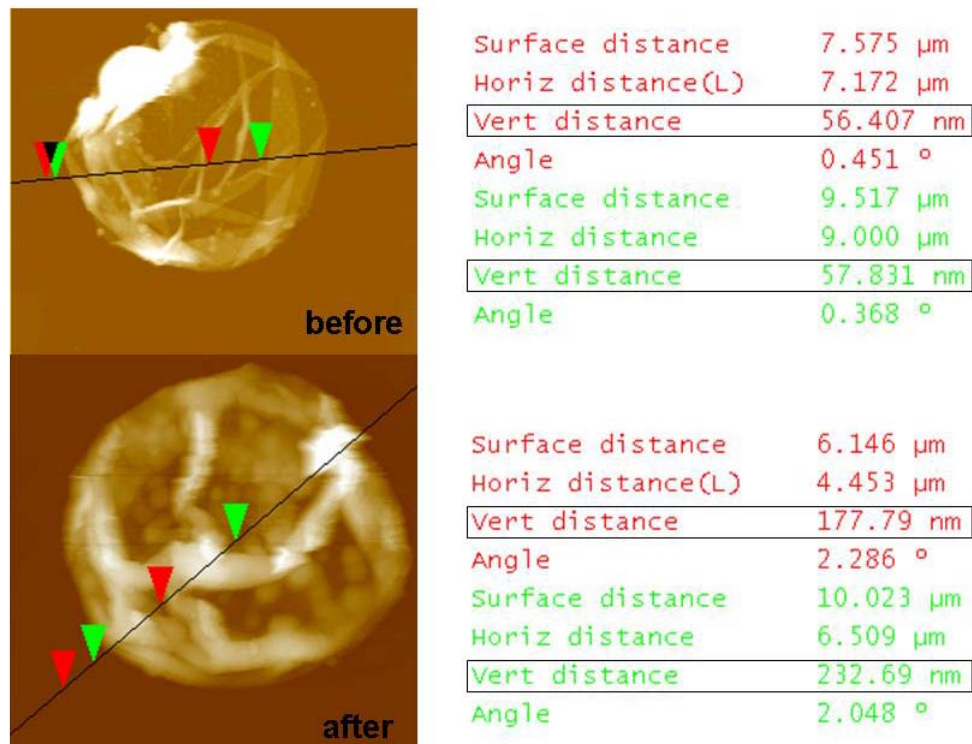


Figure 4.4. 3 AFM images of dried capsules before and after PNIPAM encapsulation. After encapsulation of PNIPAM the double wall thickness increases from 57 nm to 200 nm, an increase of almost 150nm which can be attributed to the presence of the microgel inside the capsule.

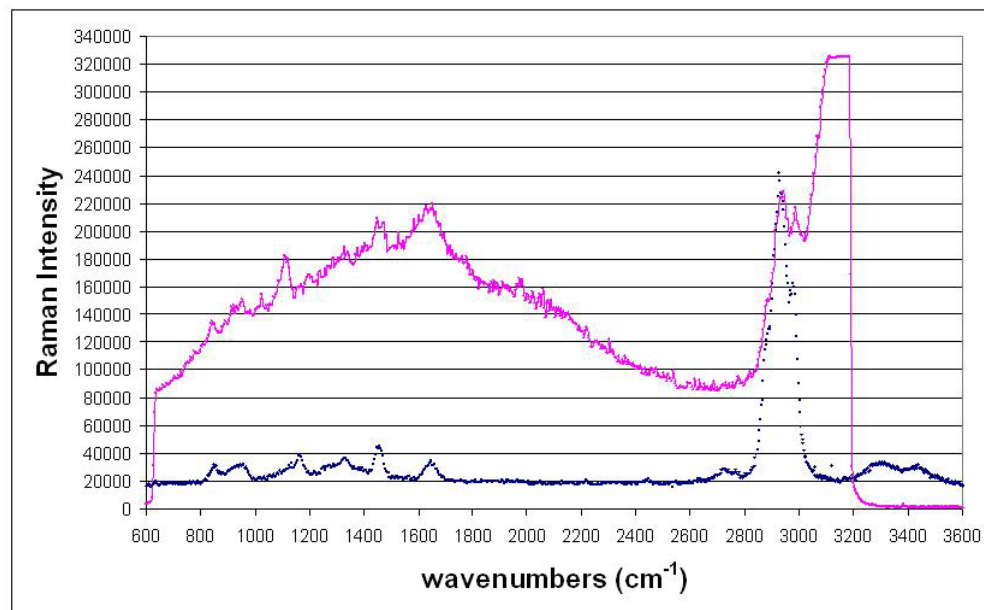


Figure 4.4. 4 Raman spectra of pure PNIPAM purchased from Aldrich (bottom) and the PNIPAM found inside the capsules (top).

Discussion

Once it was proven that PNIPAM was encapsulated the thermo-responsive properties were checked to ensure the encapsulated PNIPAM stayed responsive. In Figure 4.4.5 CLSM images are presented upon heating the capsules. When heating the filled capsule the PNIPAM undergoes a transition from a soluble phase or “coil” to an insoluble or “globule” phase at around 34°C. The pictures below are the same capsule after allowing the capsules to cool below the LCST of the PNIPAM and zoomed in. This demonstrated that the PNIPAM synthesized inside the capsule remains as responsive to temperature as it is in bulk state. Previous work has shown that capsules must be heated above 50°C to cause noticeable changes in the capsules wall permeability [16]. Therefore the effects observed at 32°C are only a result of the PNIPAM.

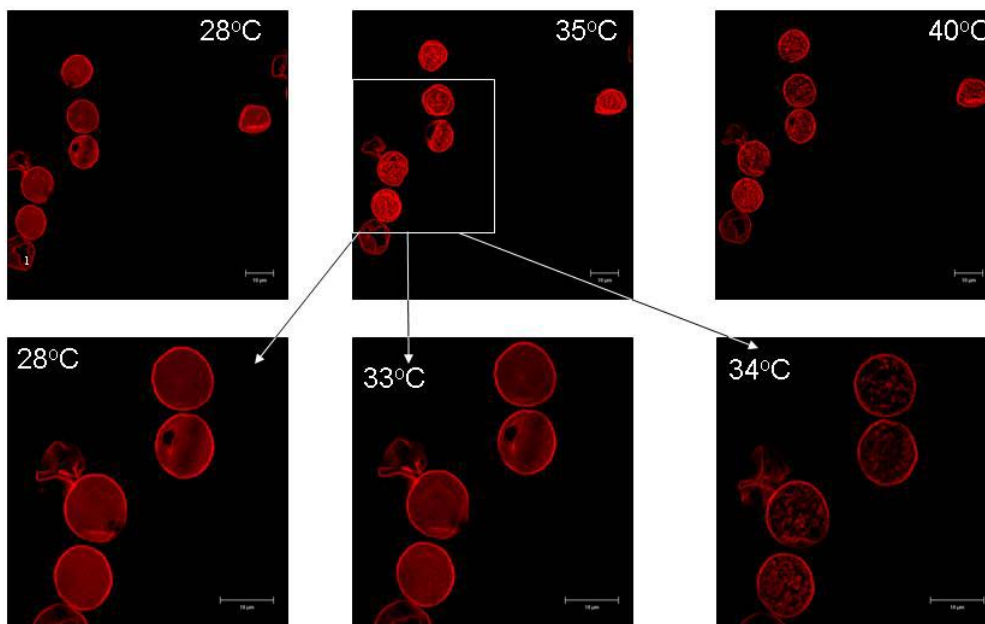


Figure 4. 4. 5: Series of confocal pictures revealing encapsulated PNIPAM only inside capsules. The PNIPAM exhibits a reversible collapse after heating. Scale bar is 10 μm .

To compare the collapse temperature of the PNIPAM inside the capsule and the bulk, the PNIPAM from the supernatant that was dialyzed and re-crystallized was then dissolved in water in order to achieve the same concentration as that inside the capsules

and that measured with DSC. The PNIPAM in the bulk had a LCST of 34°C. The LCST of PNIPAM in bulk is normally around 32°C, however the small amount of Rhodamine used to label the polymer increases the LCST. The capsule wall is comprised of the complex of two polyelectrolytes (PSS and PAH). The orientation of the PSS and PAH chains does not allow one polymer chain to fully complex one polymer chain, resulting in many uncompensated charges. The NaCl present during the capsule preparation will compensate for these uncompensated charges. The difference between the LCST of pure PNIPAM in the bulk and inside the capsules arises from the increased order of the structure of the water inside the polyelectrolyte capsule wall [17]. The result is that either the capsule wall components or their complement are structuring the water, which brings about a 2°C difference in the collapse temperature of the encapsulated and bulk PNIPAM.

4.5 PNIPAM as an absorption and release agent

It has been shown that PNIPAM can absorb a substance in its hydrophilic state. After PNIPAM is heated, PNIPAM becomes more hydrophobic and can release the absorbed substance [18]. Methylene Blue has often been suggested as a candidate for the absorption on a PNIPAM network and the subsequent release after heating. To test this effect on PNIPAM encapsulated via the “ship in a bottle” method, unlabelled PNIPAM was synthesized inside the capsules according to the previous procedure discussed above, but without the MRho. A large excess of Methylene Blue was added to the capsule suspension and left overnight. After incubation of the capsules in the Methylene Blue suspension, the capsules were centrifuged and washed until the supernatant was clear. These capsules were imaged with confocal microscopy, and when viewed with the confocal microscope the capsules were a purple-blue color, a result of the Methylene Blue absorption. An image of this is not shown, since the main excitation of Methylene Blue is 663 nm, and there is no suitable laser line available to excite at this wavelength. After the capsules were heated the intensity of the color inside the capsules decreased, but the capsule was never colorless again. This effect of the release of Methylene Blue

from the capsules was tested with UV absorption spectroscopy. Unfortunately, the concentration was never high enough to measure the amount released from the capsule. To have an understanding of how much Methylene Blue would be released from a capsule system, the release of Methylene Blue was measured with a membrane. PNIPAM from Aldrich was dissolved to have a concentration of 0.5M. To this a large excess of Methylene Blue was added and left overnight for incubation. The PNIPAM-Methylene Blue solution was put inside a membrane with a molecular cutoff of 4500 Da. This was exhaustively dialyzed until no Methylene Blue diffused from the membrane. At this point the membrane was introduced to water above the LCST of the membrane. Immediately the solution inside the membrane turned from a translucent blue to a cloudy blue, denoting the collapse of the PNIPAM. The release of Methylene Blue was followed with UV absorption spectroscopy. The graph below shows the release.

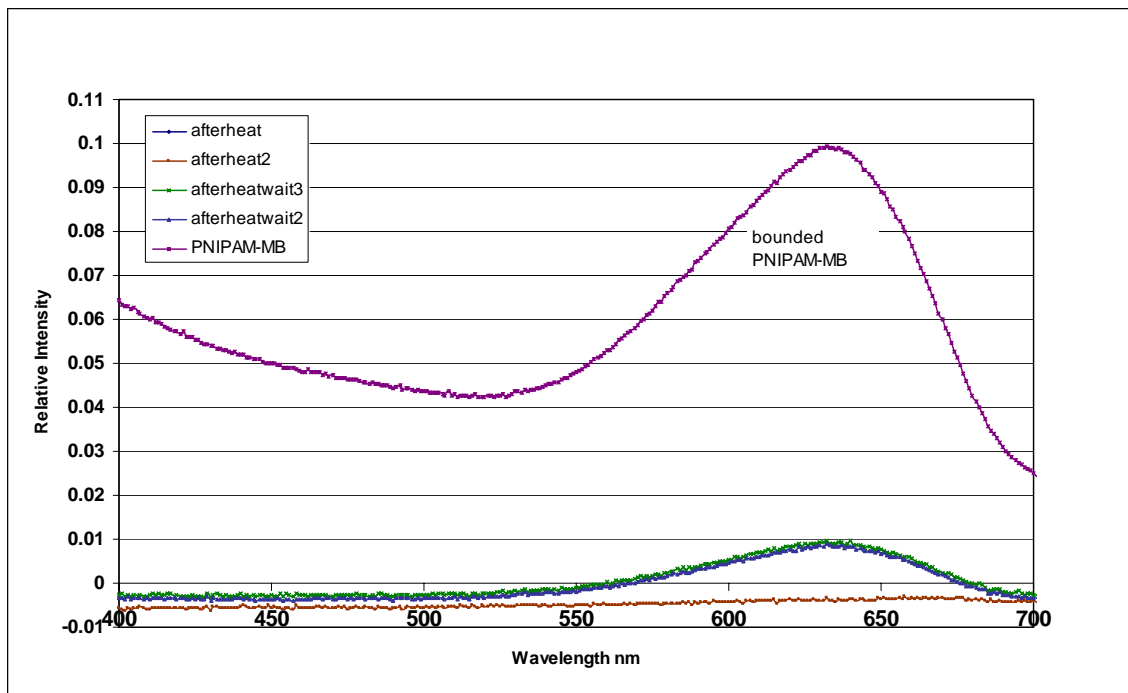


Figure 4.5.1 Release of Methylene Blue from a membrane. See text.

In Figure 4.5.1 the red curve represents the absorption spectra of the water one hour after the collapse was observed inside the membrane. The blue curve represents the spectra after the membrane had been in the heated water one night; the green curve shows

the spectra measured after one day in the water bath. The purple curve is the spectra if the membrane is broken and the solution inside the membrane is measured. From the curves it can be deduced that some of the Methylene Blue was released, but only a small amount. This confirms that a large amount could be absorbed in the capsules, but only a small amount was released. Guilherme et. al state that the Methylene Blue is absorbed on the PNIPAM network and that incomplete release occurs because of hydrophobic nature of the dye. Guilherme et. al suggests using a new, more hydrophilic, dye, Orange II [19]. To compare Orange II in our system to Methylene Blue an excess of Orange II was added to the suspension of capsules with PNIPAM encapsulated via the “ship in a bottle”. Like the Methylene Blue, Orange II was left overnight to absorb. Then the capsules were repeatedly washed. The sediment of the capsules was orange. Upon imaging with confocal microscopy it could be seen that the Orange II was leaking from the capsule. This was also confirmed with Orange II in a dialysis bag. Orange II was left with free PNIPAM overnight and then placed in a dialysis membrane. Much of the dye was released initially, due to the diffusion of the non-bound Orange II to PNIPAM. After that the diffusion was slower but never stopped until the solution inside the dialysis membrane became clear, indicating that all the Orange II was released. In an attempt to keep the Orange II inside the capsules, the matrix capsule of the capsules templated on the CaCO_3 were tried (this will be discussed below).

FITC was used to test the accumulation of capsules with PNIPAM encapsulated via co-synthesis with non-filled capsules. It was added to these samples shown in Figures 4.5.2 and 4.5.3. In both cases the FITC permeated after some time and aggregated inside the capsule. The FITC accumulated inside both the “empty” (top row) and the filled capsule (bottom row). Due to the porous structure of the core, the PAH/ PSS penetrates inside the core; when the core is removed, a matrix structure results. Then when a charged dye like FITC is added to the solution, the dye will accumulate inside the capsule. This effect is shown in the following figures.

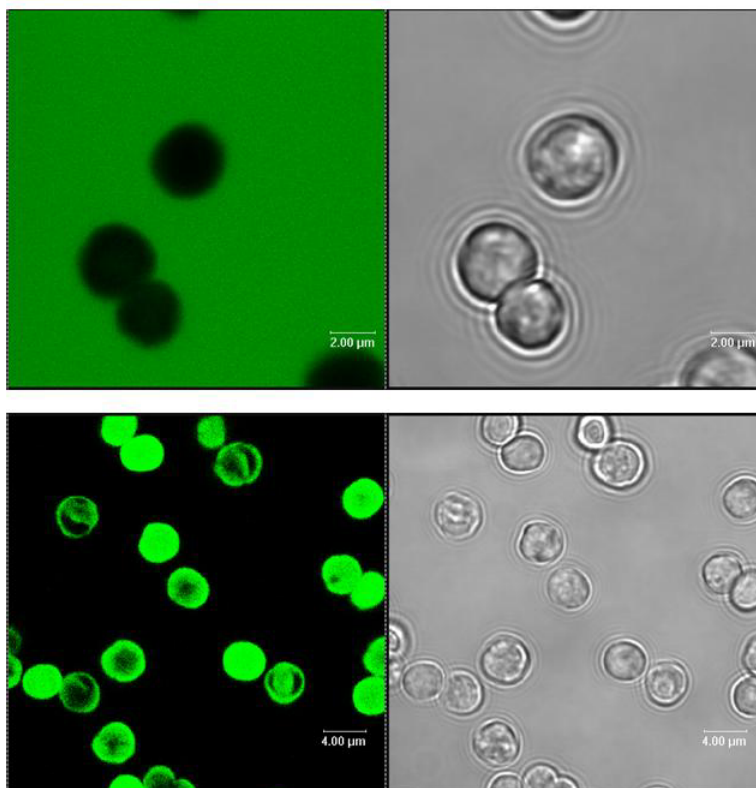


Figure 4.5.2 Confocal images of (PAH/PSS)₄ capsules from CaCO₃ cores with FITC.

Comparing the “empty” capsule and the capsules templated on co-synthesized cores, one concludes that the dye is spread inside and seems to have a strong bond with the inner material. Also, if one looks at the transmission image, the picture of the “filled” capsule appears darker, which could denote the presence of PNIPAM.

Figures 4.5.2 and 4.5.3 show pictures of FITC added to CaCO₃ capsules. These images were obtained by putting a drop of suspension onto a glass slide. To this a drop of FITC was added. In both figures the top image is taken shortly after the addition of FITC. The bottom picture of the figure set was taken after 10 minutes. Just like in section 4.2 the dye accumulates inside the capsules.

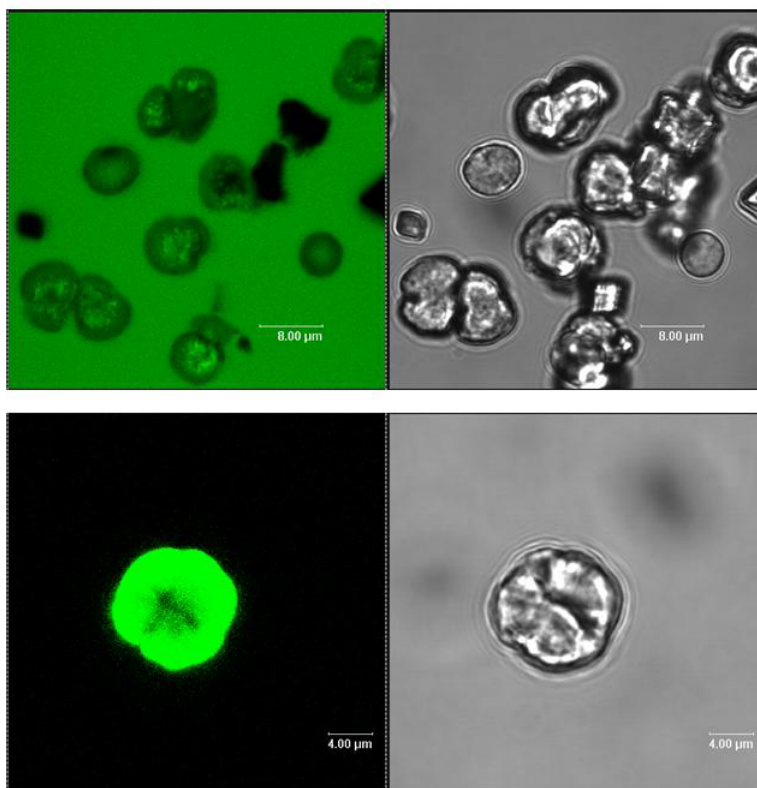


Figure 4.5.3 Confocal images of (PAH/PSS)₄ capsules from CaCO₃ cores with encapsulated PNIPAM with FITC.

Orange II was proposed in literature as a probe that is released upon heating. Like the capsules with PNIPAM encapsulated by the “ship in a bottle” method, the capsules with PNIPAM encapsulated via co-synthesis were added to a solution with a large excess of Orange II left overnight and then washed. The resulting capsules are presented in Figures 4.5.4 and 4.5.5.

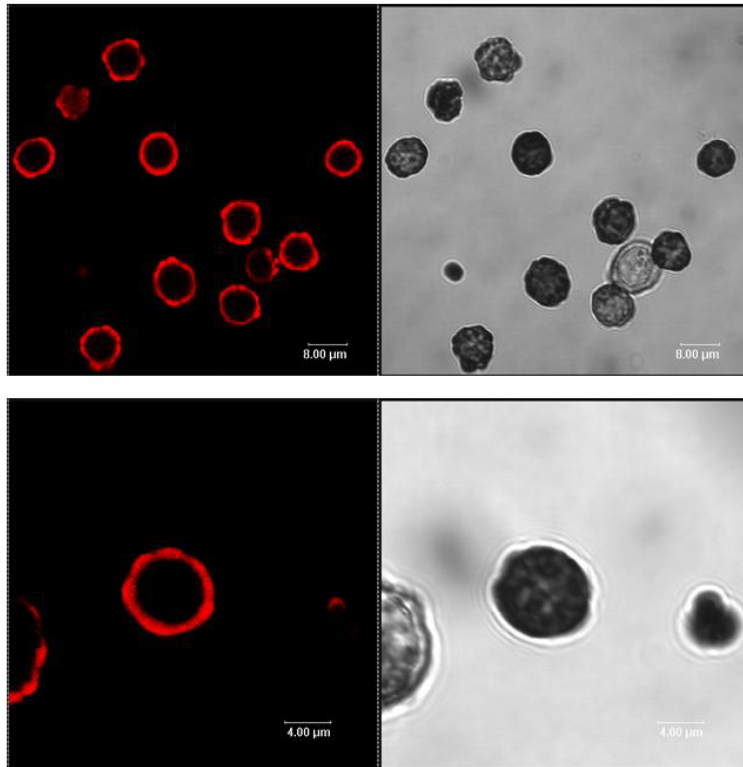


Figure 4. 5. 4 CaCO_3 encapsulated PNIPAM (PSS/PAH)4 treated with Orange II overnight and washed until supernatant was clear

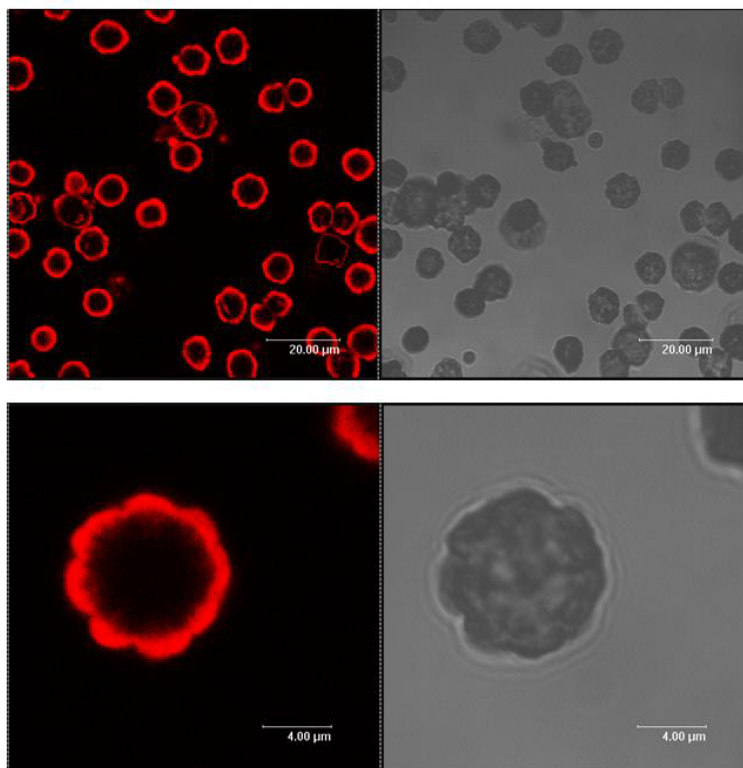


Figure 4. 5. 5 CaCO_3 encapsulated PNIPAM (PSS/PAH)4 added to microscope slide

The capsules presented in Figure 4.5.4 and 4.5.5 look similar, in that the Orange II fluorescing only from the wall. The capsules left in Orange II overnight appear to be darker in the transmission image, which could denote a higher Orange II content. There are most likely two reasons for this. First, because of the sulfonate function on the dye, it will bind preferentially to the charged PAH in the capsule wall and in the matrix structure left in the wall. Secondly, the dye that did absorb was probably released during the washing process. Due to the polar nature of Orange II if the concentration gradient is favorable it will break its hydrogen bond with the PNIPAM and release into the water outside of the membrane. Rhodamine absorption on the PNIPAM network (co-synthesis) was carried out, in an attempt to match results achieved by Quinn et al [20]. They showed the absorption and release of Rhodamine from a film including PNIPAM that released the dye after heating. In the case of the capsules the Rhodamine absorbed, but never released.

As has been shown, many attempts were made to absorb and release a dye from the PNIPAM network. To date none have been completely successful. In the case of the co-synthesis capsules the presence of the matrix definitely affects the properties of the PNIPAM. But this not the case for the “ship in a bottle” capsules. The inability to reproduce literature results lies more likely on an only partially understood system in the literature. In the case of Methylene Blue it was shown that Orange II would be a better candidate due to the hydrophobic nature of Methylene Blue. In the case in Orange II and Rhodamine, the systems were probably not in equilibrium at the point of heating the PNIPAM to release the dye. In the case of Orange II, when the concentration gradient favors the release the PNIPAM network, it will occur. In the case of the reported Rhodamine release, it appears that the authors in fact observed the release of the non-bound slowly diffusing Rhodamine.

4.6 Effect of salt on the LCST of PNIPAM

The Hofmeister series organizes cations and anions according to their chaotropic and kosmotropic abilities on the structure of water. It was first investigated in 1888 by Hofmeister [21] who found that different ions that make up salts do not behave the same when mixed with egg white proteins. In fact depending on the ions involved, different precipitation concentrations were found. The Hofmeister series has recently experienced a rebirth of interest, so much so that it was the topic of the whole August 2004 issue of *Current Opinion in Colloid & Interface Science*, including translations of the major papers from the original German text [22]. Recently Hofmeister ion investigations have been done on planar LbL films studying the thickness of the resulting films [23]. The anion series is $\text{ClO}_4^- > \text{SCN}^- > \text{I}^- > \text{NO}_3^- > \text{Br}^- > \text{Cl}^- > \text{CH}_3\text{COO}^- > \text{HCOO}^- > \text{F}^- > \text{OH}^- > \text{HPO}_4^{2-} > \text{SO}_4^{2-}$. Taking Cl^- as a middle point, ions to the left are chaotropic or water structure breaking. Ions to the right are kosmotropic or water structure making, and the effect of anions is more pronounced than that of cations [24].

PNIPAM is a polymer whose solubility in water is highly sensitive and dependent on the hydrogen bond it can make with water. The addition of salt or ions interrupts the structure of water and therefore impedes the ability of PNIPAM to form hydrogen bonds. The hydrogen bond of PNIPAM to water is also disrupted when the temperature is increased. If one adds enough salt to a PNIPAM solution it will collapse even at room temperature. This is what is observed in the cases of encapsulated PNIPAM in the presence of 1M NaCl. Moreover, if the salt concentration is decreased the collapse temperature increases, proving that the solubility of PNIPAM in water is highly dependent on temperature and salt concentration [25,26]

The supernatant of the PNIPAM was measured with DSC after dialysis, freeze drying, and dissolution in water to approximately the same concentration inside the capsules. The same amount of PNIPAM-MRho dissolved in the individual salt solution was added to every DSC measuring pan. The DSC graphs are shown in Figure 4.6.1. The height of the peaks can be compared not only because the scale on every graph is the

identical, but also because the amount added to the measurement pan was the same. In every graph two peaks are observed the first peak around 2°C is ice melting. The second peak denotes the LCST of the polymer at that salt concentration.

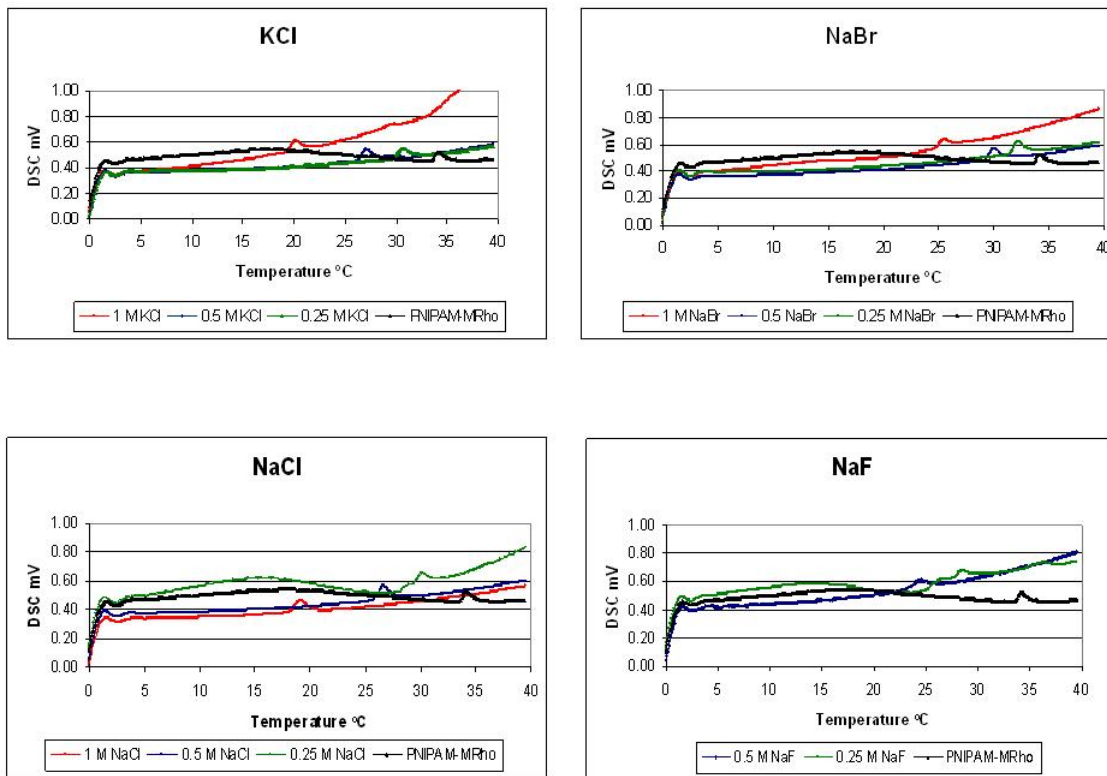


Figure 4.6.1 DSC of bulk PNIPAM with different ions and concentrations.

The LCST of bulk and encapsulated PNIPAM with different ions was investigated with DSC and confocal microscopy respectively. The observed LCST are presented in Figure 4.6.2 (Note that the collapse temperatures of PNIPAM in capsules are decreased by 5 degrees for clarity). The addition of 1M salt - independent of type - caused the collapse of the encapsulated PNIPAM at room temperature, which was around 22°C.

To observe the online heating of the capsules equal amounts of PNIPAM-filled capsule suspension (volume-wise) were added to 2M, 1M and 0.5M salt. This made an overall salt concentration of 1M, 0.5M and 0.25M respectively. A glass slide was placed atop of the capsule/salt mixture. The heating plate was then placed on top of the glass side.

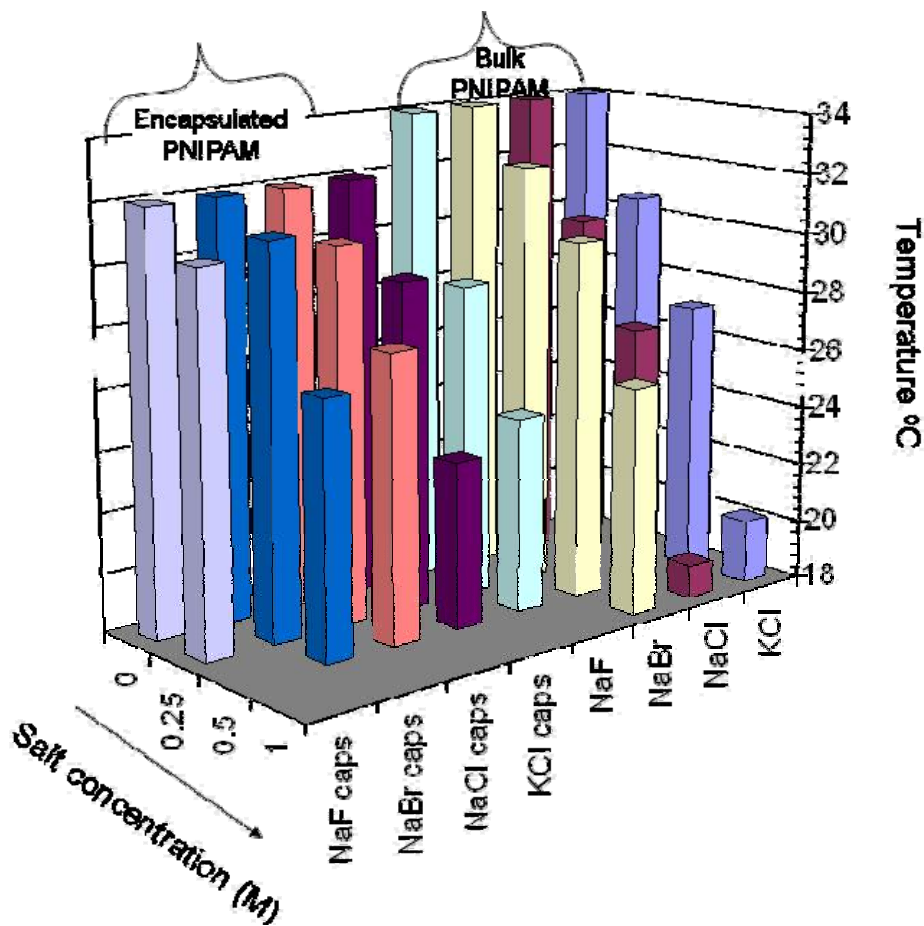


Figure 4.6.2: Dependence of LCST of PNIPAM with various concentrations of different salts.

NaCl

When comparing the bulk LCST (from DSC) with the literature value one realizes that the effect caused by NaCl on the LCST is the same as that presented by Yang et al [25], i.e., the change in the bulk LCST of 34.1 is decreased by 4°C, 7.4°C, and 15°C for 0.25, 0.5, and 1M NaCl, respectively. For the encapsulated PNIPAM, the collapse temperature in pure water is 32 °C with a decrease by 1.5 °C and 4.5 °C for 0.25, and 0.5 M NaCl, respectively, with a collapse below room temperature for 1M NaCl. The decrease in the efficiency of NaCl in collapsing the PNIPAM inside the capsules is a result of the presence of the capsule wall, which acts like a buffer, protecting the polymer. This will be discussed later.

NaBr

The collapse temperature of the PNIPAM is also extremely dependent on the type of ion used. In the case of NaBr the encapsulated PNIPAM exhibits similar behavior compared to NaCl, where the LCST decreases with increasing salt concentration; moreover, the fact that NaBr and NaCl demonstrate similar behavior is to be expected, due to their neighboring positions in the Hofmeister series. The observed LCST for encapsulated NaBr is decreased by 1 °C and 5.5 °C for 0.25, 0.5M NaBr respectively. Compared to results reported in the literature, the effect we observe is always larger than the reported change in collapse temperature being 1.9°C, 4.1°C, and 8.5°C for 0.25, 0.5, and 1M NaBr, respectively. [25,27]

NaF

In the case of NaF, -F is a smaller, harder, and more electronegative ion with a larger hydration shell compared to -Br and -Cl. Therefore -F has a higher capacity to disrupt hydrogen bonding of the PNIPAM. Exactly this is observed in the trend in the bulk. The LCST is significantly decreased in comparison to NaBr or NaCl. In the case of capsules with 1M and 0.5M NaF the PNIPAM inside the capsules collapsed below room temperature. However, at 0.25M NaF, the collapse temperature is decreased by only 1.5°C, which is similar to the effect of NaCl inside the capsules. This, again, is an effect of the capsule wall behaving as a buffer. In the case of the bulk the change in the LCST with respect to salt concentration is 5.6°C and 9.6°C for 0.25 and 0.5M NaF, respectively. In the case of 1M NaF the LCST could not be determined. This is agreement to what Zhang et al [27] found. They report that above 0.7M NaF the PNIPAM transition goes from a one- to a two-step process, making the LCST difficult to determine.

KCl

According to the Hofmeister series, anions should exhibit a stronger influence on the PNIPAM than the cation. Leaving the counterion -Cl the same, K⁺ was taken. As expected in the case of free PNIPAM, KCl has a very similar behavior, in which increasing the salt amount decreases the LCST. When comparing the effect of K⁺ to Na⁺ the effect is smaller. This is due to the larger interaction Na⁺ has than K⁺ [23]. The

collapse temperature in bulk is exactly what Freitag et al [28] present, except for the PNIPAM. Inside the capsule the LCST is changed by 3 and 8°C for 0.25M and 0.5M KCl, respectively. The observed effect for PNIPAM inside the capsule and in the bulk are similar, meaning that in the cases of cations the capsule wall does not provide much protection.

If the collapse temperatures of the encapsulated and bulk PNIPAM are compared, the trend of increased collapse temperature with decreasing salt concentration remains the same. However, the temperature at which it happens differs. Inside the capsule the PNIPAM collapse temperature is nearly the same for 0.25M. A possible explanation for this is that when salt is added to the capsule the ions tend to stay outside of the capsule wall in the polar environment. In bulk, the added salt distributes evenly throughout the solution. Inside the capsules with encapsulated PNIPAM, the environment is non-polar and the effective salt concentration is lower. With higher concentrations of added salt, the ion must go inside the capsule, giving the distinguishable Hofmeister effect of ion type on the LCST.

4.7 Comparison of encapsulation techniques

Three encapsulations methods were employed. The first method was the accumulation of dyes onto the matrix structure resulting from capsules templated on a porous CaCO₃ cores. The second technique was using the co-synthesis technique, and the third was the “ship in a bottle” method. In the second technique the presence of PNIPAM inside the CaCO₃ core resulted in a different core morphology. The third method is a much longer and involved process, but it results in a fully reversible thermo-responsive capsule. In the second method when 1M salt was added or when the capsules were heated the coil-to-globule-transition was never seen. Since the second method of encapsulation did not react to the given stimulus, it is difficult to really compare the two outside of Raman spectroscopy.

Figure 4.7.1 compares the Raman spectra from the second and third encapsulation methods, the PNIPAM purchased from Aldrich, the CaCO_3 cores with PNIPAM and (PSS/PAH) capsules. The sharp increase in the signal in the purchased PNIPAM at 3200 cm^{-1} and decrease at 600 cm^{-1} is due to the shutter. Previously, other authors have identified PNIPAM with the CH_2 vibrations at 1453 cm^{-1} [29,30] and 2800 cm^{-1} [14]. It may, however, be better to use the peak associated with the amide motive at 1600 cm^{-1} . This peak is more specific to PNIPAM and shows up in the PS capsules (“ship in a bottle”) and in the purchased PNIPAM lines. From this peak at 1600 cm^{-1} it is certain that PNIPAM is inside the capsules templated on PS cores. But this is not so evident in the capsules templated on CaCO_3 cores. Another area that could be scrutinized to prove the presence of PNIPAM in the capsules is the large band between 3200 and 3600 cm^{-1} . This band is associated with the $-\text{OH}$ stretch from water but also could denote the presence of hydrogen bonds, and can be seen in the purchased PNIPAM sample as well as in the capsules templated on co-precipitated CaCO_3 capsules. The purchased PNIPAM shows this band despite the fact that the dry powder was measured. The presences of the band could arise from the PNIPAM forming hydrogen bonds with the moisture in the air. The PSS/PAH capsules show this band, but has a later onset.

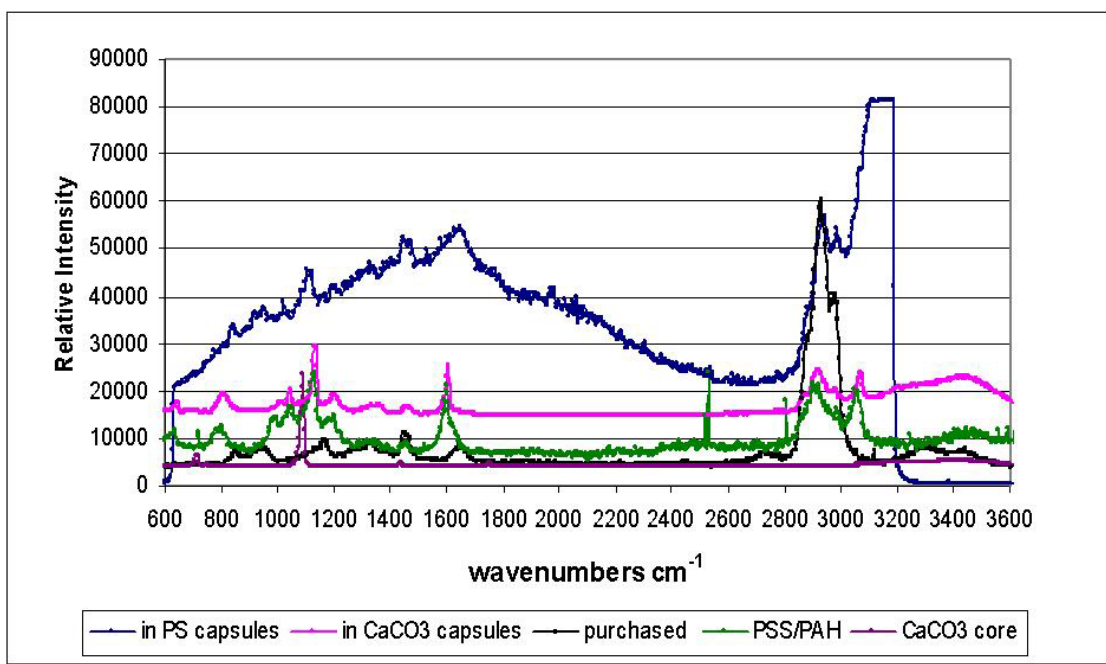


Figure 4.7.1 Raman Spectroscopy of PNIPAM encapsulated in capsules templated on CaCO_3 cores and PS cores.

Raman spectroscopy gives a proof that the “ship in a bottle” encapsulation method was successful in that PNIPAM was incorporated into the multilayer capsules. In the case of the co-precipitated CaCO_3 capsules, the Raman gives a hint that PNIPAM could be inside the capsules. However, due to the matrix residual structure inside the capsules templated on CaCO_3 the PNIPAM does not collapse, rendering this technique not useful for drug delivery applications. To have definite proof of the presence of the PNIPAM inside the co-precipitated CaCO_3 capsules, one could do MALDI-TOF mass spectroscopy. In light of this the third encapsulation method is better, since it has a fully reversible, thermo-sensitive active agent inside the multilayers.

4.8 Conclusions

In summary, we demonstrated a novel approach for fabricating polyelectrolyte microcapsules containing a gel-like polyelectrolyte matrix. The process of consecutive polyelectrolyte adsorption applied to porous calcium carbonate microparticles as templates results in polyelectrolyte matrix formation within the templating particles due to permeation of polyelectrolytes into porous micros supports during the LbL assembling procedure. After core decomposition, the formed microcapsules have a matrix-type structure consisting of an inner porous polyelectrolyte network. We demonstrated that the encapsulation of a macromolecule, such as dyes, can be performed by adsorption into this matrix within the polyelectrolyte capsules. Microcapsule morphology, structure, and adhesion capacity for entrapping macromolecules are influenced by a number of polyelectrolyte adsorption procedures used for capsule preparation. Encapsulation of macromolecules is presumably based on electrostatic interaction between macromolecules and free charges of the polyelectrolyte complex inside the capsules.

PNIPAM was successfully encapsulated into a polyelectrolyte microcapsule the “ship in a bottle” method. This confined PNIPAM maintained its thermo-responsive properties in micron-sized capsules. With different types and concentrations of ion, we

prove the ability to control and tune the LCST inside the capsule. The transition temperature inside the capsule differs from that of the bulk due to the presence of the capsule wall, but still follows the trend of lower LCST with higher salt concentration.

References

- 1 Peyratout, C. S.; Dähne, L., Tailor-made polyelectrolyte microcapsules: From multilayers to smart containers. *Angewandte Chemie, International Edition* **2004**, 43, (29), 3762-3783.
- 2 Antipov, A. A.; Sukhorukov, G. B.; Donath, E.; Möhwald, H., Sustained Release Properties of Polyelectrolyte Multilayer Capsules. *Journal of Physical Chemistry B* **2001**, 105, (12), 2281-2284.
- 3 Ai, H.; Jones, S. A.; de Villiers, M. M.; Lvov, Y. M., Nano-encapsulation of furosemide microcrystals for controlled drug release. *Journal of Controlled Release* **2003**, 86, (1), 59-68.
- 4 Trubetskoy, V. S.; Loomis, A.; Hagstrom, J. E.; Budker, V. G.; Wolff, J. A., Layer-by-layer deposition of oppositely charged polyelectrolytes on the surface of condensed DNA particles. *Nucleic Acids Research* **1999**, 27, (15), 3090-3095.
- 5 Volodkin, D. V.; Balabushevitch, N. G.; Sukhorukov, G. B.; Larionova, N. I., Model system for controlled protein release: pH-sensitive polyelectrolyte microparticles. *STP Pharma Sciences* **2003**, 13, (3), 163-170.
- 6 Donath, E.; Sukhorukov, G. B.; Caruso, F.; Davis, S. A.; Möhwald, H., Novel hollow polymer shells by colloid-templated assembly of polyelectrolytes. *Angewandte Chemie, International Edition* **1998**, 37, (16), 2202-2205.
- 7 Sukhorukov, G. B.; Antipov, A. A.; Voigt, A.; Donath, E.; Möhwald, H., pH-controlled macromolecule encapsulation in and release from polyelectrolyte multilayer nanocapsules. *Macromolecular Rapid Communications* **2001**, 22, (1), 44-46.
- 8 Radtchenko, I. L.; Sukhorukov, G. B.; Loporatti, S.; Khomutov, G. B.; Donath, E.; Möhwald, H., Assembly of alternated multivalent ion/polyelectrolyte layers on colloidal particles. Stability of the multilayers and encapsulation of macromolecules into polyelectrolyte capsules. *Journal of Colloid and Interface Science* **2000**, 230, (2), 272-280.
- 9 Dähne, L.; Loporatti, S.; Donath, E.; Möhwald, H., Fabrication of micro reaction cages with tailored properties. *Journal of the American Chemical Society* **2001**, 123, (23), 5431-5436.
- 10 Antipov, A. A.; Shchukin, D.; Fedutik, Y.; Petrov, A. I.; Sukhorukov, G. B.; Möhwald, H., Carbonate microparticles for hollow polyelectrolyte capsules fabrication. *Colloids and Surfaces, A: Physicochemical and Engineering Aspects* **2003**, 224, (1-3), 175-183.

- 11 Voron'ko, Y. K.; Dzhurinskii, B. F.; Kokh, A. E.; Sobol', A. A.; Shukshin, V. E., Raman spectroscopy and structure of InBO₃. *Inorganic Materials* **2005**, 41, (9), 984-989.
- 12 Zhanpeisov, N. U.; Ohta, K.; Kajimoto, S.; Hobley, J.; Hatanaka, K.; Fukumura, H., Density functional theory study of the origin of IR and Raman band shifts in H-bond complexes of triethylamine with water. *International Journal of Quantum Chemistry* **2005**, 105, (4), 376-386.
- 13 Leporatti, S.; Voigt, A.; Mitlohner, R.; Sukhorukov, G.; Donath, E.; Möhwald, H., Scanning force microscopy investigation of polyelectrolyte nano- and microcapsule wall texture. *Langmuir* **2000**, 16, (9), 4059-4063.
- 14 Maeda, Y.; Mochiduki, H.; Yamamoto, H.; Nishimura, Y.; Ikeda, I., Effects of ions on two-step phase separation of poly(vinyl methyl ether) in water as studied by IR and Raman spectroscopy. *Ibid.* **2003**, 19, (24), 10357-10360.
- 15 Colthup, N.; Daly, L. H.; Wiberley, S. E., Introduction to Infrared and Raman Spectroscopy. 2nd Ed. ed.; **1975**; 'Vol.' p 544 pp.
- 16 Ibarz, G.; Dähne, L.; Donath, E.; Möhwald, H., Controlled permeability of polyelectrolyte capsules via defined annealing. *Chemistry of Materials* **2002**, 14, (10), 4059-4062.
- 17 Shchukin, D. G.; Möhwald, H., Urea Photosynthesis inside Polyelectrolyte Capsules: Effect of Confined Media. *Langmuir* **2005**, 21, (12), 5582-5587.
- 18 Sershen, S. R.; Westcott, S. L.; Halas, N. J.; West, J. L., Temperature-sensitive polymer-nanoshell composites for photothermally modulated drug delivery. *Journal of Biomedical Materials Research* **2000**, 51, (3), 293-298.
- 19 Guilherme, M. R.; Silva, R.; Giroto, E. M.; Rubira, A. F.; Muniz, E. C., Hydrogels based on PAAm network with PNIPAAm included: hydrophilic-hydrophobic transition measured by the partition of Orange II and Methylene Blue in water. *Polymer* **2003**, 44, (15), 4213-4219.
- 20 Quinn, J. F.; Caruso, F., Thermoresponsive nanoassemblies: Layer-by-layer assembly of hydrophilic-hydrophobic alternating copolymers. *Macromolecules* **2005**, 38, (8), 3414-3419.
- 21 Hofmeister, F. *Arch. Exp. Pathol. Pharmacol.* **1888**, 24, 247-260.
- 22 Kunz, W.; Henle, J.; Ninham, B. W., 'Zur Lehre von der Wirkung der Salze' (about the science of the effect of salts): Franz Hofmeister's historical papers. *Current Opinion in Colloid & Interface Science* **2004**, 9, (1-2), 19-37.
- 23 Von Klitzing, R.; Wong, J. E.; Jaeger, W.; Steitz, R., Short range interactions in polyelectrolyte multilayers.. *Current Opinion in Colloid & Interface Science* **2004**, 9, (1-2), 158-162.
- 24 Salomaki, M.; Tervasmaki, P.; Areva, S.; Kankare, J., The Hofmeister anion effect and the growth of polyelectrolyte multilayers. *Langmuir* **2004**, 20, (9), 3679-3683.
- 25 Yang, Y. Y.; Zeng, F.; Tong, Z.; Liu, X. X.; Wu, S. Z., Phase separation in poly(N-isopropyl acrylamide)/water solutions. II. Salt effects on cloud-point curves and gelation. *Journal of Polymer Science Part B-Polymer Physics* **2001**, 39, (9), 901-907.
- 26 Park, T. G.; Hoffman, A. S., Sodium Chloride-Induced Phase-Transition in Nonionic Poly(N-Isopropylacrylamide) Gel. *Macromolecules* **1993**, 26, (19), 5045-5048.

- 27 Zhang, Y.; Furyk, S.; Bergbreiter, D. E.; Cremer, P. S., Specific Ion Effects on the Water Solubility of Macromolecules: PNIPAM and the Hofmeister Series. *Journal of the American Chemical Society* **2005**, (127), 14505- 14510.
- 28 Freitag, R.; Garret-Flaudy, F., Salt effects on the thermoprecipitation of poly-(N-isopropylacrylamide) oligomers from aqueous solution. *Langmuir* **2002**, 18, (9), 3434-3440.
- 29 Appel, R.; Xu, W.; Zerda, T. W.; Hu, Z., Direct Observation of Polymer Network Structure in Macroporous N-Isopropylacrylamide Gel by Raman Microscopy. *Macromolecules* **1998**, 31, (15), 5071-5074.
- 30 Appel, R.; Zerda, T. W.; Wang, C.; Hu, Z., Direct observation of interfacial profiles of polymer gels during the phase transition by Raman microimaging. *Polymer* **2001**, 42, (4), 1561-1566.

Chapter 5- Polyelectrolyte multilayer permeability alteration with wax particles

5.1 Introduction

As shown in Chapter 2, the films produced by the LbL method are soft materials which are sensitive to atmospheric humidity and other environmental conditions such as high and low pH or high ionic strength. This environment- sensitive behavior may cause the denaturation or the destruction of the film, which is disadvantageous for specific applications requiring the stability of the internal structure of the film. The diffusion of small molecules in the assembly can also be detrimental for active compounds included in the layers: One example is the diffusion of urea into myoglobin-containing multilayers reported to denature the protein [1]. In this context, different routes were investigated to improve the stability of LbL assemblies: The subsequent cross-linking of polyelectrolyte chains was employed to stabilize the internal structure of the multilayers [1,2,3,4,5,6]. The resulting films were shown to be resistant toward extreme environments, but they are still permeable for the small molecules. Moreover, cross-linking requires the presence of specific reactive moieties on polyelectrolyte chains, which may limit the versatility of the LbL technique. Another alternative consists of adsorbing a hydrophobic layer atop the films, presumably leading to a reduction of their sensitivity to water and to other small polar species. In addition, the ability of the films to prevent permeation of small hydrophilic molecules may be increased. In analogy to biological membranes, uniform lipid bilayers were deposited on polyelectrolyte multilayers [6,7,8]. These lipid layers

were shown to efficiently prevent the diffusion of small molecules in the films. However, these coatings are well-known to be unstable under mechanical stress or drying. Recently, Rouse and Ferguson [9] showed that the incorporation of uncharged, nonpolar polymers in multilayers from organic solutions strongly effects their swelling ability in a humid atmosphere.

This chapter presents a new route to improving the stability of polyelectrolyte multilayers with respect to water diffusion. This method consists of the adsorption of negatively-charged wax particles from aqueous solution atop the multilayers. The subsequent annealing of the self-assembly provides the formation of a uniform hydrophobic barrier layer. The adsorption and the fusion of wax particles have been tested on flat and spherical substrates as self-assemblies consisting of poly(allylamine hydrochloride) (PAH) and poly-(styrene sulfonate) (PSS).

Native multilayer films on spherical substrates have pores that are holes created during core dissolution, which make these films only semi-impermeable. The capsules are permeable for small dye molecules or water, but are impermeable for large molecules like polymers. Therefore, to be able to encapsulate a smaller molecule of interest for controlled delivery, the capsule needs to have a way to close the holes or pores in the film to seal in the material of interest.

5.2 Wax Particle Characterization

The wax particles used in this investigation were received as a gift from Keim-Additec GmbH (Kirchberg, Germany). The table below details the particles received and the properties relevant to this work. The exact details of the wax particle composition are proprietary information. But investigations were performed to determine the basic properties of interest in this study, the size, the charge and the melting temperature. The properties are shown in Figure 5.2.1. Figure 5.2.2 is a DSC graph of the wax particles. The peak denotes the melting temperature.

Name	Name	Size (nm)	Charge (mV)	Melting Temperature °C
Ultralube E-337	337	268.8	42	59
Ultralube E-022	022	332.8	48	45
Ultraprob E-359	- wax	72	67	57

Figure 5.2.1 Wax types and their properties

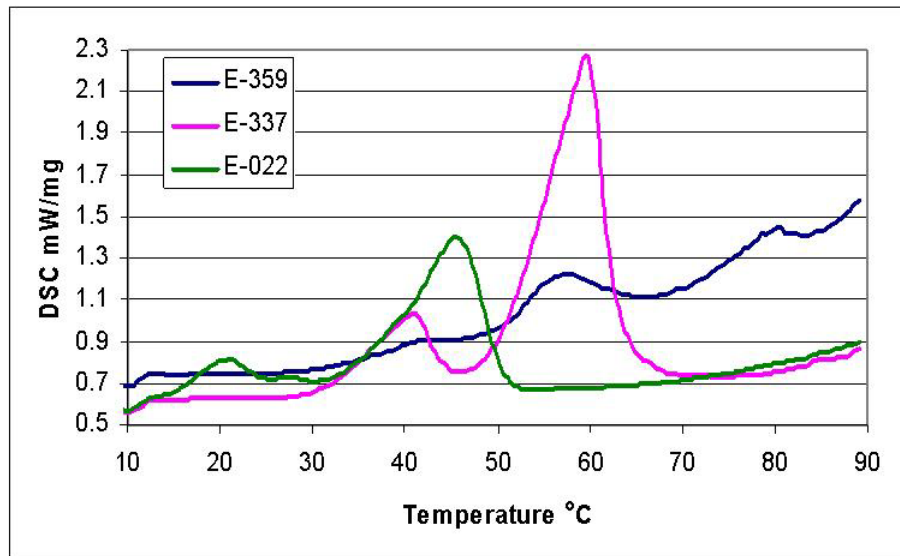


Figure 5.2.2 DSC of wax particles. The peaks denote the melting temperature of the wax.

5.3 Flat films

Preparation

The substrates used were one side-polished $\langle 100 \rangle$ silicon wafers from Silchem Handelsgesellschaft GmbH (Freiberg, Germany) cut into rectangles of 3 cm x 1 cm and two-sides-polished 8 cm x 5 cm x 1.5 cm $\langle 100 \rangle$ silicon blocks from Siliciumbearbeitung Andrea Holm (Tann/Ndb., Germany) for multilayer growth and NR experiments, respectively. The wafers were first cleaned by treatment in a hot piranha solution [H₂O₂ (30%)/H₂SO₄ (98%) 1:1 v/v] for 20 min (*caution: piranha solution is extremely*

corrosive) and then thoroughly washed with pure Milli-Q water. Polyelectrolyte multilayers were self-assembled by alternately dipping the substrate into aqueous solutions of the cationic PAH (4 mg/mL in 0.5M NaCl) and the anionic PSS (4 mg/mL in 0.5 M NaCl) for 15 min each. Note that the first layer adsorbed on the silicon wafer is PAH. After each dip, the substrate was rinsed by immersion into three beakers of pure Milli-Q water for 2 min. After the deposition of the required number of PAH/PSS bilayers, the sample with a PAH end layer was dipped in the suspension of negatively charged wax particles (3% w/w in water) for 15 min, then rinsed three times in pure Milli-Q water, and when the assembly was complete, dried with nitrogen. Such self-assemblies will be designated as (PAH/PSS) $_n$ /wax bilayers in the following. The subscript n refers to the number of PAH/PSS bilayers deposited on the silicon substrate.

Results

(PAH/PSS) $_6$ and (PAH/PSS) $_{7.5}$ were assembled on a silicon wafer. The thickness of the film was determined in air with a null ellipsometer. A film refractive index of 1.54 was assumed to determine the thickness of the films. Because the refractive index of wax is about 1.48, the total film thickness determined by ellipsometry is slightly underestimated when a layer of wax is present atop the polyelectrolyte multilayer. Figure 5.3.1 illustrates the principle of controlling the permeability of flat films by creating a barrier layer with wax particles.

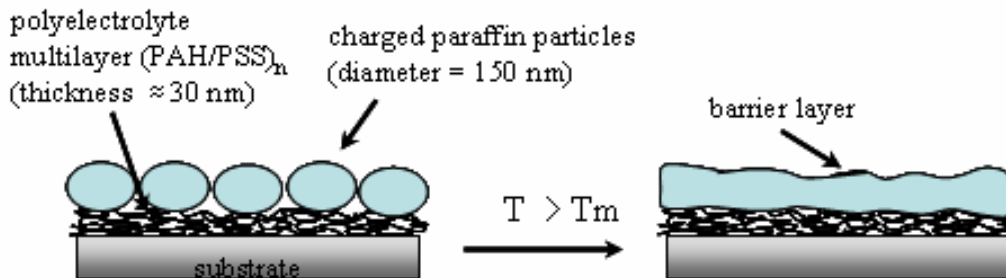


Figure 5.3.1 Schematic representation of the formation of a uniform hydrophobic barrier layer of paraffin atop the polyelectrolyte multilayer.

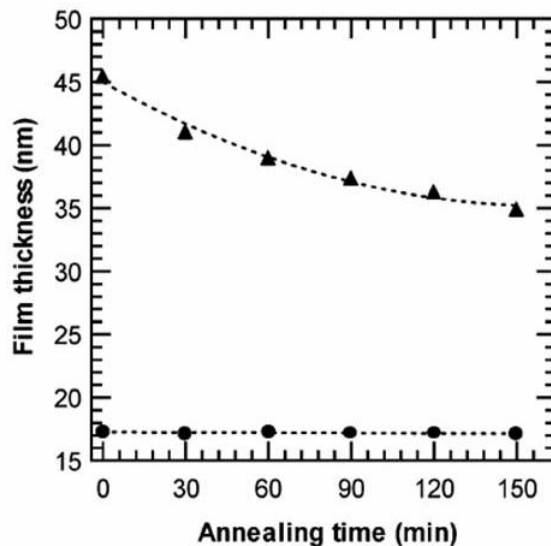


Figure 5.3.2 Variation of the ellipsometric thickness of the (PAH/PSS)₆ (circles) and (PAH/PSS)_{7.5}/wax (triangles) samples with annealing time. Lines are added to guide the eye.

In Figure 5.3.2 one should immediately notice that the film with wax is much thicker than without wax. This thickness increase cannot be attributed to the additional polyelectrolyte layers. It is due to the fact that the particles are much larger than the already absorbed layers. The second feature that one should notice is that the overall thickness decreases with time in the case of the layers with wax atop the film, whereas the polyelectrolyte film thickness remains constant.

To study the D₂O distribution within the multilayers, specular neutron reflectivity was used. As a result of the sensitivity of NR to deuterium, a direct view of the laterally averaged concentration in heavy water along a line perpendicular to the film surface is provided. The reflectivity curves of the (PAH/PSS)_{9.5} and (PAH/PSS)_{9.5}/wax multilayers before and after annealing, measured in the dry state, are shown in Figure 5.3.3a. The SLD profiles computed from the best fits of the experimental data are shown in Figure 5.3.3b. In these measurements performed in air, no significant difference was observed between the wax-coated and wax-free films. This is due to the low SLD of the wax ($r \sim -4 \times 10^{-7} \text{ \AA}^{-2}$), which is close to that of the air; [10] consequently, the wax layer does not discriminate against air, and the profiles of wax-free and wax-coated films are very similar. From these profiles, the average thickness of the (PAH/PSS)_{9.5} part of the

film was determined to be about 26 nm. This value is slightly lower than that expected from previous ellipsometry measurements on thinner films as a result of the uncertainties in the refractive index of the film and the presence of the native oxide layer at the surface of the silicon wafer. The annealing does not lead to noticeable variations of the structure of the PAH/PSS part of the films. The reflectivity curves and SLD profiles of samples measured in D₂O are presented in Figure 5.3.4a Figure 5.3.4b, respectively. Kiessig fringes, which correspond to interferences resulting from multiple reflections at the interfaces, are more visible for wax-free films than for wax-coated films as a result of the considerable increase of the roughness of the surface after wax adsorption. For (PAH/PSS)_n films lacking the final wax coating, the value of the SLD increases after immersion in D₂O because of the sorption of D₂O molecules in the multilayer. This sorption results in the swelling of the polyelectrolyte film, whose thickness increases from 26 to 37 nm; from the average SLD of the film, the amount of D₂O in the film was estimated to be about 50%. In addition, for such films, no significant difference could be detected before and after annealing (Figure 5.3.3b, compare curves 1 and 2). These results confirm that the annealing process itself does not affect the swelling of the film by water, in agreement with previous reports by others [11].

In contrast, the amount of D₂O incorporated in the wax-covered unannealed sample is much lower and decreases with increasing proximity to the silicon substrate (Figure 5.3.4b, curve 3). This is more pronounced after annealing (Figure 5.3.4b, curve 4): the fusion of the wax particles now almost completely prevents the sorption of water in the film. Interestingly, for all films, water seems to be more excluded with closer proximity to the silicon substrate, possibly due to a difference in the structure of the film as postulated by others [12,13].

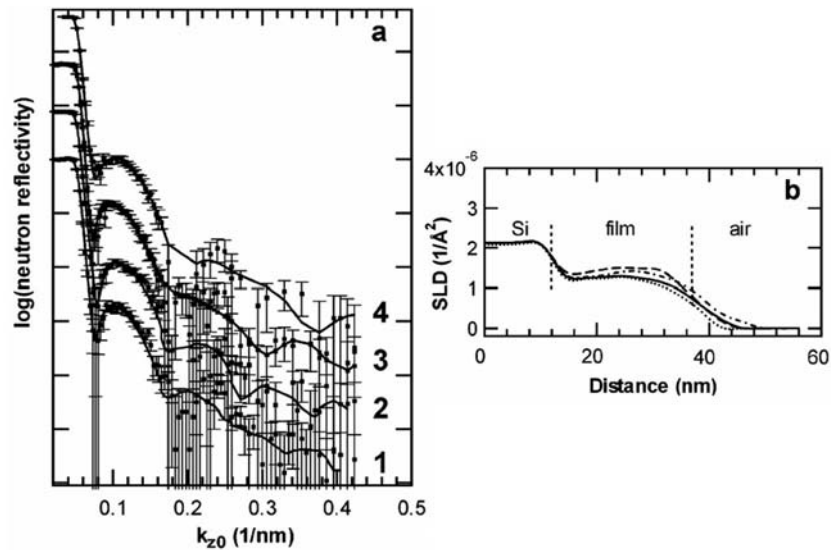


Figure 5.3.3 (a) Neutron reflectivity of multilayers measured in air: (PAH/PSS)9.5 unannealed (1), (PAH/PSS)9.5 annealed at 60 °C (2), (PAH/PSS)9.5/wax unannealed (3), and (PAH/PSS)9.5/wax annealed at 60 °C (4). Dots are experimental data, and lines are fits using the SLD profiles shown in part b. For clarity, curves have been displaced vertically. (b) The SLD profiles of (PAH/PSS)9.5 unannealed (continuous line), (PAH/PSS)9.5 annealed at 60 °C (dotted line), (PAH/PSS)9.5/wax unannealed (dotted and dashed line), and (PAH/PSS)9.5/wax annealed at 60 °C (dashed line).

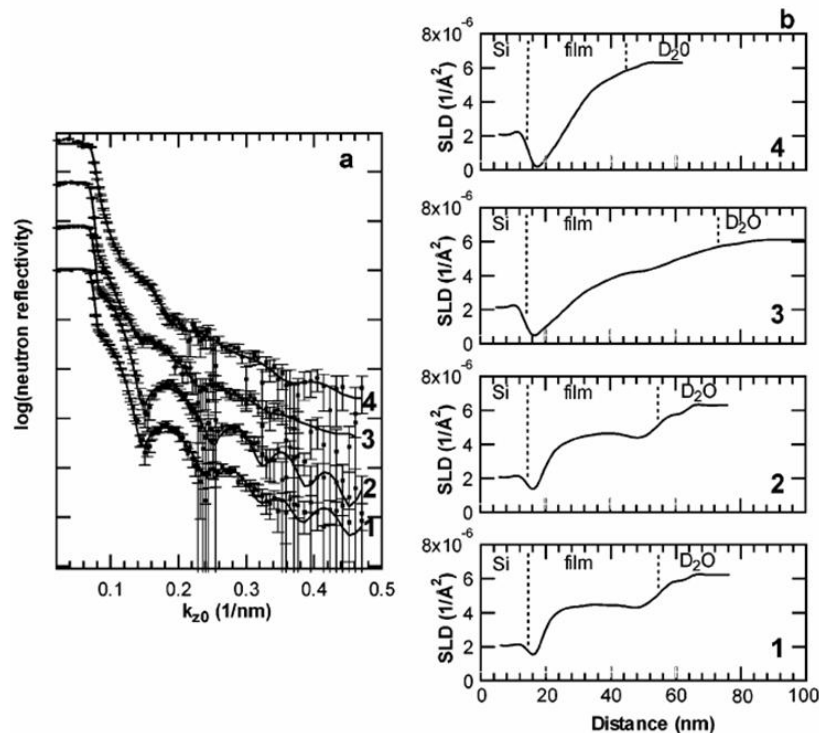


Figure 5.3.4 (a) Neutron reflectivity of multilayers measured in D₂O: (PAH/PSS)9.5 unannealed (1), (PAH/PSS)9.5 annealed at 60 °C (2), (PAH/PSS)9.5/wax unannealed (3), and (PAH/PSS)9.5/wax annealed at 60 °C (4). Dots are experimental data, and lines are fits using the SLD profiles shown in the right side. For clarity, curves have been displaced vertically. (b) Corresponding SLD profiles.

5.4 Capsules

In light of the ability to control the permeability of flat films, it was thought that this could be applied to control the permeability of capsules. To achieve this, three core types were implemented to test the resulting permeability the resulting capsules as the core type plays a large role in the capsule permeability: The effect of the core type is most seen in the dissolution process. The three core types investigated were CaCO_3 , MF, and PS.

To fabricate impermeable capsules the core was coated with PSS or PAH. Once all the polymer layers were deposited, the wax layer was added. If the layer of wax was added before the core removal it is referred to as method 1, and if the wax layer was added after the core was removed it is referred to as method 2.

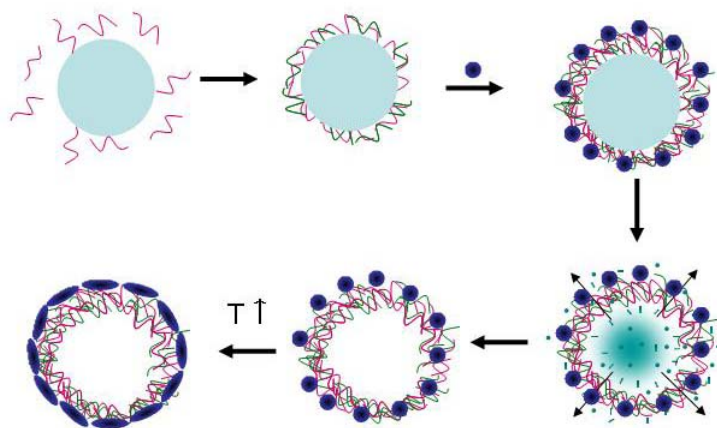


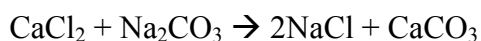
Figure 5.4.1 Scheme of capsule fabrication with wax layer via method 1.

5.4.1 Capsules- CaCO_3

Preparation

Capsules were prepared first on CaCO_3 cores as a model system because of their ease of synthesis and low cost. Various capsules were prepared with varying types of wax suspensions and charges. SEM provided a fast microscopic way to determine if the wax particles could be incorporated in the polyelectrolyte multilayer surface.

To prepare the CaCO₃ cores, an equal amount of 1 M Na₂CO₃ was added to 1M CaCl₂ all at once in a small glass beaker, while vigorously stirring. Upon addition of the second salt, the solution immediately became cloudy, denoting the nucleation and growth of the CaCO₃ cores. After allowing the CaCO₃ to grow for 30 seconds, stirring was stopped and the solution was transferred into Eppendorf tubes. The solution was centrifuged (3000 rpm, 1 minute) and washed 3 times to remove the excess NaCl, CaCl₂, Na₂CO₃, to stop the CaCO₃ growth, and to remove the cores that were much smaller than the 5μm average. After washing the cores, the layer-by-layer assembly of polyelectrolytes and wax particles was performed. Once the desired number of layers was assembled, the core was removed with two washings in 0.1M HCl and then washed in pure water until a neutral pH was reached.



Equation 5.4. 1 CaCO₃ crystallization reaction

Results

Polyelectrolyte capsules templated on CaCO₃ with 4 bilayers are presented in Figure 5.4.1.1, with their heated counted parts shown in Figure 5.4.1.2. Capsules with wax as a layer constituent are shown in Figure 5.4.1.3 and Figure 5.4.1.4. As discussed in the previous chapter, all capsules templated on CaCO₃ have porous structures resulting from the porous nature of the CaCO₃ core. In the case of capsules with wax the porosity decreases a little. This observed change in the structure of the capsule wall is due to the wax presences. More detailed SEM pictures can be seen in Appendix II.

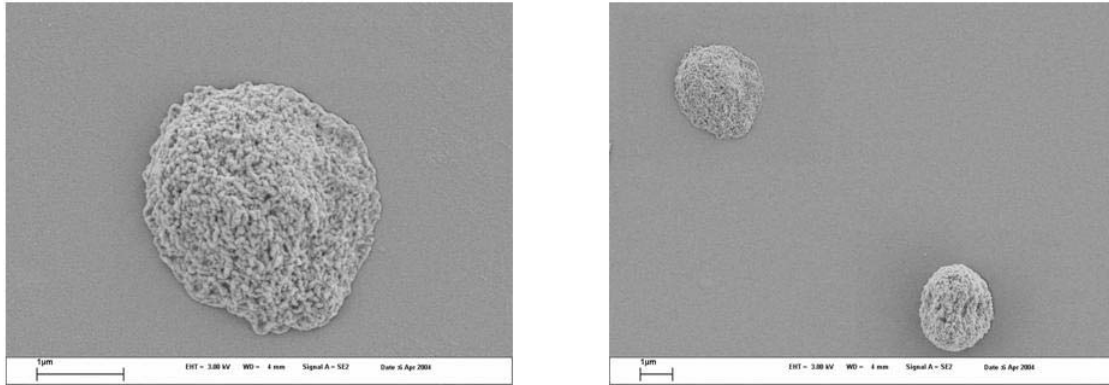


Figure 5.4.1.1 CaCO₃ templated (PAH/PSS) 4 capsules (core has been removed)

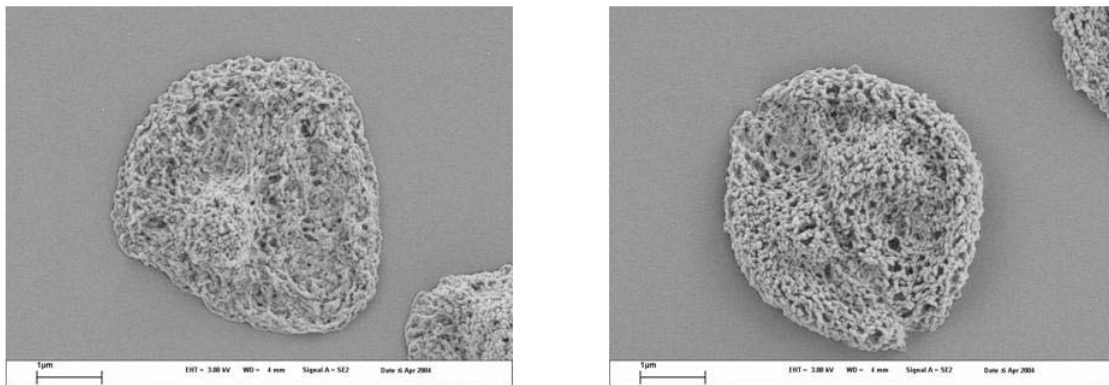


Figure 5.4.1.2 CaCO₃ templated (PAH/PSS) 4 capsules after heating.

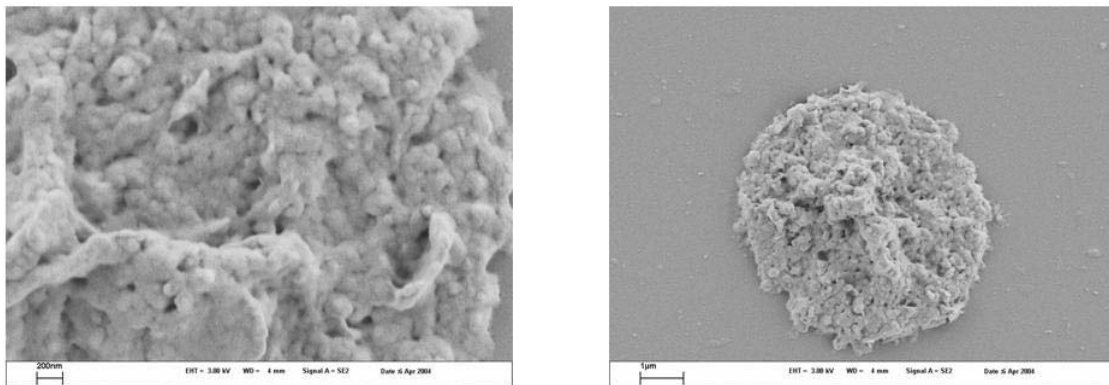


Figure 5.4.1.3 CaCO₃ templated (PAH/PSS)₂ (PAH/-wax) ₂

In the figure above one can see that the addition of wax layers to the core leads to the decrease in the amount of pores on the capsule wall. This is even more dramatic in the pictures below, which display the heated capsules. These capsules do not show any large pores as in the case of the capsules without wax and the unannealed wax. This change in the wall structure proves that the wax adsorbs and melts when the temperature is increased above the melting temperature.

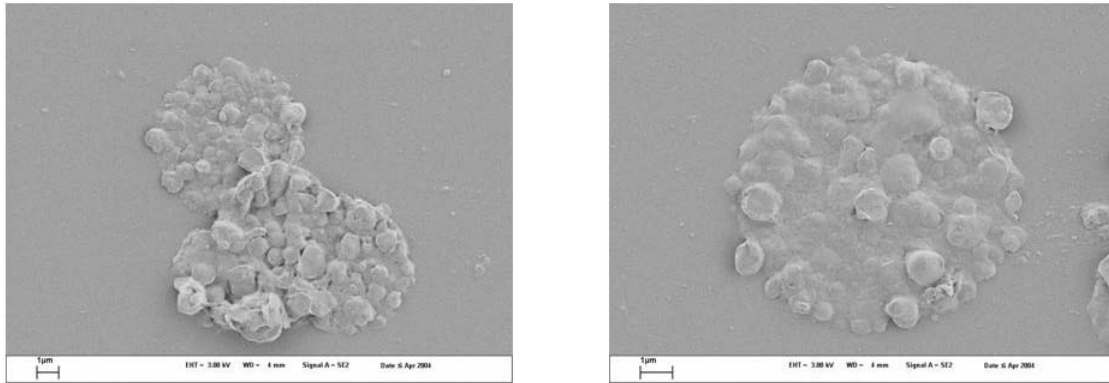


Figure 5.4.1.4 CaCO₃ templated (PAH/PSS)₂ (PAH/-wax)₂ capsules after heating.

The following pictures display the use of the positive particles received from Keim Additec. These particles reveal that the morphology of these capsules is, unfortunately, no longer spherical. Another problem is the large aggregation of the capsules assembled with positive wax.

Aggregation was also observed in capsules with 3 or 4 layers of wax. As a result the assembly with positive wax and multiple layers of the negative wax layers was halted to prevent aggregation.

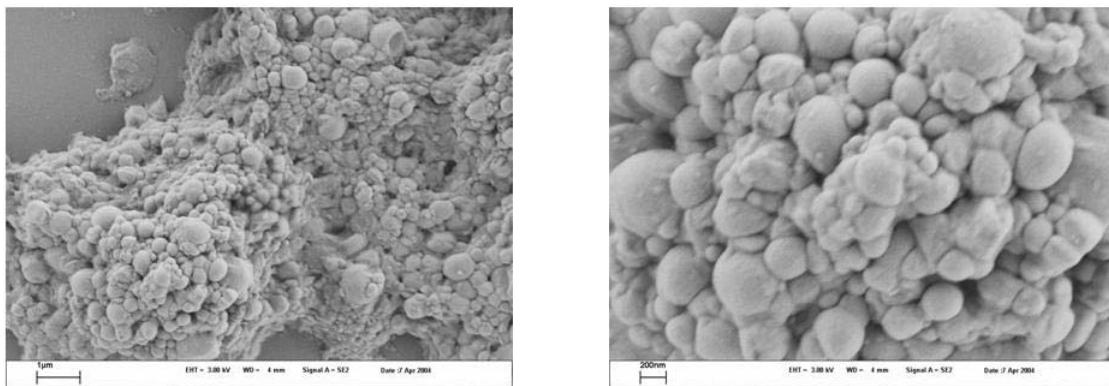


Figure 5.4.1.5 CaCO₃ (PAH/PSS)₂ (+wax022/PSS)₂ The left scale bar is 1µm. The right scale bar is 200nm.

Now that it was shown that the wax can be absorbed and annealed to change the capsule morphology the core was changed to MF to avoid the matrix structure of the capsule.

5.4.2 Capsules -Melamine Formaldehyde

Preparation

Melamine Formaldehyde particles (5 μm , positively charged) were purchased from Microparticles GmbH (Berlin, Germany). After particles were washed 3 times with pure water, capsules were prepared using the LbL method with 4 bilayers of PSS, PAH, or negative wax. The negative species was always absorbed first.

Results

The following capsules were prepared, (PAH/PSS) 4 and (PAH/PSS) 3 (PAH/-wax) according to the standard capsule procedure. These capsules were examined with FRAP using FITC as the fluorescent species. The results of FRAP are shown below.

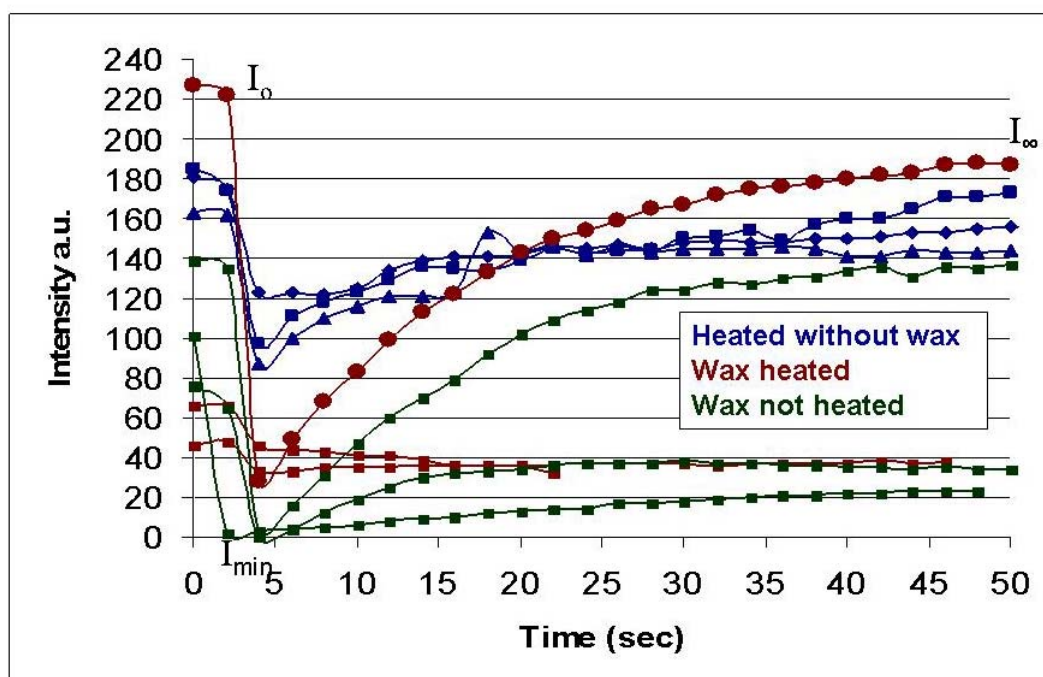


Figure 5.4.2.1 FRAP curves of MF templated capsules

Upon bleaching it was seen that the recovery time does increase with the presence of wax. In the case of the wax heated in the attempt to form a barrier layer, recovery did not take so long, however the difference between the initial intensity and the final intensity is large. This denotes that perhaps the wax is on the way to forming a barrier layer, which is not complete due to the large pores formed in the capsule wall. It is

known that MF cores do not fully dissolve in HCl. Instead of dissolving and being washed away, the MF leaves oligomers in the capsule wall. These oligomers also affect the permeability and are probably the reason why the recovery times from capsule to capsule is different. After these results were obtained it was decided to change the core material again to PS because this core is completely dissolvable and the PS diffuses through the capsule wall in smaller particles resulting in less destruction of the capsule wall. Figure 5.4.2.2 presents a confocal picture of a (PAH/PSS)4 and heated (heated without wax). Figure 5.4.2.3 shows (PAH/PSS)3 (PAH/-wax) (wax not heated) and Figure 5.4.2.4 illustrates (PAH/PSS)3 (PAH/-wax) and heated (wax heated).

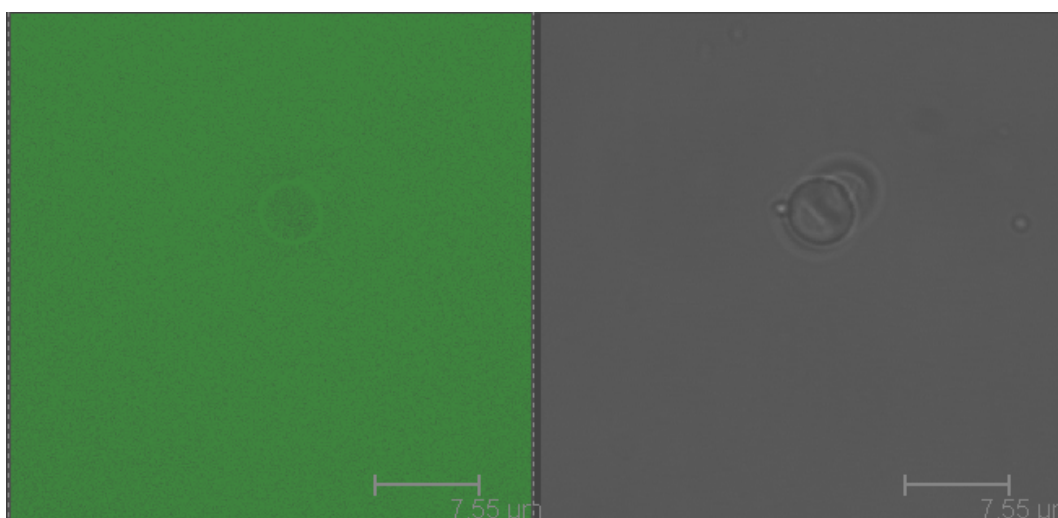


Figure 5.4.2.2 (PAH/PSS)4 MF templated capsule

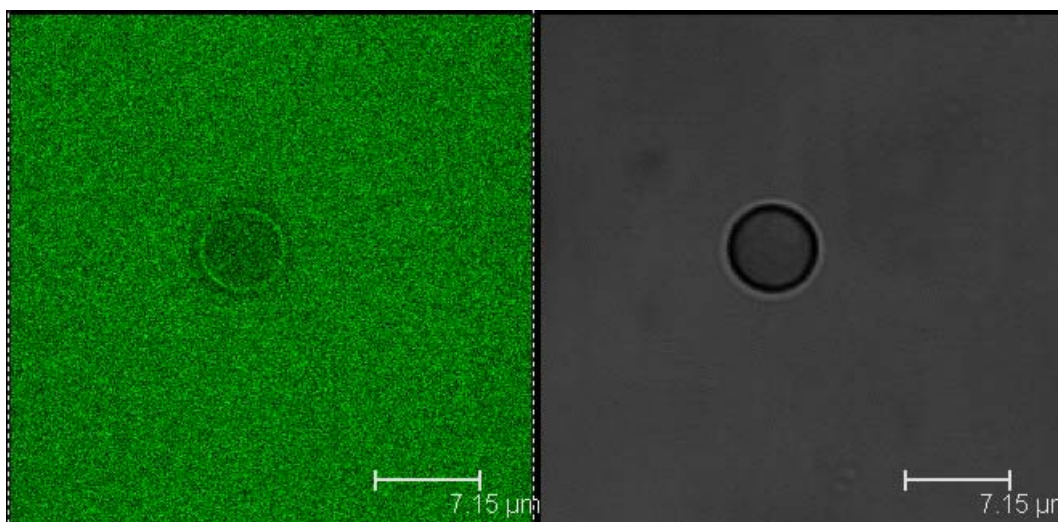


Figure 5.4.2.3 (PAH/PSS)3 (PAH/-wax) (wax not heated) templated capsule

To compare the bleaching curves one could apply the following formula

$$\frac{I_o - I_\infty}{I_o - I_{\min}} = \text{fraction of sealed capsules}$$

Equation 5.4 2.1

where I_o is the initial intensity of the fluorescence, I_∞ is the intensity at equilibrium, and I_{\min} is the intensity directly following bleaching. Applying this to the curves seen in Figure 5.3.2.1 one obtains averages of 0.27, 0.45, and 0.82 for the capsules heated without wax, with wax and heated with wax, respectively. From this one can see that the addition of wax leads to capsules that are less permeable to FITC, and the subsequent heating further decreases the permeability. The difference between I_o and I_{\min} denotes the mobile fraction of dye molecules and the difference between I_o and I_∞ and shows the amount of immobile molecules. The introduction of wax and the heating of the wax causes the amount of immobile or molecules trapped inside the capsule to increase.

As can be seen in Figure 5.4.2.1, the reproducibility of the recovery within the capsules prepared on MF is low. This is particularly the case for the capsules with a wax layer absorbed on the capsule wall. The irreproducibility of the permeability and the major problem of aggregation are illustrated in Figure 5.4.2.4 which shows (PAH/PSS)₃ (PAH/-wax) heated capsules. In addition to the severe aggregation, one can also see that there are some capsules that are fully permeable to the FITC. Other capsules are still black inside, which denotes that the capsule permeability has been significantly altered or that these capsules are impermeable. Unfortunately, single capsules of this type could never be found. Nevertheless this does show that in principle the addition of wax and subsequent heating does form a partial barrier layer and decrease the film permeability.

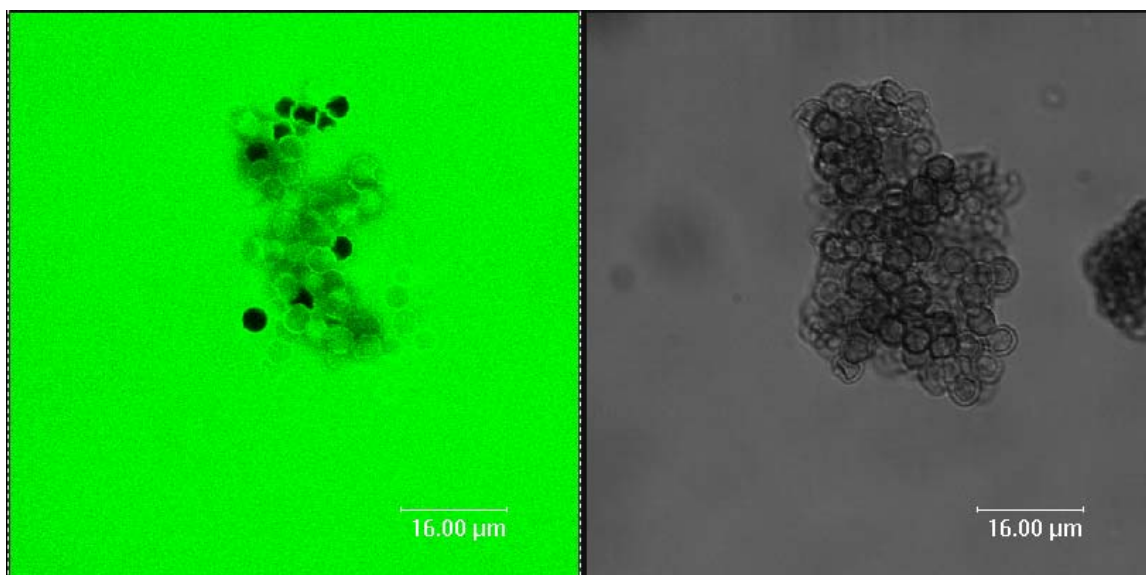


Figure 5.4.2.4 CLSM image of heated (PAH/PSS)₃ (PAH/-wax) MF templated capsules

5.4.3 Capsules- Polystyrene

Preparation

Polystyrene particles (10 μ m, negatively charged) were purchased from Microparticles GmbH (Berlin, Germany). After the particles were washed 3 times with pure water, capsules were prepared using the LbL method with 8.5-10 bilayers of PSS, PAH, or -wax. More layers are required in the case of PS core, due to the size of the template. With a core 10 μ m in size the number of layers must be increased to at least 8 bilayers to yield a stable membrane once the core is removed. The positive species was always absorbed first.

Results

The capsules resulting from PS cores were analyzed with SEM, AFM and CLSM. The SEM images show the morphology of the capsule wall before and after wax deposition. AFM gives information about the dry thickness of the wall and the roughness. Roughness is an important measurement in the analysis of capsules with wax, as the wax

particles are small, but are not closely packed. This results in a large roughness of capsules with wax. With CLSM the diameter of capsules and the permeability can be determined. To measure the permeability of the capsules Fluorescence Recovery and Photobleaching (FRAP) was performed. Below is a table listing those capsules prepared on PS cores that were investigated as part of this study.

Capsules prepared on PS cores		
2	(PAH/PSS) 8.5bil	
3a	(PAH/PSS) 8.5bil (-wax) (before core dissolution)	
3b	(PAH/PSS) 8.5bil (-wax) (after core dissolution)	
4	(PAH/PSS) 9 bil	
2_h	(PAH/PSS) 8.5bil	heated (60°C 1hr)
3a_h	(PAH/PSS) 8.5bil (-wax) (before core dissolution)	heated (60°C 1hr)
3b_h	(PAH/PSS) 8.5bil (-wax) (after core dissolution)	heated (60°C 1hr)
4_h	(PAH/PSS) 9 bil	heated (60°C 1hr)

Figure 5.4.3.1 Capsule layer continent layout.

As can be seen from the table, capsules on PS were prepared using method 1 and method 2. A scheme of method 2 is shown in Figure 5.4.3.2.

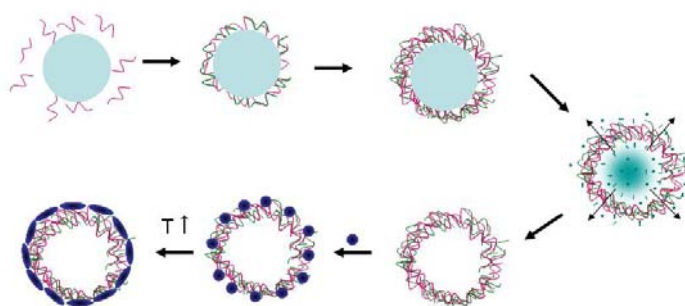


Figure 5.4.3.2 Scheme of capsule fabrication with wax layer via method 2

Polyelectrolyte capsules templated on PS with 8.5 bilayers are presented in Figure 5.4.3.3 with their heated counterparts shown in Figure 5.4.3.4. Capsules with wax as a

layer constituent (method 1) are shown in Figure 5.4.3.5 and Figure 5.4.3.6. In the case of capsules without wax, heating does not appear to cause a change in the capsule surface. The capsules with a wax layer are different from the capsules without the wax in that they appear to be rougher and a little stiffer. Heated capsules with wax appear to be smoother than the capsules with the wax, but they also appear to be much stiffer, which can be seen in the larger and sharper folds. More detailed SEM pictures are provided in Appendix II.

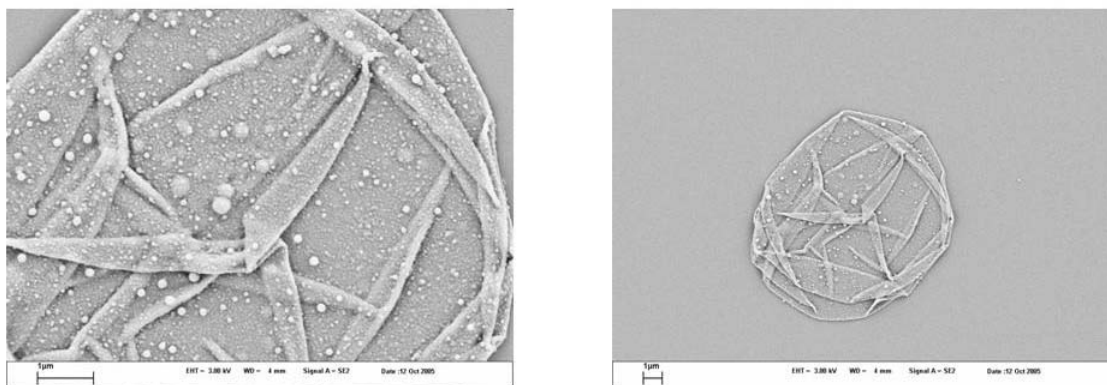


Figure 5.4.3.3 Sample 2 (PAH/PSS)_{8.5bil}. Scale bar in both images is 1 μm.

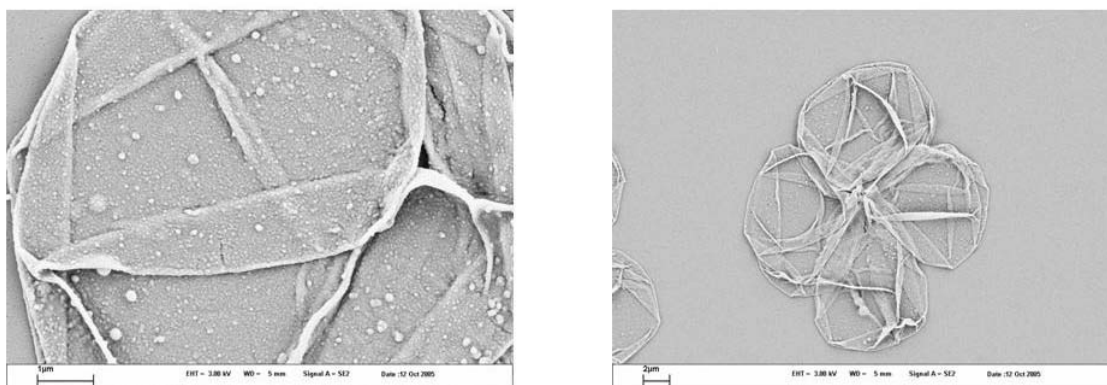


Figure 5.4.3.4 Sample 2h (PAH/PSS)_{8.5bil} heated (60°C 1hr). The scale bar in the left image is 1 μm. The scale bar in the right image is 2 μm.

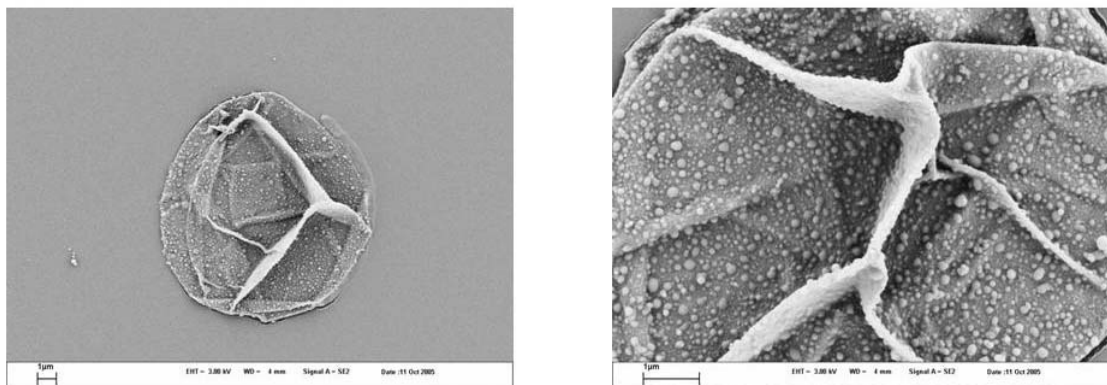


Figure 5.4.3.5 Sample 3a (PAH/PSS)_{8.5bil} + (-wax) (before core dissolution). Scale bar in both images is 1 μm.

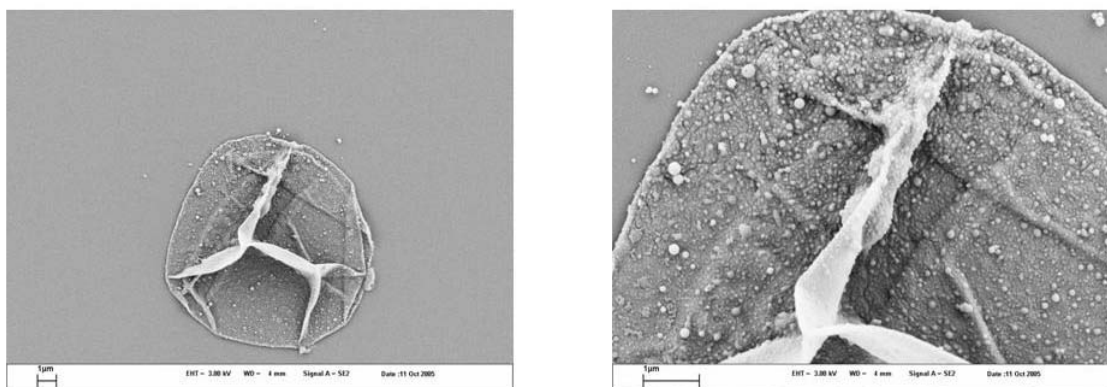


Figure 5.4.3.6 Sample 3ah (PAH/PSS)_{8.5bil} + (-wax) (before core dissolution) heated (60°C 1hr) Scale bar in both images is 1 μm.

Capsules with wax as layer constituent (method 2) are shown in Figure 5.4.3.7 and Figure 5.4.3.8.

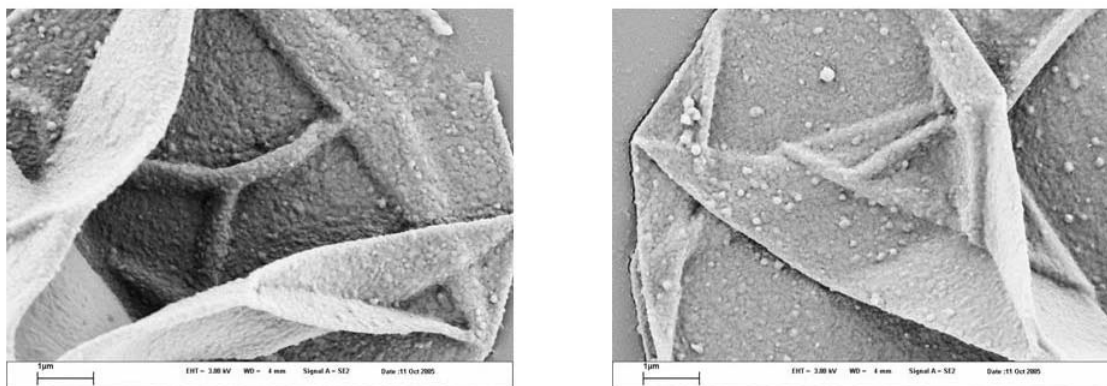


Figure 5.4.3.7 Sample 3b (PAH/PSS)_{8.5bil} + (-wax) (after core dissolution) Scale bar in both images is 1 μm.

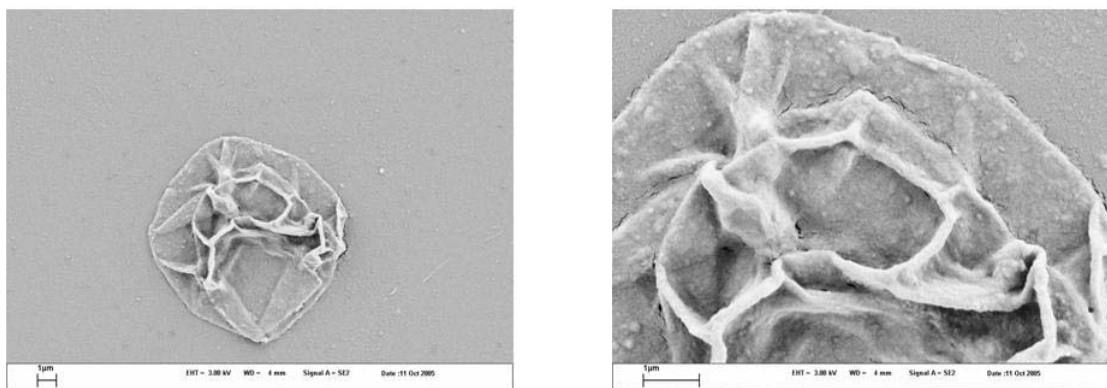


Figure 5.4.3.8 Sample 3bh (PAH/PSS)_{8.5bil} + (-wax) (after core dissolution) heated (60°C 1hr)
Scale bar in both images is 1 μm.

As can be seen from the SEM pictures, the stage at which the wax is added to the capsules does make a large difference in the surface morphology of the capsules. In the cases of capsules with wax added before the core is removed, some wax particles do absorb and anneal. But in the case of the wax added via the second method, a drastic change in the capsule surface can be seen. If the wax is added after core removal, the surface has a homogeneous coating after the deposited wax particles are annealed. AFM images of the samples are available in Appendix III. There, it is shown that the roughness increases after the wax layers are added. In addition the layers are a little thicker after heating due to the rearrangement of the polyelectrolytes. To test how this coating on the capsules affects the permeability, FRAP measurements were performed.

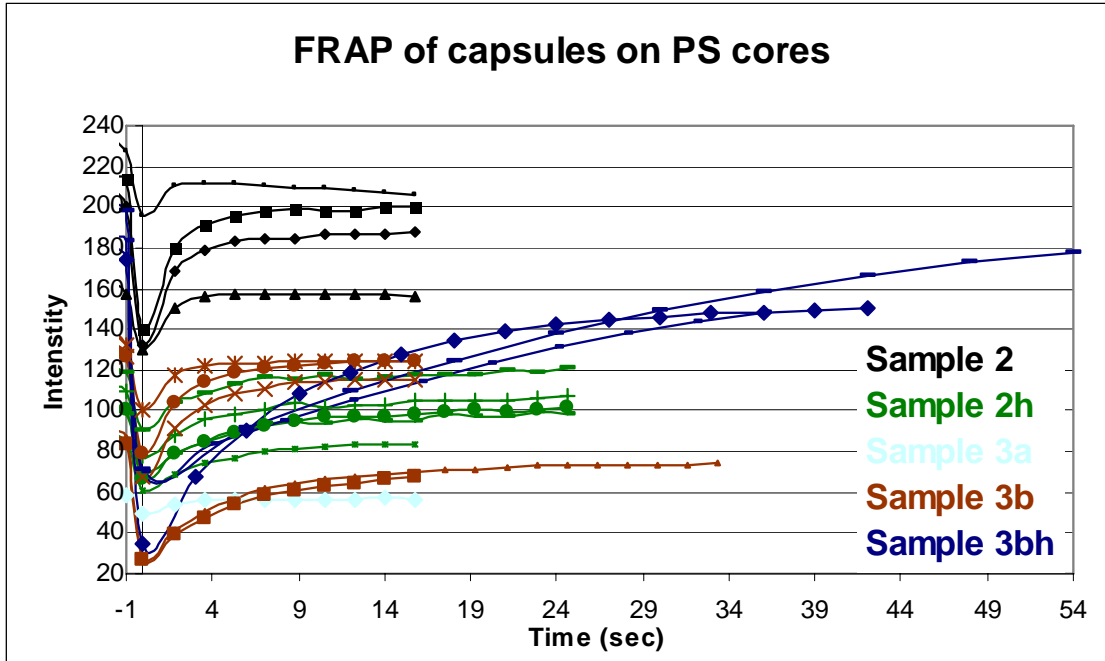


Figure 5.4.3.9 FRAP curves of PS templated capsules

When the recovery curves are separated for more clarity they provide the graphs shown in Figure 5.4.3.10.

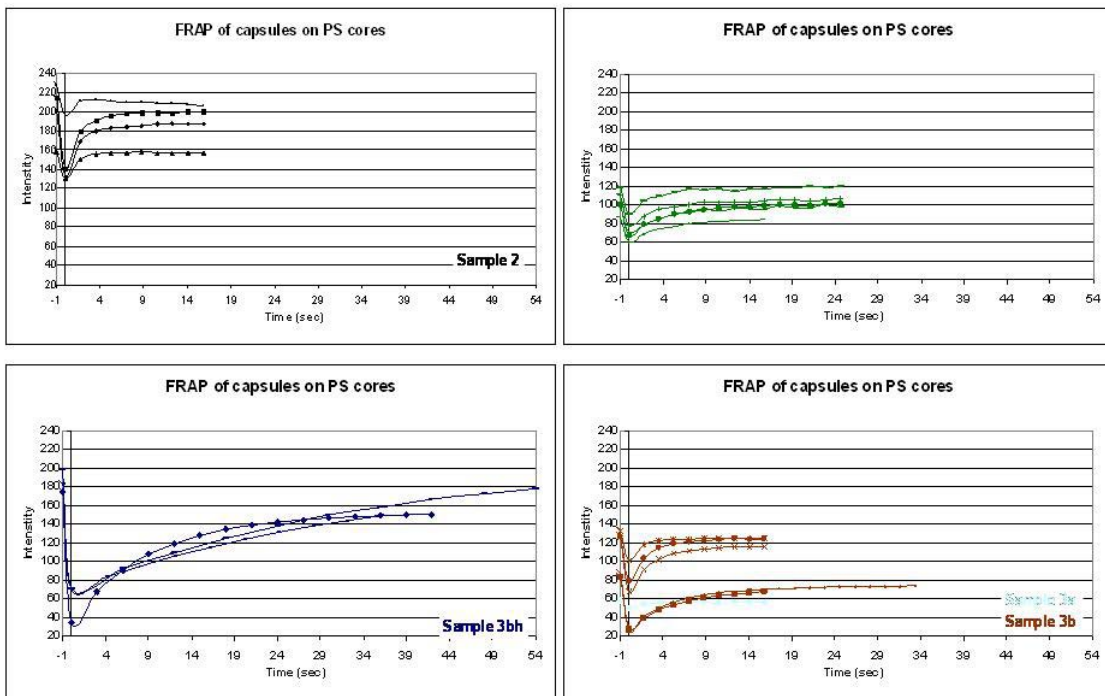


Figure 5.4.3.10 Separated FRAP curves of PS templated capsules

From the graph above it can be seen that the recovery time is on the order of five seconds for sample 2. If the sample 2 is heated the recovery time increases to 10 seconds. The permeability of sample 3a is not shown, as the sample was highly aggregated, as shown in Figure 5.4.3.11.

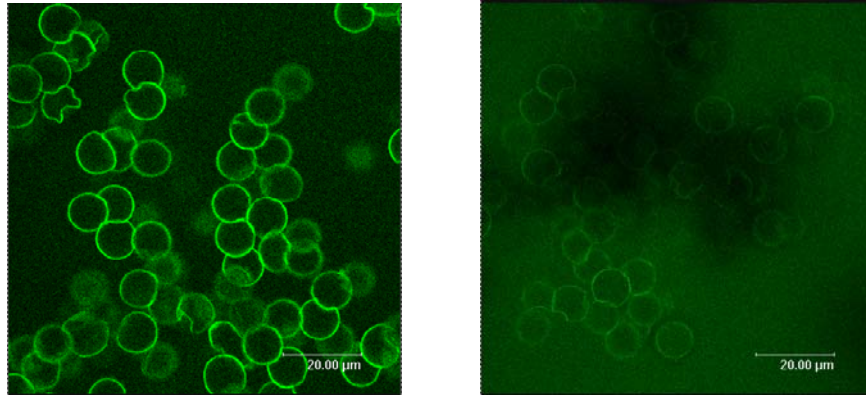


Figure 5.4.3.11 Confocal image of Sample 3a right and 3ah left.

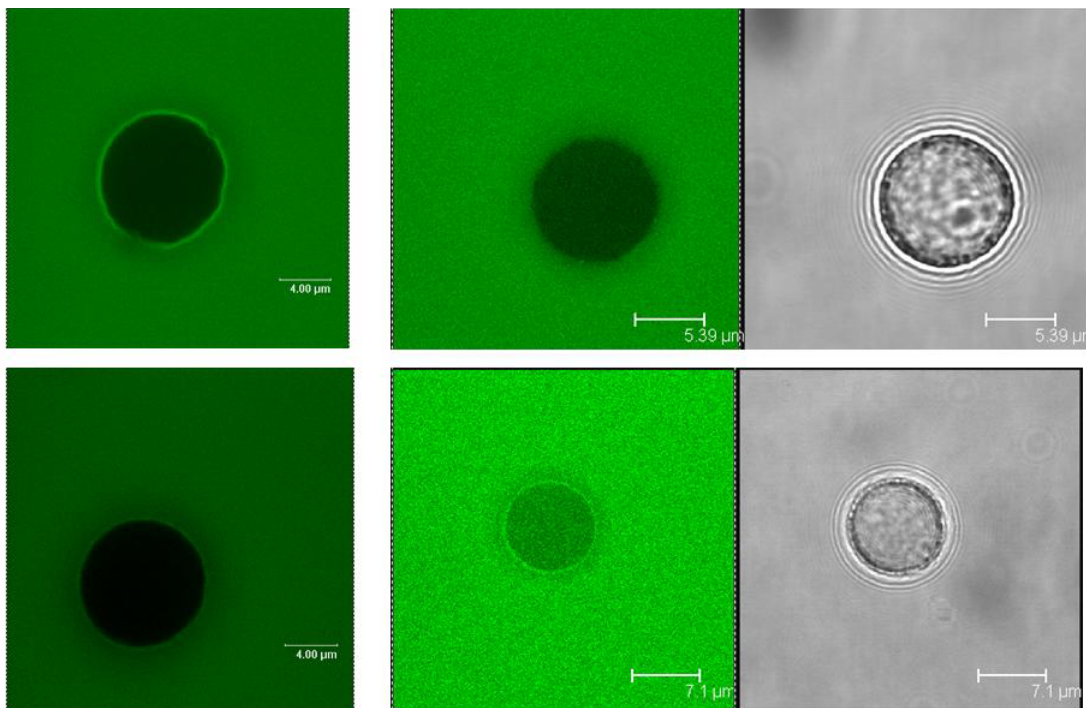


Figure 5.4.3.12 Confocal image of Sample 3bh

As can be seen, the timing of the wax addition plays a major role in the resultant permeability of the capsules. This can be explained in many ways. If the wax is added before the core is removed, it is obviously affected by the THF. In a separate Eppendorf, THF was added to wax. After the addition of THF, the appearance of the wax changed, leading to the belief that the wax is partially soluble in THF. So it possible that the wax can be removed from the capsule wall in the presence of THF. This is why sample 3a was so aggregated. If some of the wax is removed from the surface, the charge of the outermost layer is no longer homogenous, increasing the probability of aggregation. Another reason why the results of method 2 are more favorable can be the fact that THF is very hygroscopic. This means that the water in between the polyelectrolyte is removed in the presence of THF, leaving a more hydrophobic shell, which is more favorable for the absorption of wax. Also, when the water is removed from the shell fluorescent species do not have the ability to transport through the shell. And, finally, the wax added after the core is removed closes the pores caused during the core dissolution. Trying to add solvent “melted” wax was also briefly attempted. Acetone was found to be a suitable solvent for the wax. The results are seen in the Figure below.

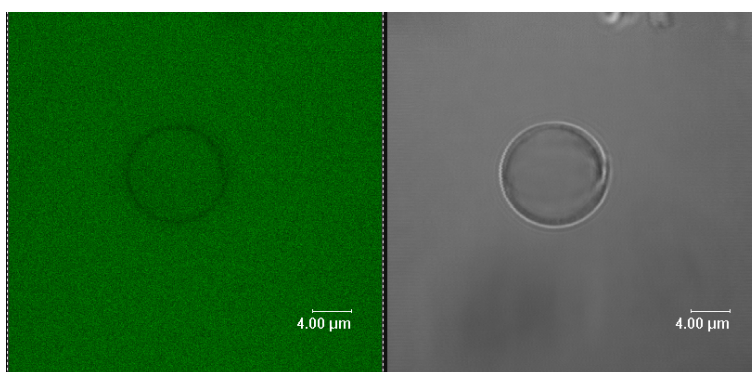


Figure 5.4.3.113 PS (10 μ m core) (PSS/PAH)₁₄. (after core removal) (added –wax dissolved in acetone). Not heated

Despite the problems with the solvent, in general the capsules templated on PS can be made reproducibly impermeable, whereas capsules templated on MF are always different. In this light, it can be shown that wax-coated capsules can made impermeable for small molecules. This is already a big advancement over previously discussed permeability changes [14, 15].

5.5 Conclusions

The use of wax as a permeability controlling agent was successfully introduced to planar and spherical polyelectrolyte multilayer films. In both cases once the wax was heated the melted wax did indeed form a barrier layer preventing the diffusion of small molecules. In the case of planar films it was proven that the resulting film is water-tight. The capsules that had wax added after the core dissolution show impermeability against FITC. In light of this, active molecules can be encapsulated and held inside the capsules. If the release of the active material is desired, the remote control release of active molecules by Skirtach et al could be easily applied [16].

References

- 1 Panchagnula, V.; Kumar, C. V.; Rusling, J. F., Ultrathin Layered Myoglobin-Polyion Films Functional and Stable at Acidic pH Values. *Journal of the American Chemical Society* 2002, 124, (42), 12515-12521.
- 2 Vuillaume, P. Y.; Jonas, A. M.; Laschewsky, A., Ordered Polyelectrolyte "Multilayers". 5. Photo-Cross-Linking of Hybrid Films Containing an Unsaturated and Hydrophobized Poly(diallylammonium) Salt and Exfoliated Clay. *Macromolecules* 2002, 35, (13), 5004-5012.
- 3 Harris, J. J.; DeRose, P. M.; Bruening, M. L., Synthesis of Passivating, Nylon-Like Coatings through Crosslinking of Ultrathin Polyelectrolyte Films. *Journal of the American Chemical Society* 1999, 121, (9), 1978-1979.
- 4 Chen, J.; Huang, L.; Ying, L.; Luo, G.; Zhao, X.; Cao, W., Self-Assembly Ultrathin Films Based on Diazo-resins. *Langmuir* 1999, 15, (21), 7208-7212.
- 5 Dai, J.; Jensen, A. W.; Mohanty, D. K.; Erndt, J.; Bruening, M. L., Controlling the Permeability of Multilayered Polyelectrolyte Films through Derivatization, Cross-Linking, and Hydrolysis. *Ibid.* 2001, 17, (3), 931-937.
- 6 Georgieva, R.; Moya, S.; Leporatti, S.; Neu, B.; Baeumler, H.; Reichle, C.; Donath, E.; Moehwald, H., Conductance and Capacitance of Polyelectrolyte and Lipid-Polyelectrolyte Composite Capsules As Measured by Electrorotation. *Ibid.* 2000, 16, (17), 7075-7081.
- 7 Moya, S.; Donath, E.; Sukhorukov, G. B.; Auch, M.; Baeumler, H.; Lichtenfeld, H.; Moehwald, H., Lipid Coating on Polyelectrolyte Surface Modified Colloidal Particles and Polyelectrolyte Capsules. *Macromolecules* 2000, 33, (12), 4538-4544.

- 8 Kugler, R.; Knoll, W., Polyelectrolyte-supported lipid membranes. *Bioelectrochemistry* **2002**, 56, (1-2), 175-178.
- 9 Rouse, J. H.; Ferguson, G. S., Stepwise Incorporation of Nonpolar Polymers within Polyelectrolyte Multilayers. *Langmuir* **2002**, 18, (20), 7635-7640.
- 10 Sears, V.F. *Neutron News* **1992**, 3, 26.
- 11 Kurth, D. G.; Volkmer, D.; Klitzing, R. V., Multilayers on solid planar substrates. From structure to function. *Multilayer Thin Films* **2003**, 393-426.
- 12 Schmitt, J.; Gruenewald, T.; Decher, G.; Pershan, P. S.; Kjaer, K.; Loesche, M., Internal structure of layer-by-layer adsorbed polyelectrolyte films: a neutron and x-ray reflectivity study. *Macromolecules* **1993**, 26, (25), 7058-63.
- 13 Ladam, G.; Schaad, P.; Voegel, J. C.; Schaaf, P.; Decher, G.; Cuisinier, F., In Situ Determination of the Structural Properties of Initially Deposited Polyelectrolyte Multilayers. *Langmuir* 2000, 16, (3), 1249-1255.
- 14 Antipov, A. A.; Sukhorukov, G. B.; Donath, E.; Mohwald, H., Sustained release properties of polyelectrolyte multilayer capsules. *Journal of Physical Chemistry B* 2001, 105, (12), 2281-2284.
- 15 Antipov, A. A.; Sukhorukov, G. B., Polyelectrolyte multilayer capsules as vehicles with tunable permeability. *Advances In Colloid And Interface Science* 2004, 111, (1-2), 49-61.
- 16 Skirtach, A. G.; Antipov, A. A.; Shchukin, D. G.; Sukhorukov, G. B., Remote activation of capsules containing Ag nanoparticles and IR dye by laser light. *Langmuir* **2004**, 20, (17), 6988-6992.

Chapter 6- General Conclusions

In this work it has been shown that introducing a non-polar substance into the polyelectrolyte multilayer is no trivial matter. In Chapter 4, active molecules were encapsulated within polyelectrolyte multilayer capsules, in this case Poly-(N-isopropyl acrylamide), (PNIPAM). In Chapter 5, the incorporation of charged wax particles into the polyelectrolyte film, leads to the decrease in the film permeability.

In Chapter 4, many encapsulation methods were discussed, three of which were attempted to incorporate active molecules inside capsules. The stimuli-responsive polymer, PNIPAM, encapsulated with the “ship in a bottle” was successful proven with Raman spectroscopy, AFM, and SEM. The “ship in a bottle” is fabricating capsules with the layer-by-layer (LbL) technique, adding the capsules to the monomer solution, polymerizing the monomer, and the washing away the polymer that is on the outside. PNIPAM added to the capsules with the “ship in a bottle” method maintained all of its thermo-sensitive properties, which was not the case for the other attempted encapsulation methods. In addition, it was shown with DSC and CLSM, that the LCST of the PNIPAM depends not only on the type and the concentration of ions present but also if the capsule wall is present. The presence of the capsule wall decreases the effective salt concentration the PNIPAM feels. With this, it was shown that the temperature at which the LCST was seen could be tuned. This work is extremely promising as it could be used as a sensor, for drug delivery applications, or waste water treatment. In many other publications active molecules were observed and released upon heating.

In Chapter 5, wax particles were implemented as a permeability control agent. First, the wax particles were characterized to ascertain their properties of interest, i.e. size, charge and melting temperature. On flat films, it was shown that wax particles introduced into the polyelectrolyte films covered the film which increased the contact angle and roughness. The increase in the roughness was proven by ellipsometry and Atomic Force Microscopy, (AFM) denoting the presence of the hydrophobic particles. The particles comprised of wax form a barrier layer after heating that repelled water. This was proven with neutron reflectivity studies against D₂O. In the case of capsules many different core materials were employed, as the permeability of the capsule wall is mostly affected by the core removal process. Again, in this case, wax particles could be introduced into the polyelectrolyte multilayers, proven by the morphology changes in the SEM images and the thickness increase of the wall shown with AFM. Capsules templated on Polystyrene cores, showed the largest decrease in the permeability to FITC after heating the incorporated wax particles. The reason the PS templated capsules showed the largest decrease in permeability is a result of the THF used to remove the core. The THF removed not only the core, but also the water within the membrane of the capsule wall. The increase in hydrophobicity of the wall created a more favorable environment for the wax particles to absorb, that after heating created a barrier layer that was resistant to FITC.

In general, two advanced methods of possible delivery systems have been proposed. In both cases, if biocompatible elements are used as the capsule wall constituents, the resulting capsule systems give a stable method of encapsulating active molecules that with the ability to tune the wall thickness, gives the ability to control the release profile of the molecule of interest.

Einbettung unpolarer, temperaturempfindlicher Substanzen in Polyelektrolytkapselsysteme zur Wirkstofffreisetzung

Verkapselung ist ein vielseitiges Werkzeug, das zum Schutz und zum Transport von Molekülen ebenso eingesetzt werden kann, wie zur Verbindung von Reaktionspartnern in einem gemeinsamen, von der Umgebung abgeschirmten Raum. Es basiert auf einem einfachen Vorbild der Natur. Pflanzen schützen ihren Samen zum Beispiel durch eine harte, nahezu undurchdringbare Schale (Nüsse) oder durch eine selektiv durchlässige Hülle, wie bei Weizen, der sobald er feucht wird zu keimen beginnt. Die Natur setzt durch den Einsatz des Hülle-Kern Prinzips sehr effizient die Kontrolle über Durchlässigkeit und Anpassung an bestimmte Aufgaben um.

Wird das Hülle-Kern-Prinzip zum Schutz oder Transport von Molekülen eingesetzt, so sind die zu verwendenden Kapseln nur wenige Mikrometer groß. Sie werden dann als Mikrokapseln bezeichnet. Zur Erzeugung dieser Mikrokapseln werden verschiedene Methoden verwendet. Der heute übliche Weg geht von einer ca. 5-10 Mikrometer großen Kugel (Kern) aus, die mit einer stabilen und an die gewünschten Eigenschaften angepassten Schicht von wenigen Nanometern versehen wird. Im Anschluss wird der Kern herausgelöst und eine hohle, stabile Kapsel erhalten.

Schichten von wenigen Nanometern Dicke können aus Polyelektrolyten durch das Layer-by-Layer-Verfahren (LbL) hergestellt werden. Dieses Verfahren eignet sich auf Grund seiner vielen Anpassungsmöglichkeiten besonders zum Aufbau der Schichten für Mikrokapseln, da sich die Eigenschaften der Beschichtung bereits beim Aufbau der Schicht auf die Bedürfnisse maßschneidern lassen.

Diese Arbeit befasst sich mit der Erzeugung von Mikrokapseln, deren Eigenschaften temperaturabhängig sind. Dies wurde auf zwei Wegen erreicht. Zum einen wurden Kapseln aus Polyelektrolyten und Wachs aufgebaut. Bei Temperaturerhöhung schmilzt das Wachs und versiegelt die Kapsel. Zum anderen werden Kapseln mit einem Wärme empfindlichen Polymer gefüllt. Bei Temperaturerhöhung kollabiert das Polymergerüst. Der enthaltene Wirkstoff wird freigesetzt.

Introduction of a Thermo-sensitive Non-polar Species into Polyelectrolyte Multilayer Capsules for Drug Delivery

The layer-by-layer assembly (LbL) of polyelectrolytes has been extensively studied for the preparation of ultrathin films due to the versatility of the build-up process. The control of the permeability of these layers is particularly important as there are potential drug delivery applications. Multilayered polyelectrolyte microcapsules are also of great interest due to their possible use as microcontainers. This work will present two methods that can be used as employable drug delivery systems, both of which can encapsulate an active molecule and tune the release properties of the active species.

Poly-(N-isopropyl acrylamide), (PNIPAM) is known to be a thermo-sensitive polymer that has a Lower Critical Solution Temperature (LCST) around 32°C; above this temperature PNIPAM is insoluble in water and collapses. It is also known that with the addition of salt, the LCST decreases. This work shows Differential Scanning Calorimetry (DSC) and Confocal Laser Scanning Microscopy (CLSM) evidence that the LCST of the PNIPAM can be tuned with salt type and concentration. Microcapsules were used to encapsulate this thermo-sensitive polymer, resulting in a reversible and tunable stimuli- responsive system. The encapsulation of the PNIPAM inside of the capsule was proven with Raman spectroscopy, DSC (bulk LCST measurements), AFM (thickness change), SEM (morphology change) and CLSM (in situ LCST measurement inside of the capsules). The exploitation of the capsules as a microcontainer is advantageous not only because of the protection the capsules give to the active molecules, but also because it facilitates easier transport.

The second system investigated demonstrates the ability to reduce the permeability of polyelectrolyte multilayer films by the addition of charged wax particles. The incorporation of this hydrophobic coating leads to a reduced water sensitivity particularly after heating, which melts the wax, forming a barrier layer. This conclusion was proven with Neutron Reflectivity by showing the decreased presence of D₂O in planar polyelectrolyte films after annealing creating a barrier layer. The permeability of capsules could also be decreased by the addition of a wax layer. This was proved by the increase in recovery time measured by Florescence Recovery After Photobleaching, (FRAP) measurements.

In general two advanced methods, potentially suitable for drug delivery systems, have been proposed. In both cases, if biocompatible elements are used to fabricate the capsule wall, these systems provide a stable method of encapsulating active molecules. Stable encapsulation coupled with the ability to tune the wall thickness gives the ability to control the release profile of the molecule of interest.

Acknowledgements

"If I have seen further than others, it is by standing upon the shoulders of giants."

Newton, Isaac

One can not do everything alone. And that is true of this work. Without the assistance of many, this work would not have been possible. First and foremost, I would like to thank Prof. Dr. Ronald S. Besser, Prof. Dr. Yuri Lvov, and Prof. Dr. Helmuth Möhwald. Without Dr. B and Prof. Dr. Lvov introduction to science, LbL, and bringing to MPI for collaboration with Prof. Dr. Sukhorukov one will never know if I would have moved to Europe. I thank Prof. Dr. Helmuth Möhwald for accepting me, welcoming me into the MPI, for the many tips, helpful discussions and fun on the soccer field.

Many of the measurements presented in this work would also been not possible, or at least much more difficult without the following people. I would like to thank Roy Knocke and Wenfei Dong for Raman measurement that also gave another perspective of my system. I would like to thank, Heidemarie Zastrow for her friendly personality and very competent electrophoresis measurements. I would like to thank, Anneliese Heilig many things: for her patience and friendliness even when I had many, many samples for AFM; and assistance with CLSM. I am grateful to Guntram Schwarz for nice discussions and assistance of DSC. I would like to thank Dmitry Shchukin (for showing me the SEM here in house) and Dr. Jürgen Hartmann and Rona Pitschke of many very specific questions of SEM analysis. Keim Additec GmbH is greatly acknowledged for the gift of the wax particles.

I would like to express my gratitude to my many group members over the years. Karine Glinel, Ana Cordeiro, Radostina Georgieva, Oliver Kreft, Alexei Antipov, Claire Peyratout, Daria Andreeva, Sajanikumari Sadasivan, André Skirtach, Lidong Li., Gemma Ibarz-Ric, Annegret Praast, Karen Köhler, Dmitry Volodkin, and Tatjana Mauser. I would like especially thank two people: Concetta Tedeschi for helping with the transition of moving to Germany, and Christophe Déjughnat for sooooo much assistance in the lab, helpful discussions and patience with me and the many problems we had with the system.

I have to thank my soccer buddies. Audrée Andersen, Marc Schneider, Miles Page, Chris(topher) Haluska, and Arne Thomas. There are too many others, but I thank you all for keeping “the wall” of sound mind and body.

I would to say thanks to the lunch bunch and coffee/tea corner people. Marc Nolte, Marc Schneider, Ralf Köhler, Annika Vergin, Nils Elsner, Ingo Dönch, Renate Müller, Tatjana Mauser, Goran Bogdanovic, and Christian Radüge. I thank you guys for exciting and pleasure filled discussions. I can not imagine how I could have survived the canteen without you!!!

I am indebted to my wonderful officemates over the last years. Anja, Goran, Matthias, and Torsten. Thanks for teaching many things and help keeping me sane when yet again something else went wrong in the lab. The “Princess of the Dawn” would like to recognize her fellow “*Moscher*” for being distinguished loyal subjects. Ihr wisst schon wer gemeint ist!!!!!!!

I would also like to thank my church community, AVA and my girl friends for being such great people and dear, life long friends. I would like to specially recognize Mary Wurm, Dr. Alissa Prosser, and Sarah Benz. Without “y’all” the stay in Berlin would not have been the same.

And last but definitely not least I would like to thank Adam Reppond, Amanda Foster and my family back in America. Thanks for your constant love, support and encouragement.

Appendix I-Materials

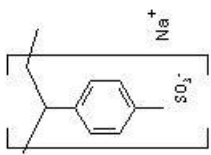
The sources of the chemicals used in this work are as follows: sodium poly(styrene sulfonate) (PSS, Mw \approx 70 kDa) and poly(allylamine hydrochloride) (PAH, Mw \approx 70 kDa) (Aldrich, USA), fluorescein isothiocyanate (FITC, Sigma, USA), ethylenediaminetetraacetic acid (EDTA, Sigma), calcium chloride dihydrate ($\text{CaCl}_2 \cdot 2\text{H}_2\text{O}$, Ultra, Sigma), Na_2CO_3 (pro analysis, Merck, Germany), bovine serum albumin (BSA, Sigma), and dextran-FITC (4 kDa, Aldrich) Orange II (Tropaeolin 000 Nr2), Potassium Chloride and Methylene Blue (Fluka)

Ammonium persulfate, (APS), N-isopropylacrylamide (NIPAM), N,N,N',N'-Tetramethyl-ethylenediamine (TMEDA) and dialysis membranes with a 12,400 kDa molecular cut off were purchased from Sigma-Aldrich (Germany). Tetrahydrofuran (THF), and NaCl were acquired from Roth (Germany). Monodispersed polystyrene (PS) with a mean diameter of 10.25 μm were obtained from Microparticles GmbH (Berlin) cores. Methacryloxyethyl thiocarbonyl rhodimine B (MRho) (used to label the NIPAM) was purchased from Polysciences, Inc (Warrington USA). The water used in all experiments was prepared in a three-stage Millipore Milli-Q Plus 185 purification system and had a resistivity higher than 18 $\text{M}\Omega \text{ cm}$. NaBr, NaF, KCl were purchased from Roth GmbH (Karlsruhe, Germany).

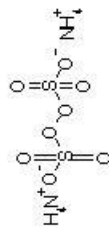
To prepare PAH-FITC, two solutions (PAH and FITC) were mixed in 50mM borate buffer (pH 9.5) at a ratio of 100:1 (amino group of PAH/FITC) and dialyzed against water overnight after 2 h of incubation at room temperature.

BSA was labeled with FITC by mixing of BSA and FITC solutions in 50 mM borate buffer (pH 9.5) at a molar ratio of 1:1. After stirring for 2h at room temperature, the solution was dialyzed against water overnight and used for further study.

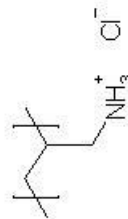
The molecular structures of the more complicated molecules are displayed below.



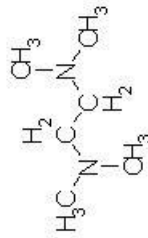
Poly (styrene - sulfonate) (PSS)



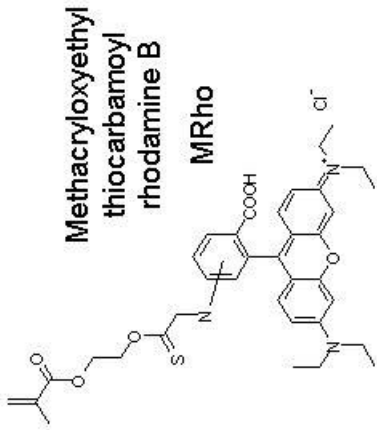
Ammonium peroxodisulfate (APS)



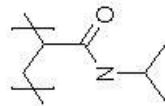
Poly (allylamine hydrochloride) (PAH)



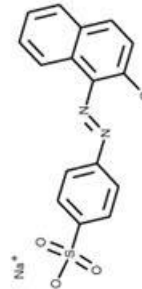
Tetramethylethylenediamine (TMEDA)



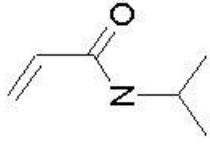
Methacryloxyethyl thiocarbamoyl rhodamine B (MRho)



PNIPAM



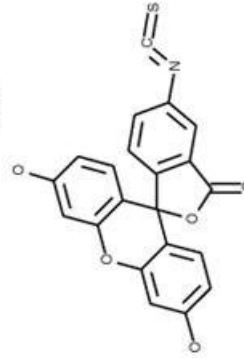
Orange II



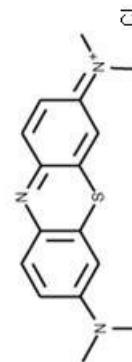
N-isopropyl acrylamide (NIPAM)



Tetrahydrofuran (THF)



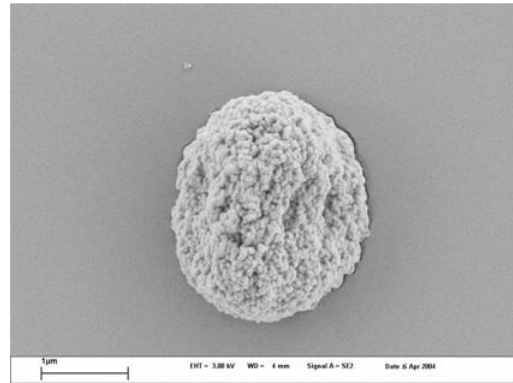
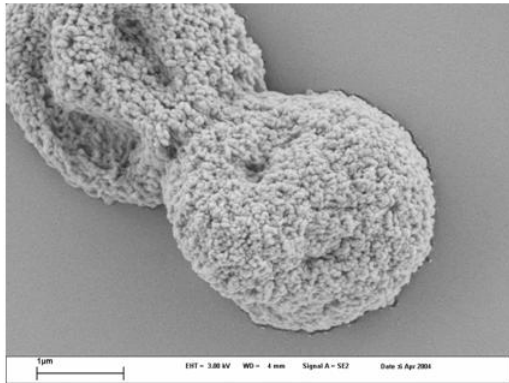
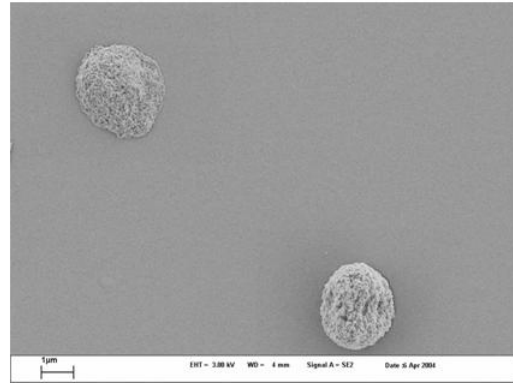
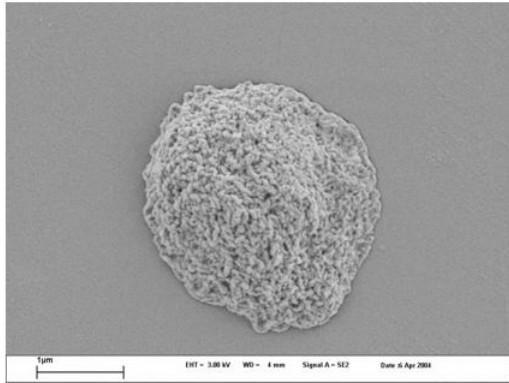
Fluorescein isothiocyanate (FITC)



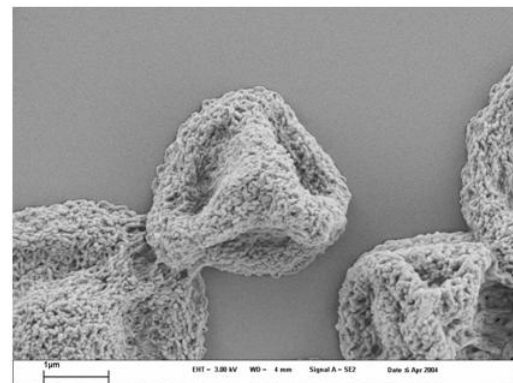
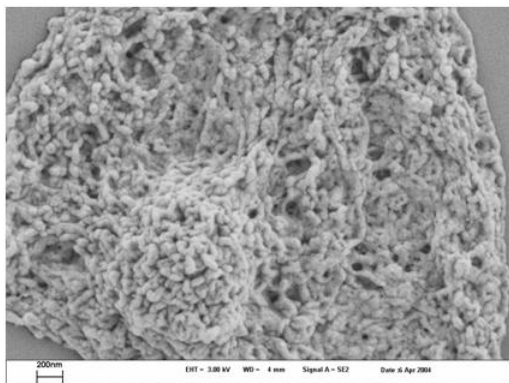
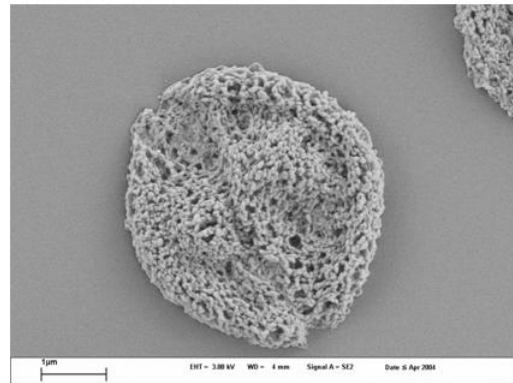
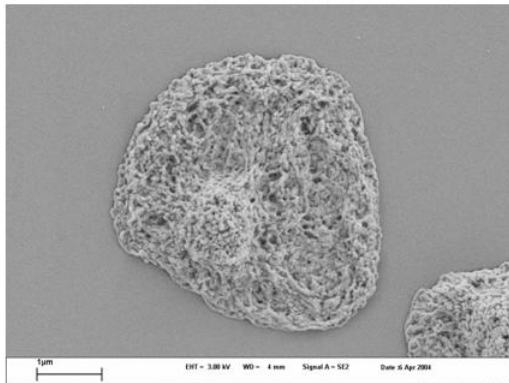
Methylene Blue

Appendix II Supporting SEM Images

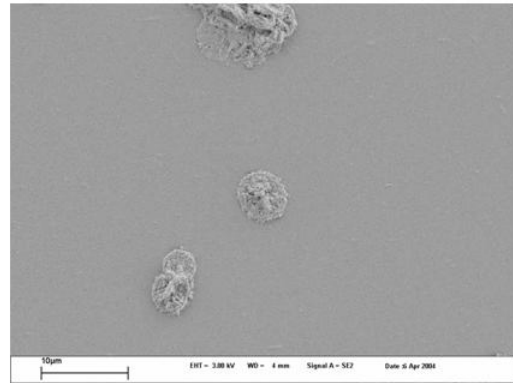
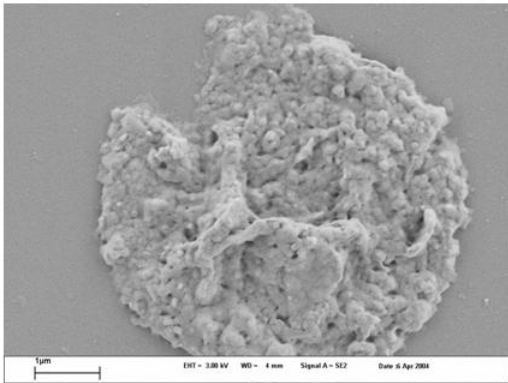
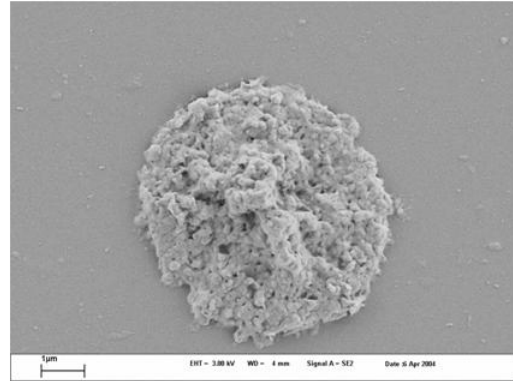
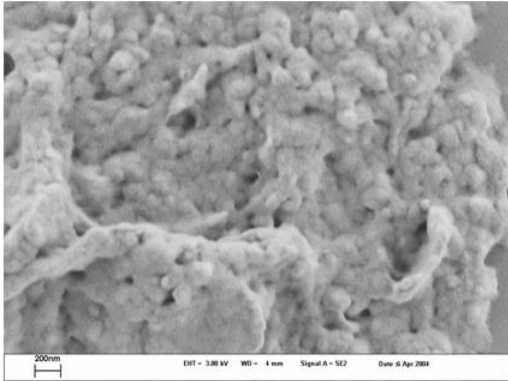
In the next pages SEM images of the capsules discussed in Chapter 5 are shown. The images display the change in the surface morphology of capsules with, and without wax as well as when the wax is present and the wax is annealed. Pages 2-4 are pictures of capsules templated on CaCO_3 and pages 5-7 are of capsules on PS cores.



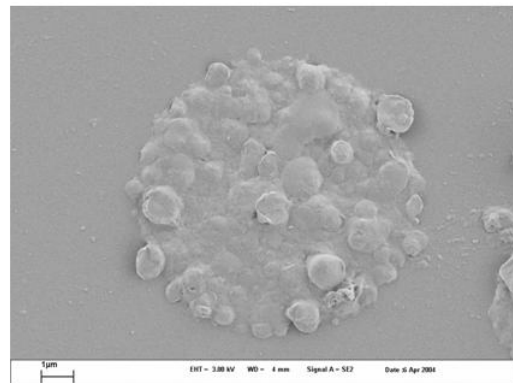
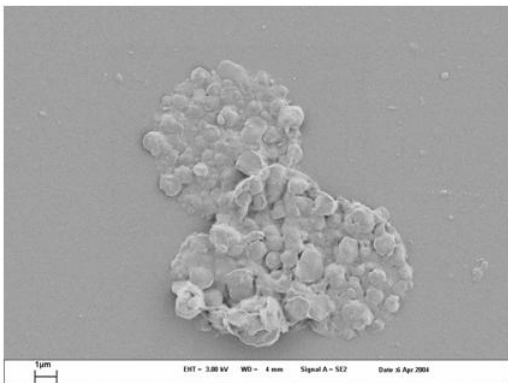
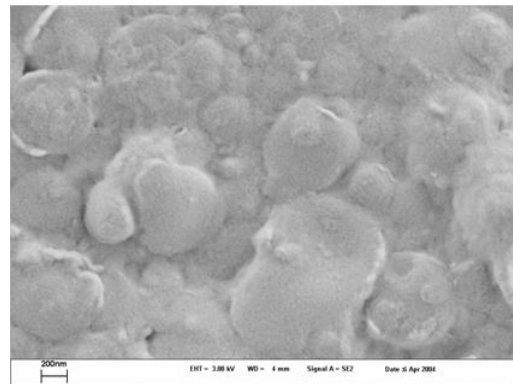
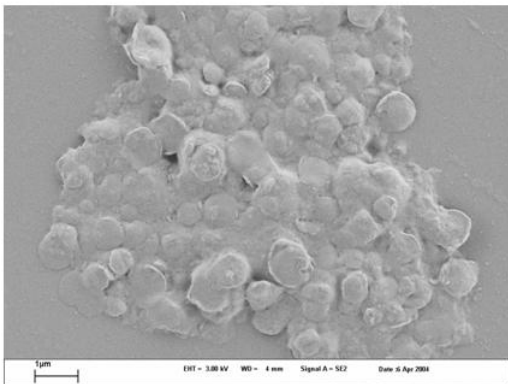
CaCO₃ (PAH/PSS) 4



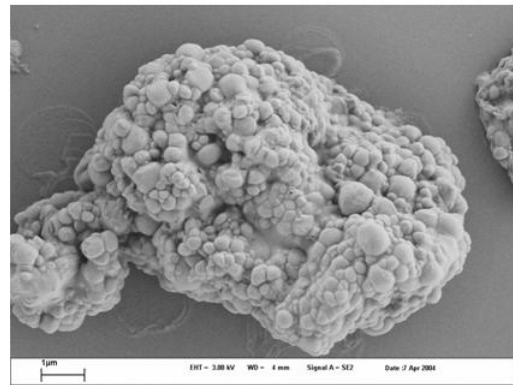
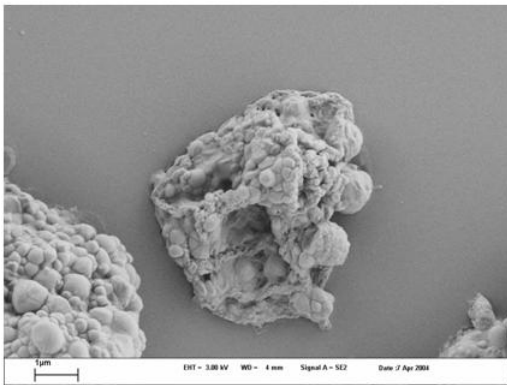
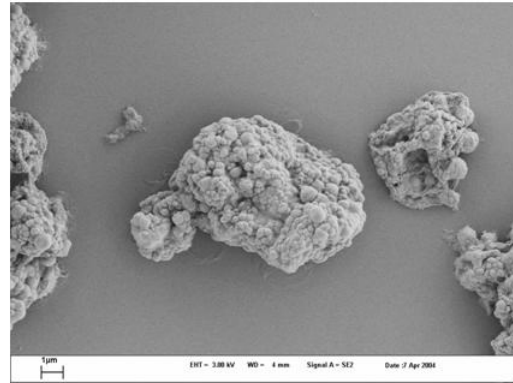
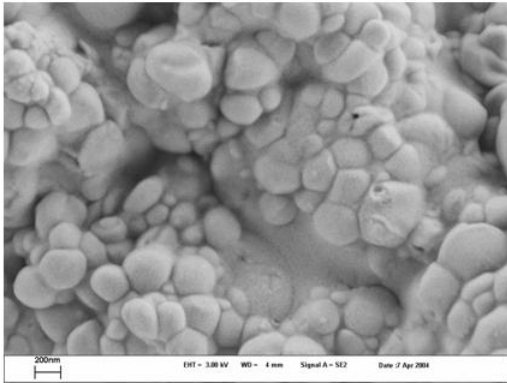
CaCO₃ (PAH/PSS) 4 then heated 2 hours 70°C



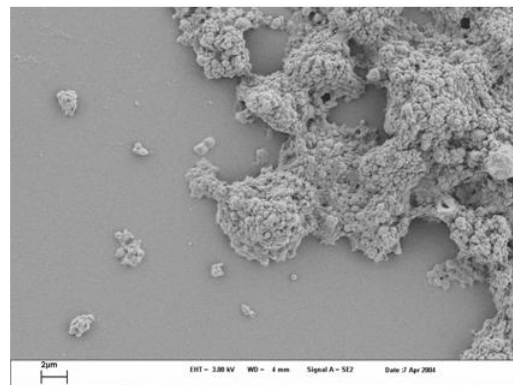
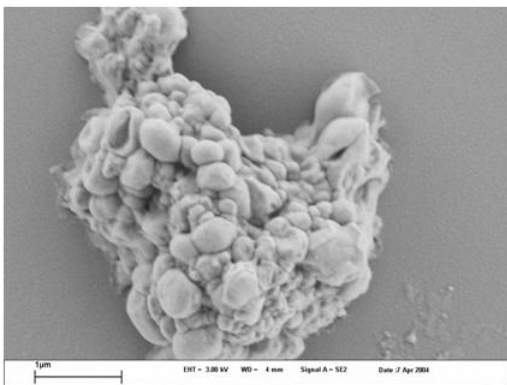
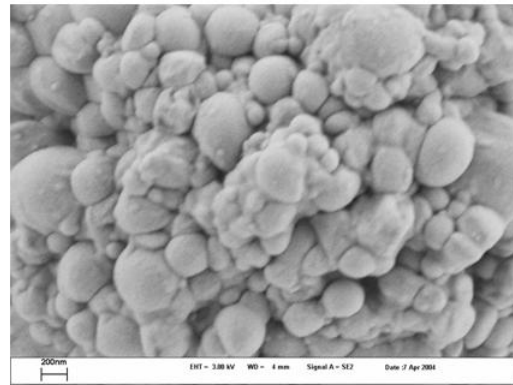
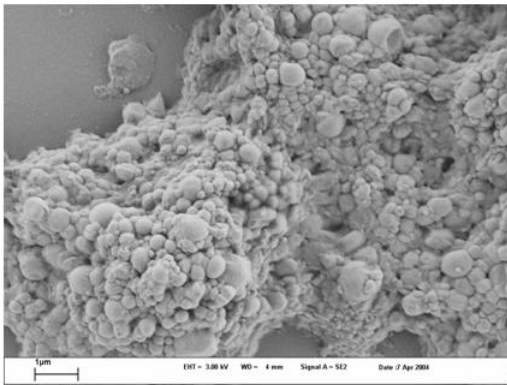
CaCO_3 (PAH/SS)2 (PAH-wax)2



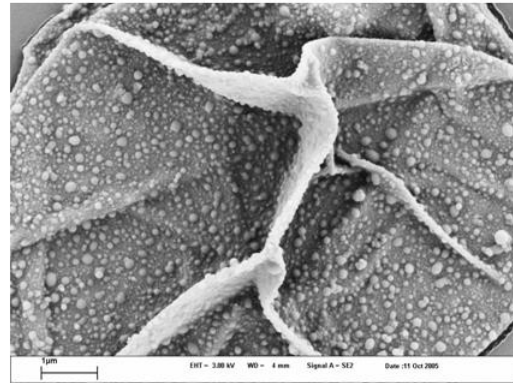
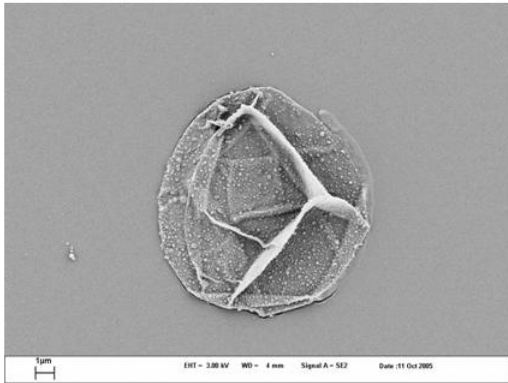
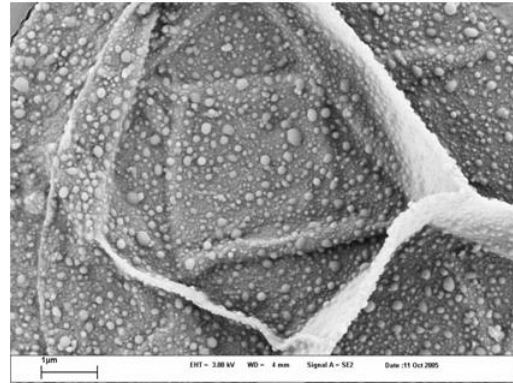
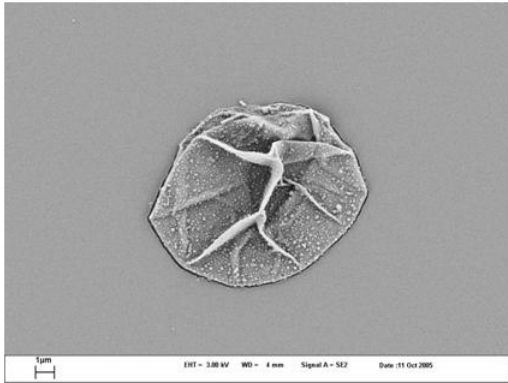
CaCO_3 (PAH/PSS)2 (PAH-wax)2 then heated 2 hours 70°C



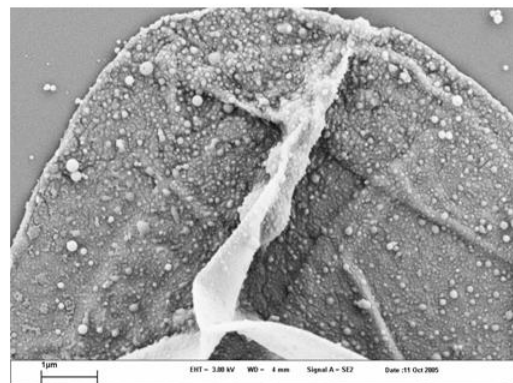
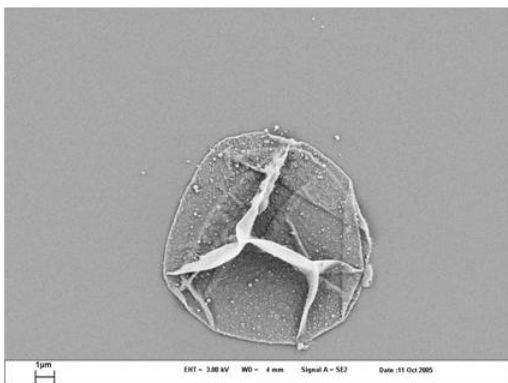
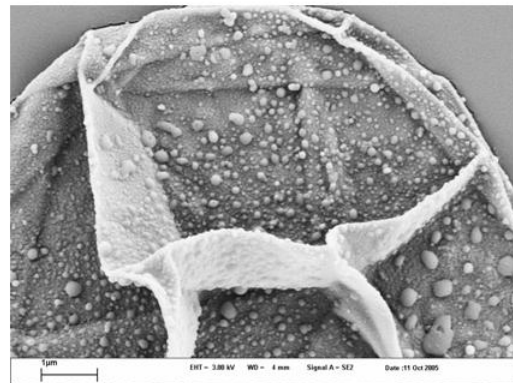
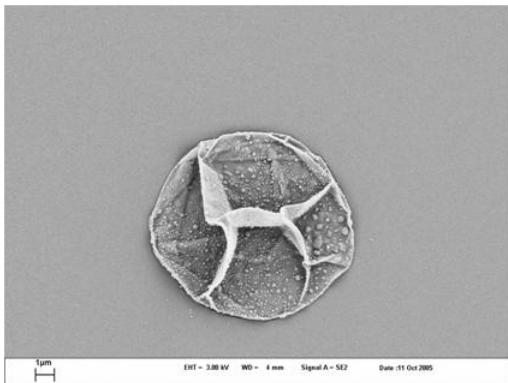
CaCO_3 (PAH/PSS)₂ (+wax022/PSS)₂ then heated 2 hours 70°C



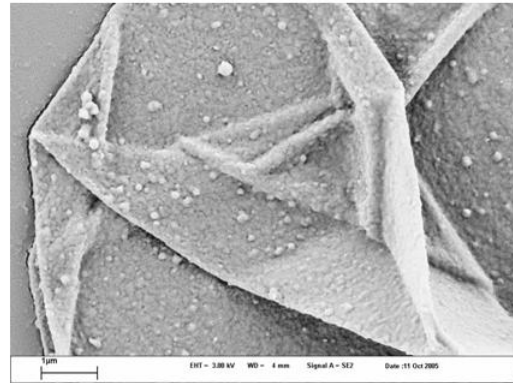
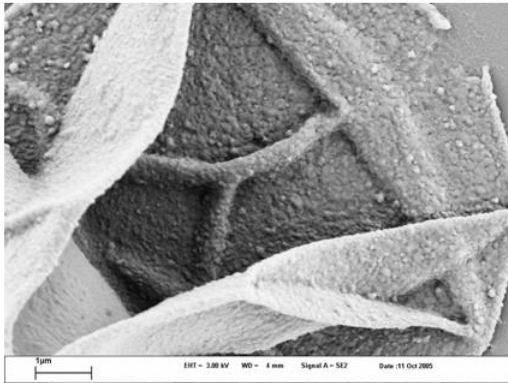
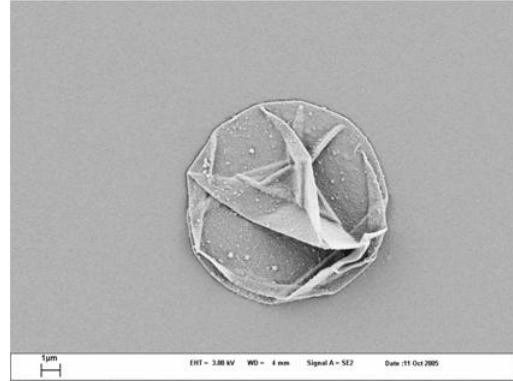
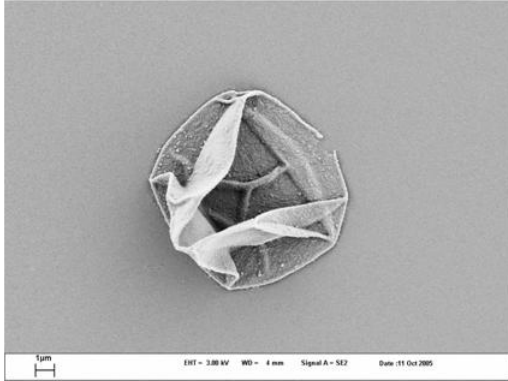
CaCO_3 (PAH/PSS)₂ (+wax022/PSS)₂



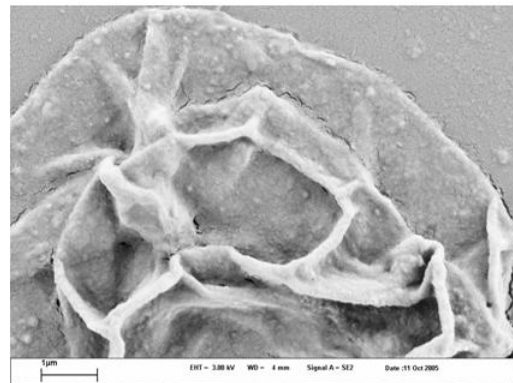
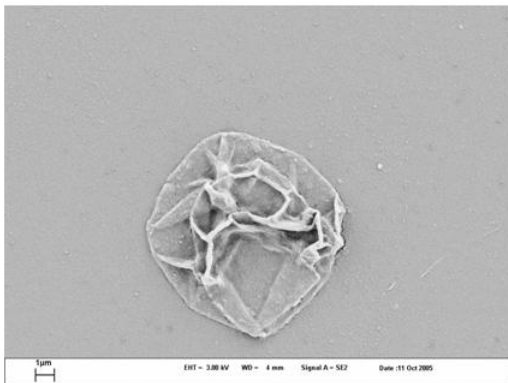
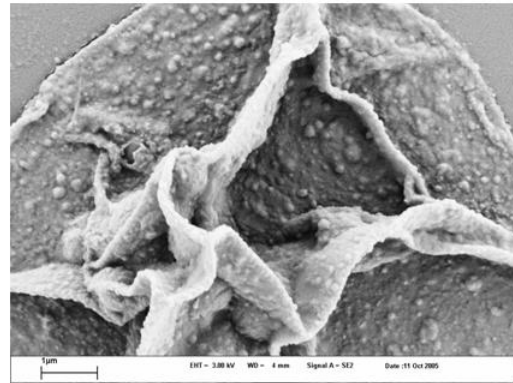
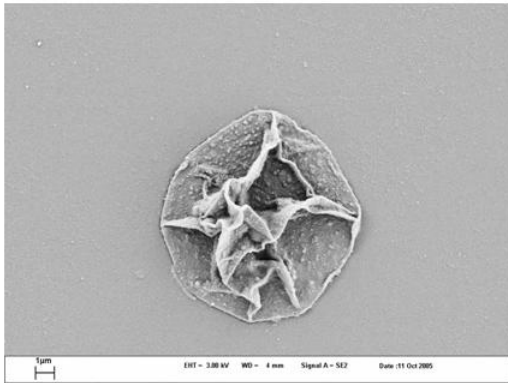
Sample 3a PAH/PSS) 8.5bil + (-wax) (before core dissolution)



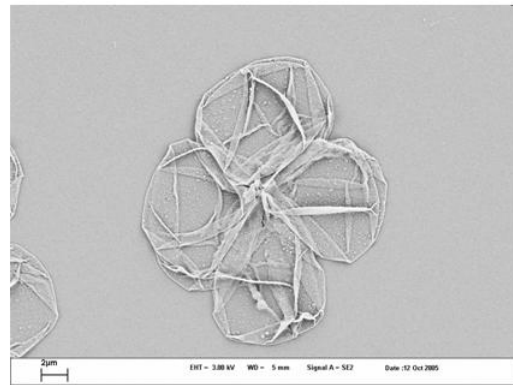
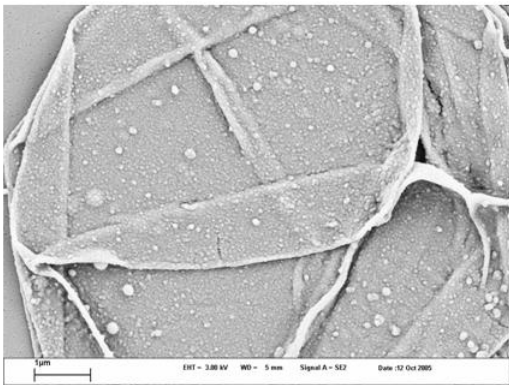
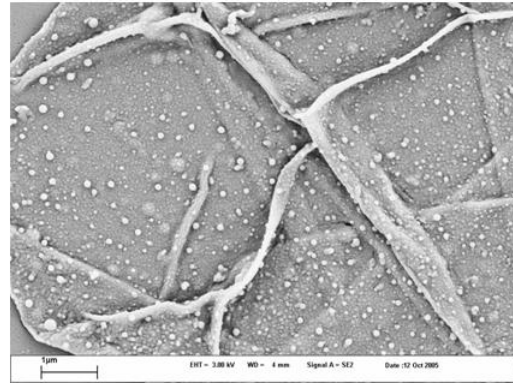
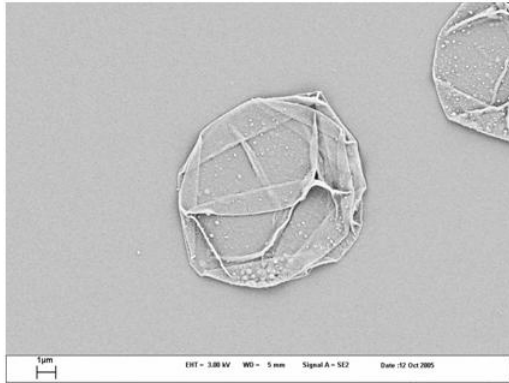
Sample 3ah (PAH/PSS) 8.5bil + (-wax) (before core dissolution) heated (60°C 1hr)



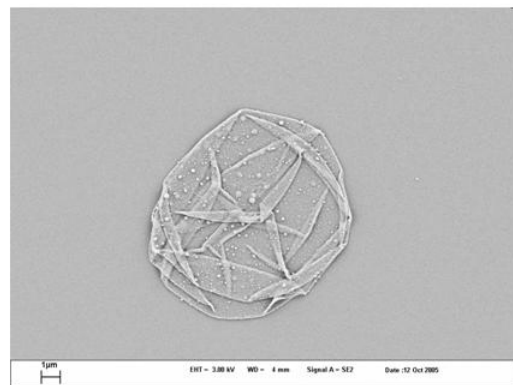
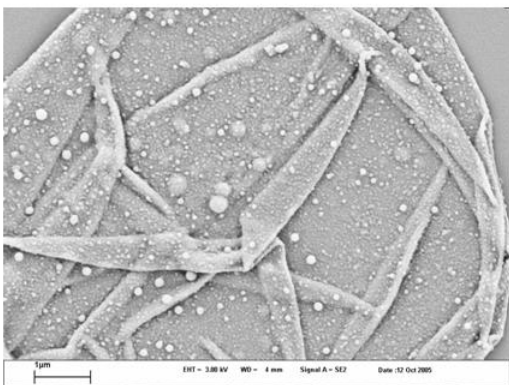
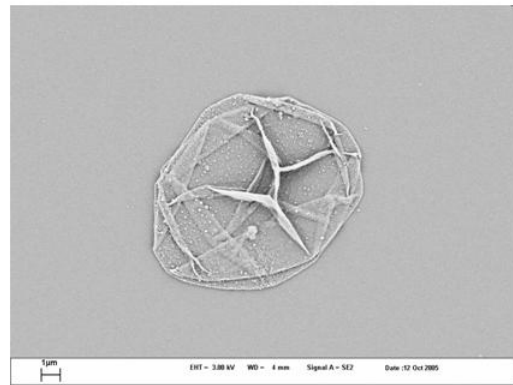
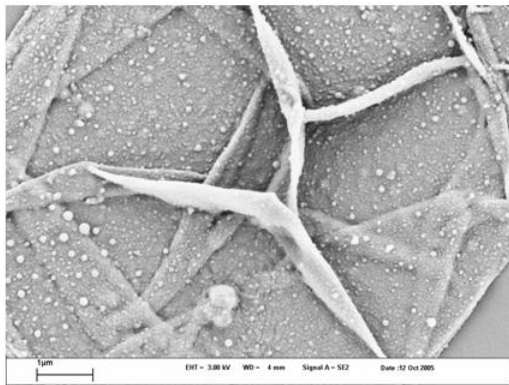
Sample 3b (PAH/PSS) 8.5bil + (-wax) (after core dissolution)



Sample 3bh (PAH/PSS) 8.5bil + (-wax) (after core dissolution) heated (60°C 1hr)



Sample 2h (PAH/PSS) 8.5bil heated (60°C 1hr)



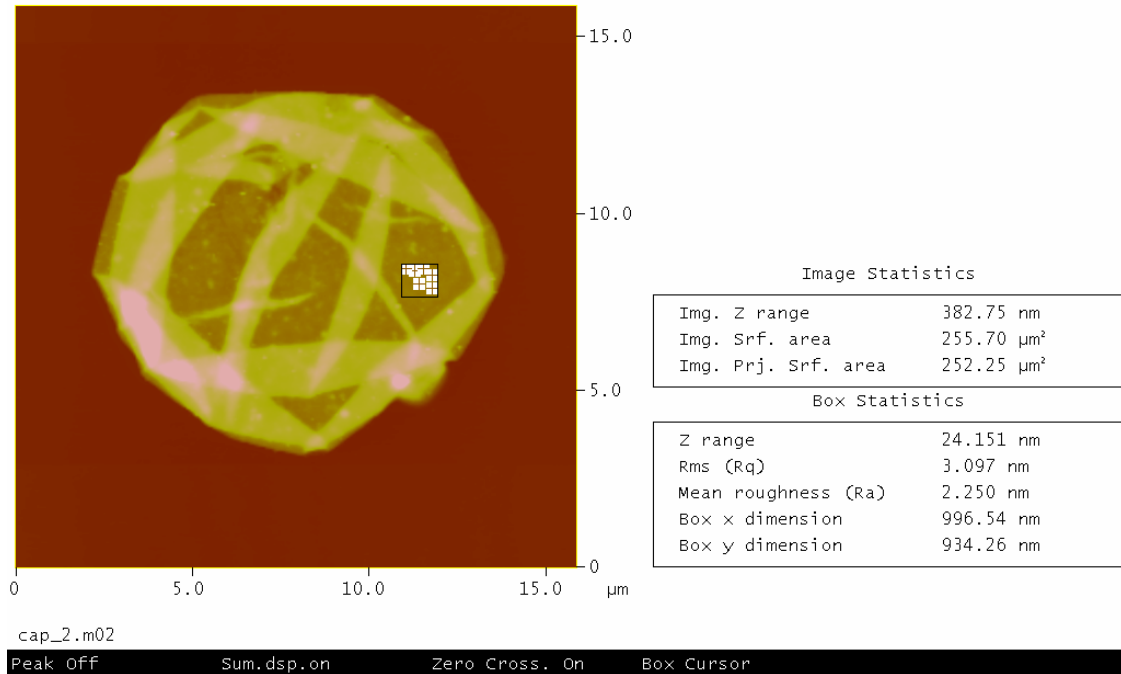
Sample 2 (PAH/PSS) 8.5bil

Appendix III Supporting AFM Images

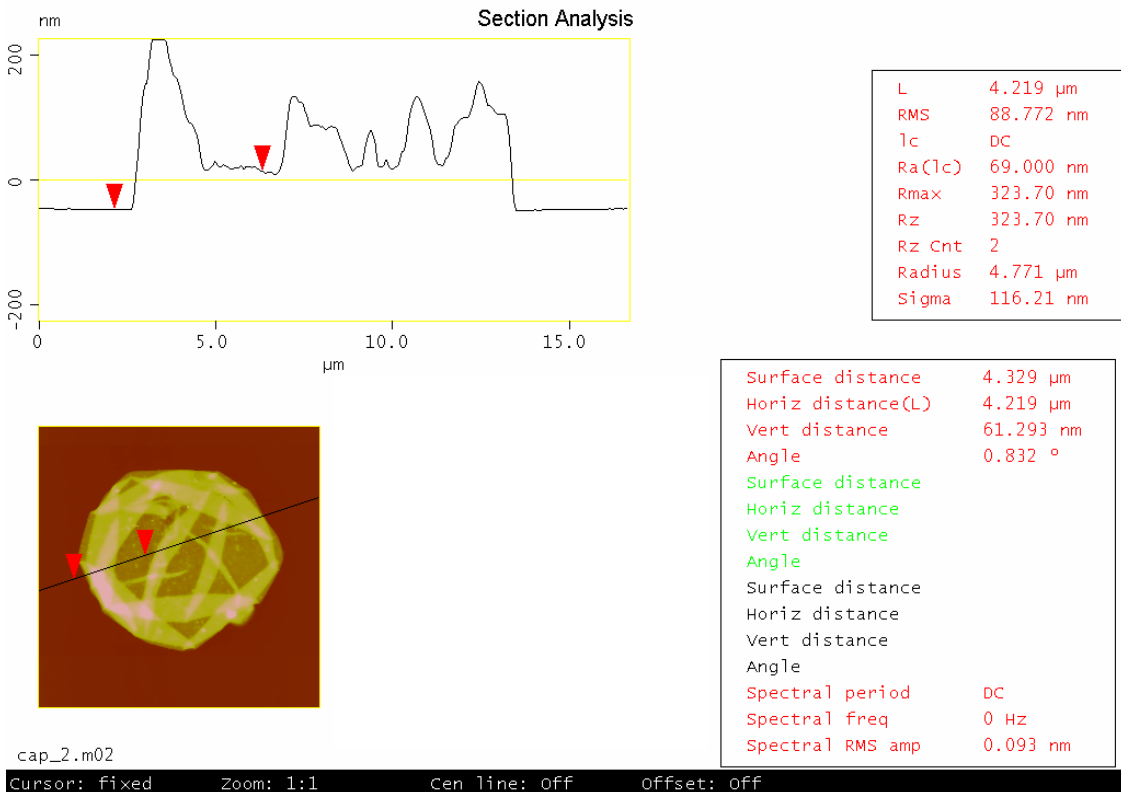
In the next pages images of the capsules discussed in Chapter 5 are shown. The images display the roughness and thickness dependency on the number of layer, the presence of wax and the effect of heat.

Peak Surface Area Summit Zero Crossing Stopband Execute Cursor

Roughness Analysis

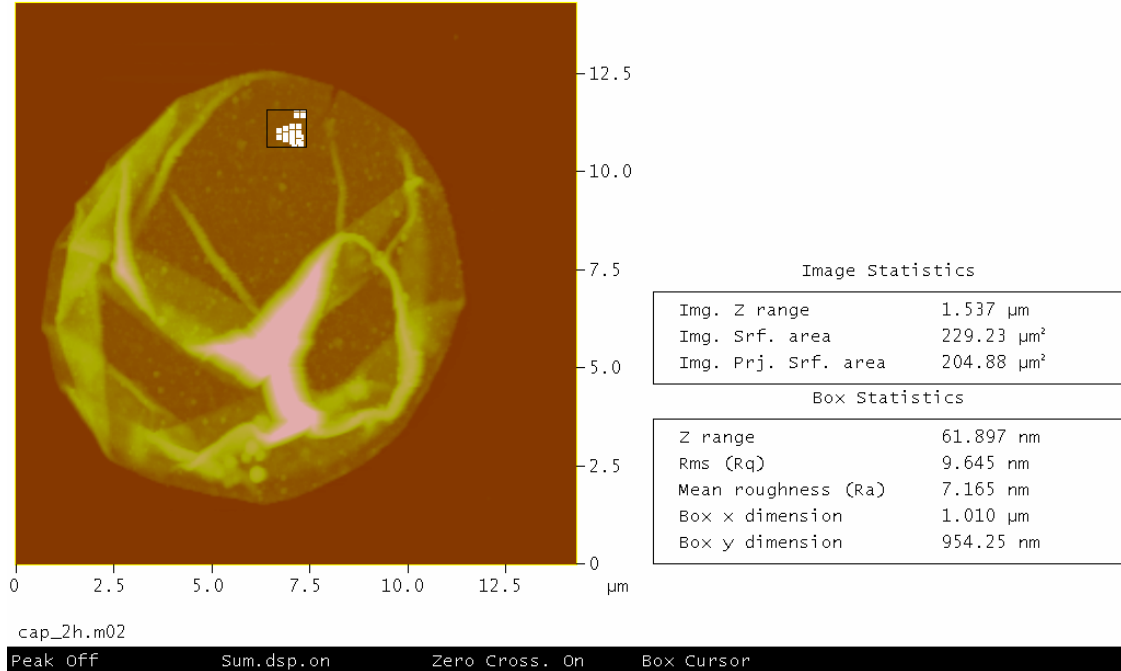


Cursor Marker Spectrum Zoom Center Line Offset Clear

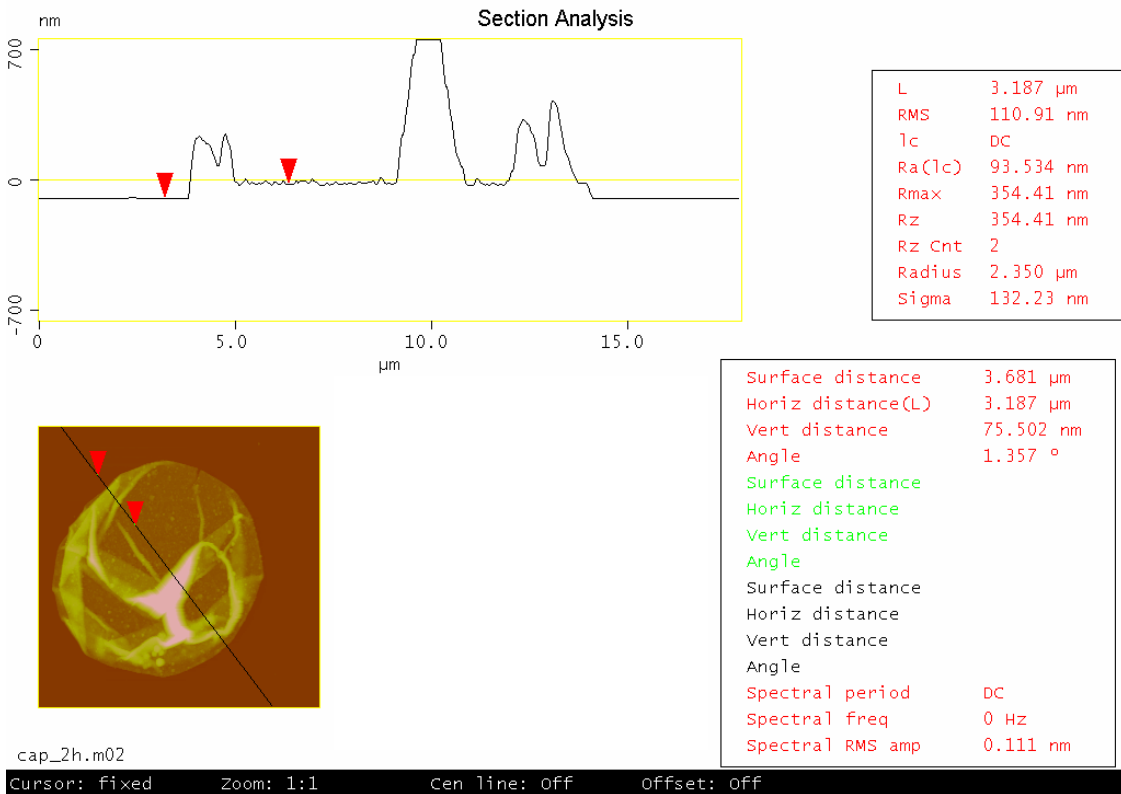


Peak Surface Area Summit Zero Crossing Stopband Execute Cursor

Roughness Analysis

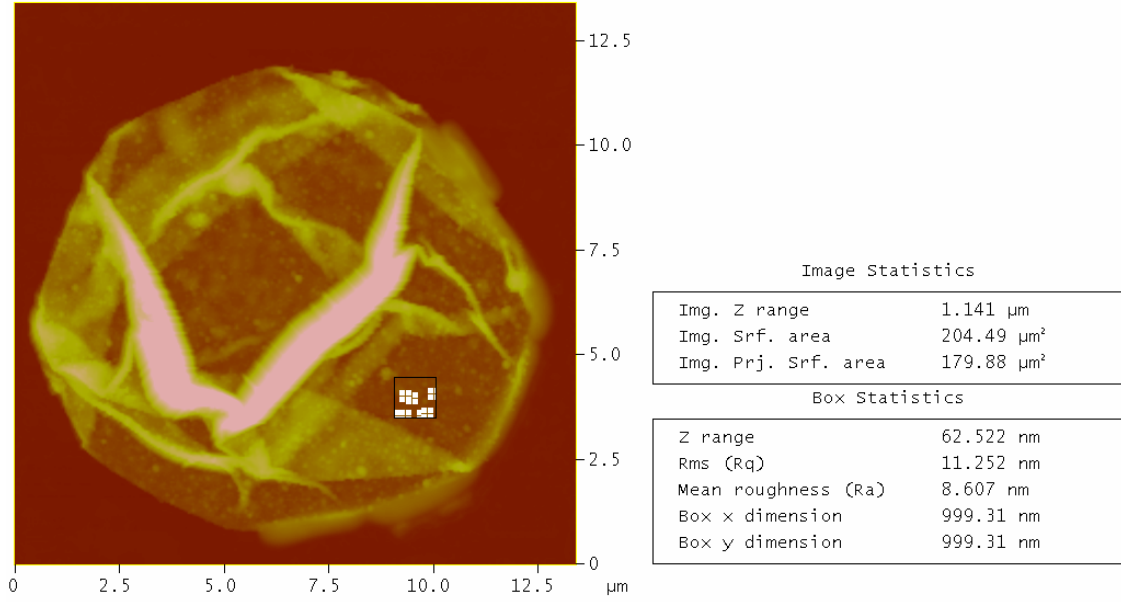


Cursor Marker Spectrum Zoom Center Line Offset Clear



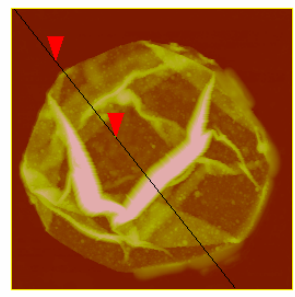
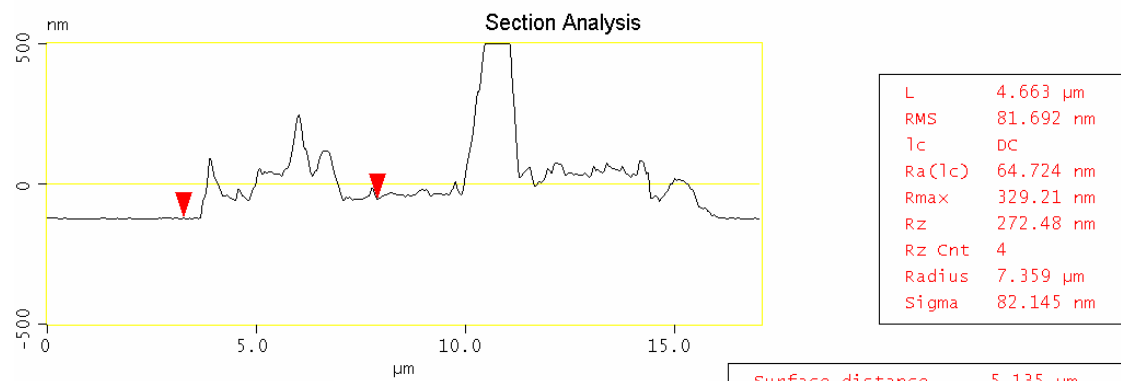
Peak Surface Area Summit Zero Crossing Stopband Execute Cursor

Roughness Analysis



Peak Off Sum.dsp.on Zero Cross. On Box Cursor

Cursor Marker Spectrum Zoom Center Line Offset Clear



Surface distance	5.135 μm
Horiz distance(L)	4.663 μm
Vert distance	68.371 nm
Angle	0.840 $^\circ$
Surface distance	
Horiz distance	
Vert distance	
Angle	
Surface distance	
Horiz distance	
Vert distance	
Angle	
Spectral period	DC
Spectral freq	0 Hz
Spectral RMS amp	0.019 nm

3a.m04
 Cursor: fixed Zoom: 1:1 Cen line: Off Offset: Off

Peak Surface Area Summit Zero Crossing Stopband Execute Cursor

Roughness Analysis

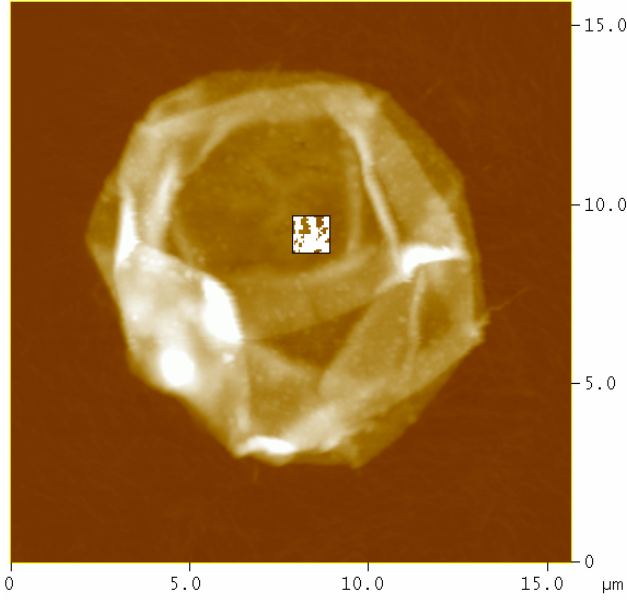


Image Statistics

Img. Z range	1.067 μm
Img. Rms (Rq)	188.70 nm
Img. Ra	154.61 nm
Img. Rmax	1.078 μm
Img. Srf. area	265.34 μm^2

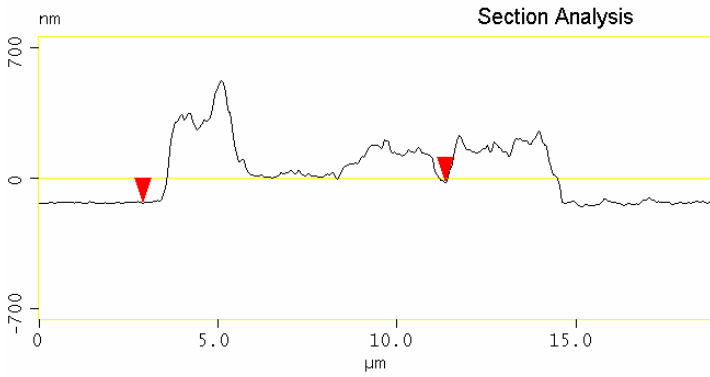
Box Statistics

Rms (Rq)	18.159 nm
Mean roughness (Ra)	14.903 nm
Box x dimension	1.046 μm
Box y dimension	1.046 μm

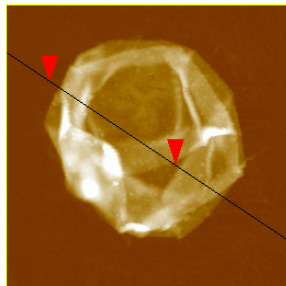
3a_h.m01

Peak On Summit On Zero Cross. Off Box Cursor

Cursor Marker Spectrum Zoom Center Line Offset Clear



L	8.456 μm
RMS	144.96 nm
lc	DC
Ra(lc)	115.40 nm
Rmax	668.73 nm
Rz	445.89 nm
Rz Cnt	4
Radius	2.567 μm
Sigma	1.166 μm



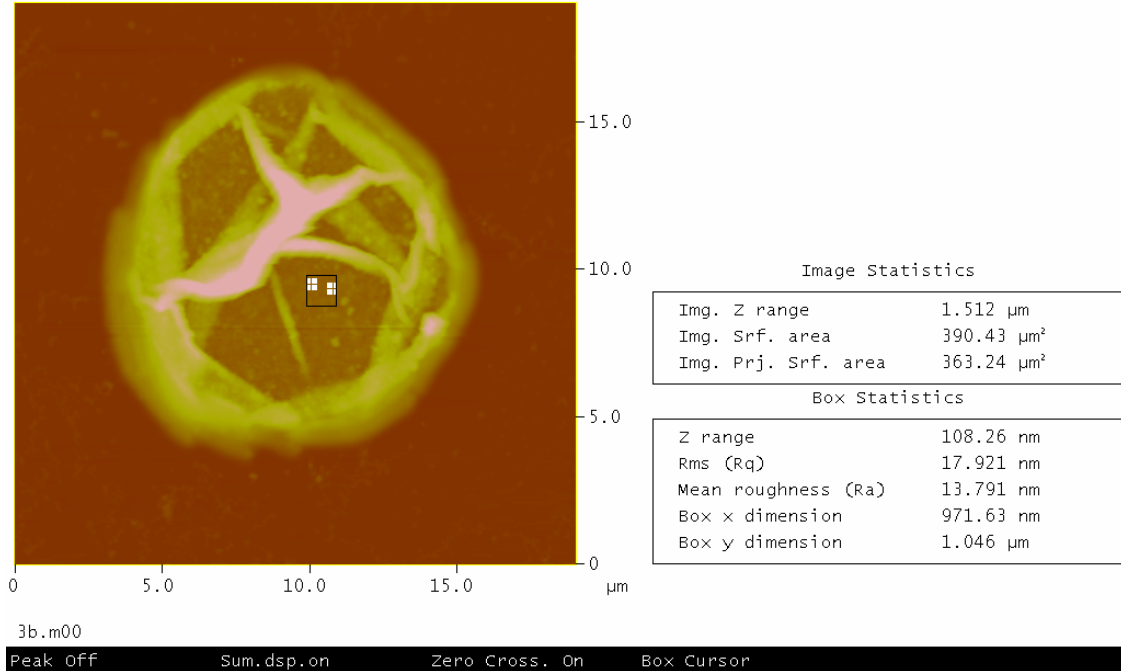
Surface distance	9.181 μm
Horiz distance(L)	8.456 μm
Vert distance	109.15 nm
Angle	0.740 $^\circ$
Surface distance	
Horiz distance	
Vert distance	
Angle	
Spectral period	DC
Spectral freq	0 Hz
Spectral RMS amp	0.082 nm

3a_h.m01

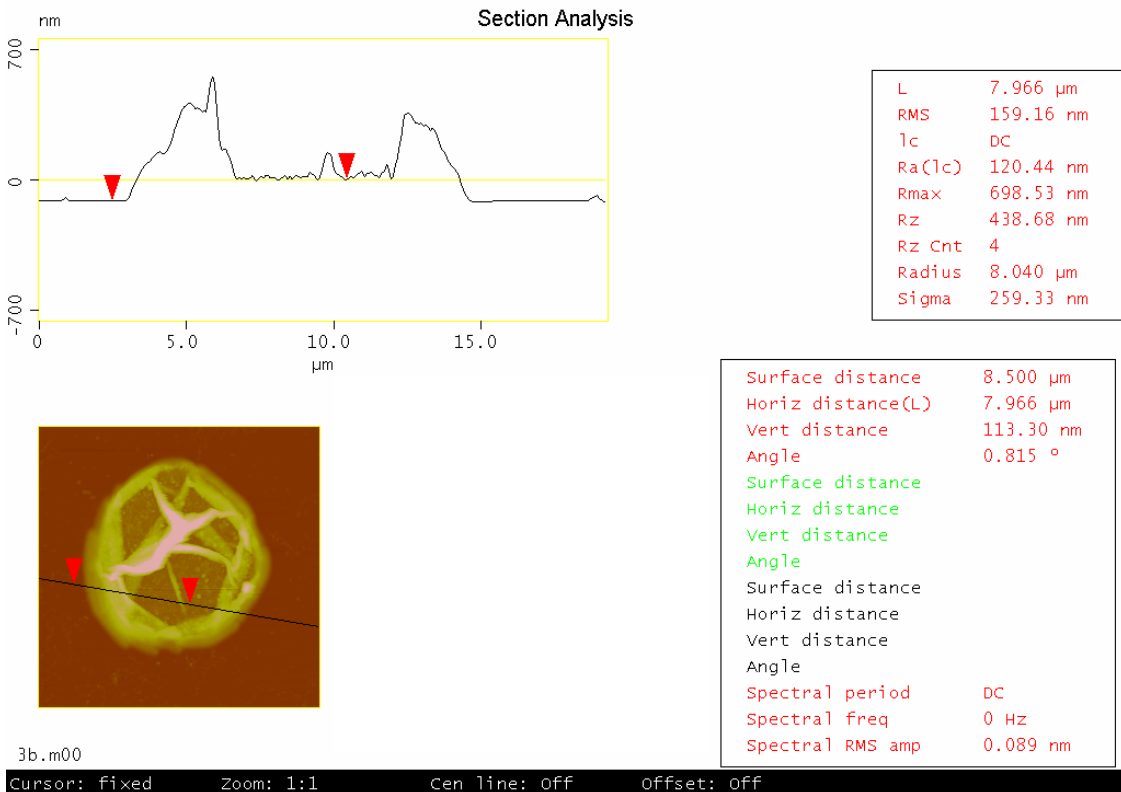
Cursor: fixed Zoom: 1:1 Cen line: Off Offset: Off

Peak Surface Area Summit Zero Crossing Stopband Execute Cursor

Roughness Analysis



Cursor Marker Spectrum Zoom Center Line Offset Clear



Peak Surface Area Summit Zero Crossing Stopband Execute Cursor

Roughness Analysis

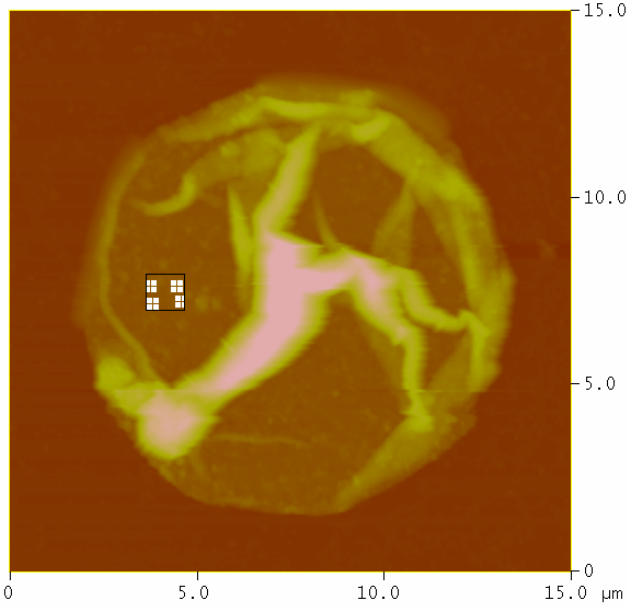


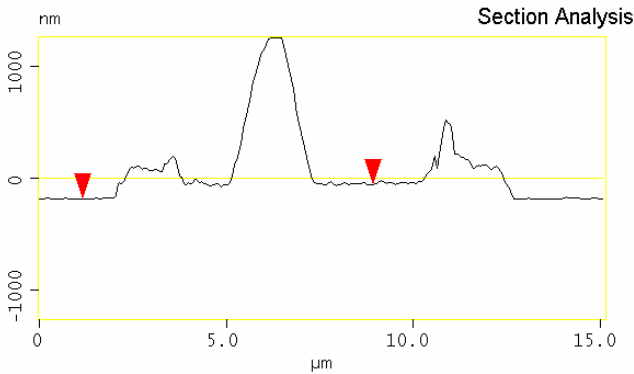
Image Statistics	
Img. Z range	2.265 μm
Img. Srf. area	265.02 μm^2
Img. Prj. Srf. area	225.00 μm^2

Box Statistics	
Z range	118.65 nm
Rms (Rq)	17.953 nm
Mean roughness (Ra)	13.987 nm
Box x dimension	1.000 μm
Box y dimension	941.18 nm

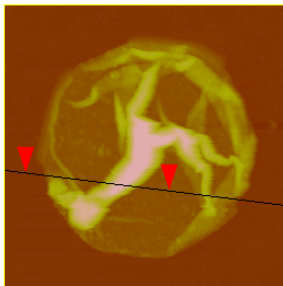
3b_h.m01

Peak Off Sum.dsp.on Zero Cross. On Box Cursor

Cursor Marker Spectrum Zoom Center Line Offset Clear



L	7.734 μm
RMS	422.12 nm
lc	DC
Ra(lc)	301.31 nm
Rmax	1.483 μm
Rz	692.13 nm
Rz Cnt	6
Radius	3.323 μm
Sigma	624.71 nm



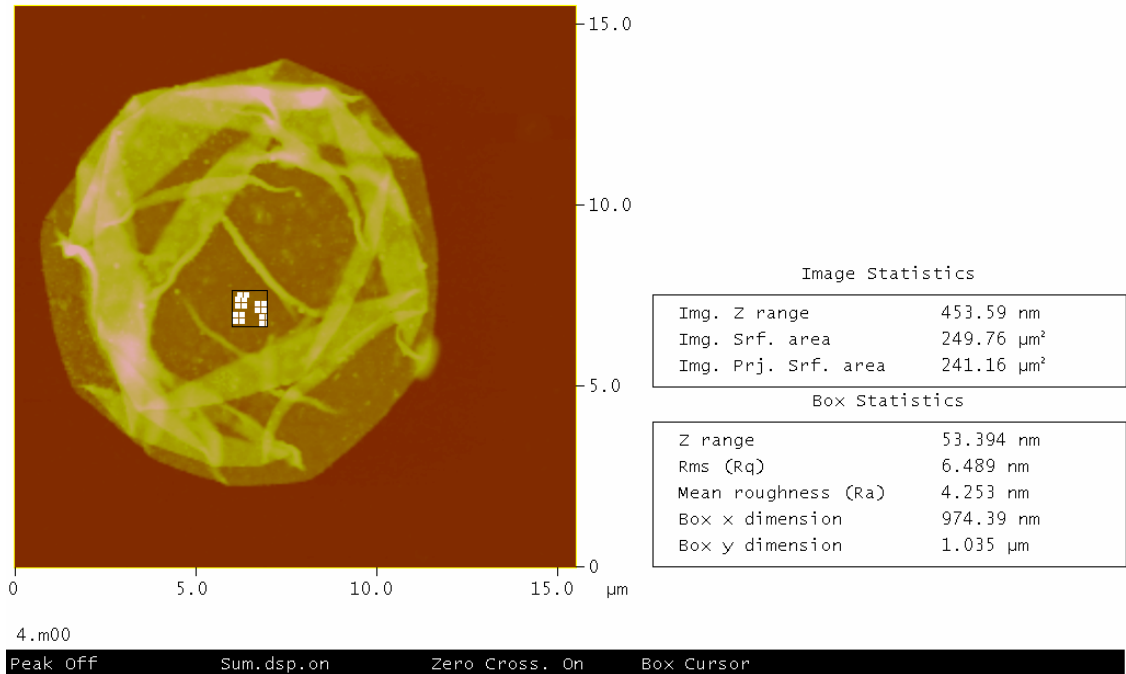
Surface distance	9.451 μm
Horiz distance(L)	7.734 μm
Vert distance	125.35 nm
Angle	0.928 $^\circ$
Surface distance	
Horiz distance	
Vert distance	
Angle	
Surface distance	
Horiz distance	
Vert distance	
Angle	
Spectral period	DC
Spectral freq	0 Hz
Spectral RMS amp	0.209 nm

3b_h.m01

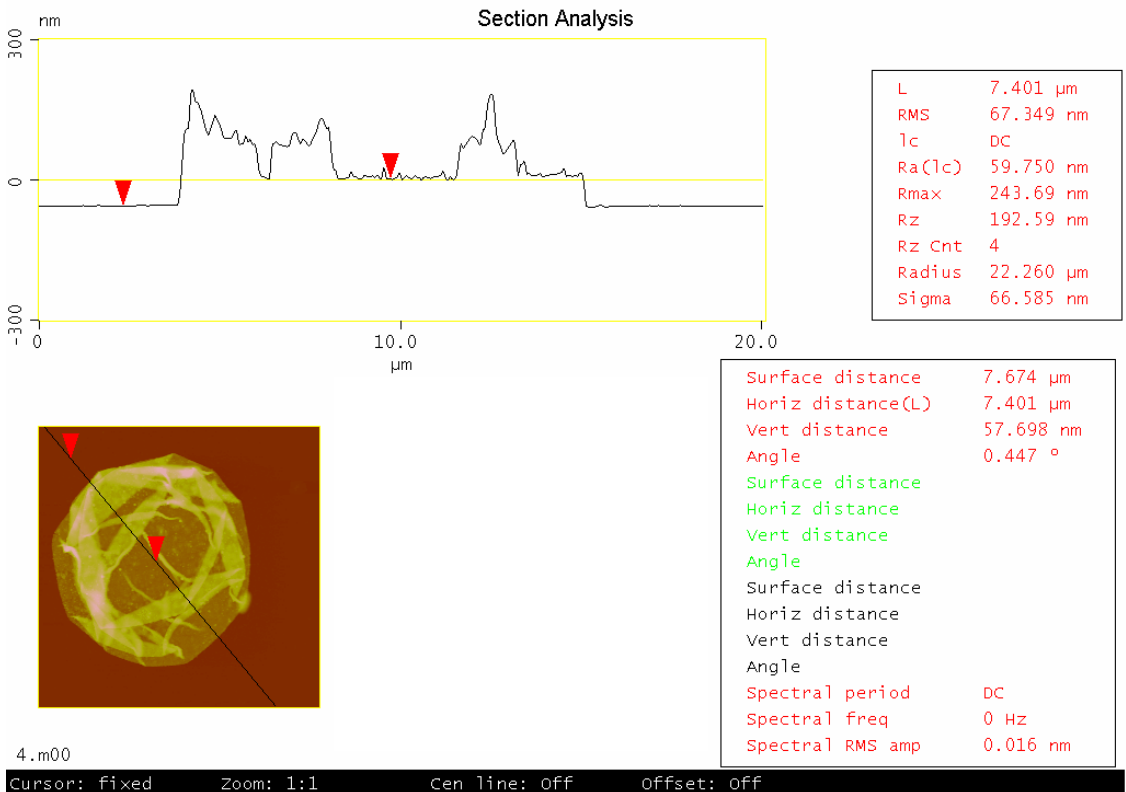
Cursor: fixed Zoom: 1:1 Cen line: Off Offset: Off

Peak Surface Area Summit Zero Crossing Stopband Execute Cursor

Roughness Analysis



Cursor Marker Spectrum Zoom Center Line Offset Clear



Peak Surface Area Summit Zero Crossing Stopband Execute Cursor

Roughness Analysis

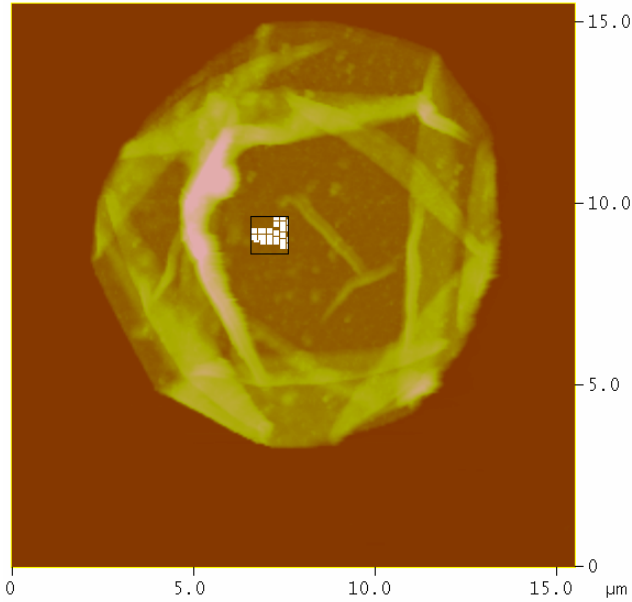


Image Statistics

Img. Z range	874.41 nm
Img. Srf. area	257.83 μm^2
Img. Prj. Srf. area	241.16 μm^2

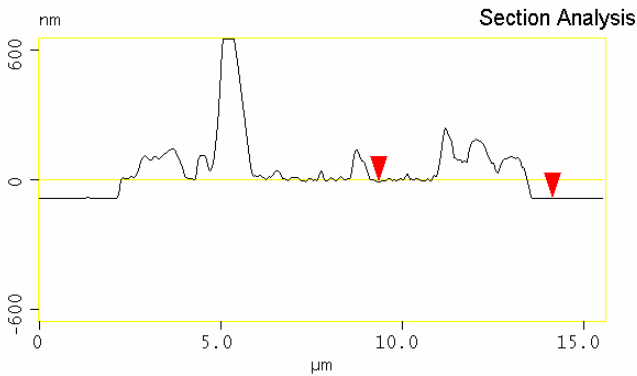
Box Statistics

Z range	53.780 nm
Rms (Rq)	8.397 nm
Mean roughness (Ra)	6.327 nm
Box x dimension	1.035 μm
Box y dimension	1.035 μm

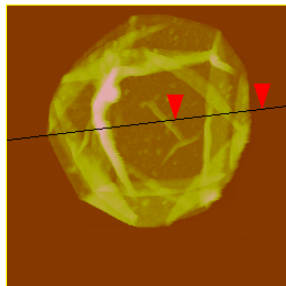
4_h.m02

Peak Off Sum.dsp.on Zero Cross. On Box Cursor

Cursor Marker Spectrum Zoom Center Line Offset Clear



L	4.792 μm
RMS	84.047 nm
lc	DC
Ra(lc)	71.937 nm
Rmax	316.79 nm
Rz	225.39 nm
Rz Cnt	4
Radius	8.263 μm
Sigma	67.255 nm



Surface distance	5.105 μm
Horiz distance(L)	4.792 μm
Vert distance	78.281 nm
Angle	0.936 $^\circ$
Surface distance	
Horiz distance	
Vert distance	
Angle	
Surface distance	
Horiz distance	
Vert distance	
Angle	
Spectral period	DC
Spectral freq	0 Hz
Spectral RMS amp	0.118 nm

4_h.m02

Cursor: fixed Zoom: 1:1 Cen line: Off Offset: Off

Appendix IV Publications

Prevot, M.; Cordeiro, A. L.; Sukhorukov, G. B.; Lvov, Y.; Besser, R. S.; Möhwald, H., Design of a microfluidic system to investigate the mechanical properties of layer-by-layer fabricated capsules. *Macromolecular Materials and Engineering* **2003**, 288, (12), 915-919.

Volodkin, D. V.; Petrov, A. I.; Prevot, M.; Sukhorukov, G. B., Matrix polyelectrolyte microcapsules: New system for macromolecule encapsulation. *Langmuir* **2004**, 20, (8), 3398-3406.

Glinel, K.; Prevot, M.; Krustev, R.; Sukhorukov, G. B.; Jonas, A. M.; Möhwald, H., Control of the Water Permeability of Polyelectrolyte Multilayers by Deposition of Charged Paraffin Particles. *Langmuir* **2004**, 20, (12), 4898-4902.

Prevot, M.; Déjugnat, C.; Möhwald, H.; Sukhorukov, G., Behaviour of Temperature-Sensitive PNIPAM Confined in Polyelectrolyte Capsules. *ChemPhysChen* **2006**. *Submitted*

Prevot, M.; Möhwald, H.; Sukhorukov, G., Water Permeability Control of Capsules on Various Cores through Charged Paraffin Particle Deposition. **2006**. *In preparation*